DIFFRACTIVE PHOTON PRODUCTION

THE UNIVERSITY of MANCHESTER

A thesis submitted to the University of Manchester
for the degree of Doctor of Philosophy
in the Faculty of Science

By

Norman G. Evanson

Department of Physics and Astronomy

September 1999

Contents

List of Figures

List of Tables

Abstract

UNIVERSITY OF MANCHESTER

ABSTRACT OF THESIS submitted by **Norman G. Evanson** for the Degree of Doctor of Philosophy and entitled **Diffractive Photon Production**

Month and Year of Submission: September 1999

We study the diffractive production of photons in γp, $\gamma\gamma$ and e^+e^- collisions. We specifically compute the rates for $\gamma^* p \to \gamma X$, $\gamma^*\gamma^* \to \gamma X$ and for $\gamma^*\gamma^* \to \gamma\gamma$, where X denotes the dissociation products of the proton or photon. Our calculations are performed using the leading logarithmic formalism of Balitsky, Fadin, Kuraev and Lipatov (BFKL), and are used to make estimates for cross sections at HERA, LEP and a future linear collider. We focus on the rates at large momentum transfers, $-t \gg \Lambda^2$, where we are most confident in the use of QCD perturbation theory. However, our calculations do allow us to study the $-t \to 0$ behaviour of the $\gamma^*\gamma^* \to \gamma\gamma$ process in the region where the incoming photons are sufficiently virtual.

Declaration and Copyright Notice

No portion of the work referred to in this thesis has been submitted in support of an application for another degree or qualification of this or any other university or other institution of learning.

The Author

The author was born in 1973 and lived in the small Shropshire town of Wem until the age of 18. He then moved to Leeds where he completed a B.Sc. in Physics at Leeds University, graduating with a 1^{st} class degree in 1994. Having always intended to pursue a Ph.D. he decided to have a break during the year 1994-95 to see what happened. After a period of unemployment, he spent enough of the year covered in coal during the privatisation of the coal industry to be able to travel and spend freely until he moved on. He returned to education in October 1995 and got himself involved in the heady world of BFKL phenomenology. During the course of his studies he has given presentations at the ECFA/DESY future LC workshop at Oxford University in 1999, and at the I.o.P Particle Physics Conference twice; Manchester University in 1998 and Salford University in 1999. He also won 1^{st} prize for the end of 2^{nd} year poster exhibition. He has had the results of his work published by the APS:- Phys. Rev. **D60** (1999) 034016. He currently resides in the Unix cluster of Manchester University Theoretical Physics group and would really like a dog.

Acknowledgements

There are far too many people who contributed, in some guise or other, to the completion of this thesis, to be mentioned here. Many apologies to those of you not listed, but you know who you are. To my peers from Manchester theory group: Anne Keinappel, Hiroko Short have been good friends for the duration. Scott Jones and Keith Richardson have had the unfortunate distinction of having lived with me (SSJ) and shared an office with me (KGR). Many thanks also go to Agustin Sabio Vera for proofreading this thesis.

The members of the particle physics community whom I have met and worked with deserve special praise for often pointing out the right direction in times of crisis: Mike Seymour, Martin McDermott, Peter Sutton, Phil Burrows, and in particular Mark Wüsthoff, who has been fantastically helpful during my time at Manchester.

To my friends from Shropshire, Leeds and Manchester, all of you have been a source of relaxation, mirth, wit, mental stimulation and recently financial support. (The cash is on the way when I get a job !!) My heart goes out to Ross who has put up with me as a flat mate for the last two years.

Thanks to PPARC who have supported me through the first three years of this work and Manchester University who have provided P/T employment in several forms to supplement the meager grant. Many thanks to the staff at Levenshulme employment service office and Manchester benefit service, whose relaxed attitude, mind numbing ineptitude (MBS), and, tellingly, phenomenal staff turnover rate have made "benefit fraud" over the last year easier than it could have been.

On the downside, the author finds, and must point out, that it is utterly ridiculous that this situation need occur in the first place. You cannot expect people to complete a piece of work in four years if you cut them off financially after three, with seemingly no support structure for those not fortunate enough to have friends or family who are either willing or able to support them. The "get a job and do it part time" option was lost when the four year deadline was introduced. Enough said.

My parents, Norman and Margaret, have been a constant source of encouragement, patient advice, and bottomless love for all my life and this thesis is about their pride in their son as much as anything else. Also to Jude who has been such a wonderful, elegant, witty,.. partner to me since we first met working in the union bar. She has become one of the cornerstones of my life over the last two years and truly knows what makes me tick.

Lastly, I must mention the great deal of support and encouragement that I have received from my supervisor, Jeff Forshaw. Jeff has been a most patient and inspirational teacher throughout the duration of my Ph.D. His level of understanding of physics is truly admirable and puts us mere mortals to shame. I doubt that I would have gotten this far if it had not been for his guidance.

Chapter 1

Introduction

The current pedagogy of physics relies on the premise that there are four fundamental forces in the universe: gravity, electromagnetism, the weak and strong nuclear forces. Historically, the first of these to be identified was gravity which today stands alone and remains the most difficult to reconcile with quantum mechanics. In stark contrast to gravity is electromagnetism where the application of the ideas of quantum field theory (QFT) and the Abelian gauge principle have produced a theory, QED, that has been predicated by the accuracy of its predictions to measurement. The success of QED owes to the almost universal application of perturbation theory where the fine structure constant $\alpha(\approx 1/137)$ is usually sufficiently small to justify the perturbation expansion in it, which is so eloquently displayed by the technique of Feynman diagrams. The study of the nuclear forces can be said to have begun with the discovery of the neutron by Chadwick in 1932 and throughout its history there have been numerous attempts to arrive at a satisfactory theory which stands up to the scrutiny of experiment. With the successful application of QED in the 1950's the push to understand the nuclear forces in the same field theoretic language intensified until the weak nuclear force was unified with QED by the work of Weinberg, Glashow and Salam in 1967 which lead to the conception of electro-weak theory based on the gauge group $SU(2)_L \times U(1)_Y$. The strong nuclear force was eventually brought into the domain of quantum field theories with the invention of QCD in 1973, based on the non-Abelian group $SU(3)_c$. Thus the description of elementary particle physics today is based on the unified gauge group

$SU(3)_C \times SU(2)_L \times U(1)_Y$, universally referred to as the Standard Model.

Within the strong sector of the Standard Model one of the major challenges is to gain an understanding of the phenomena of diffraction. Diffraction in optics refers to the scattering of different frequency components of light at differing angles off the same target, i.e. all the original frequency components are still there but they have each been differently scattered by the target which is itself unaffected: the scattered wave is regarded as the shadow of the target. Hadronic diffraction was first observed in cosmic ray data [1] and is entirely analogous [2] in that the "projectile" hadron is regarded as being a superposition of diffractive eigenstates each of which scatter *elastically* off the "target" hadron, which remains intact. Each of the eigenstates will scatter off the hadronic target with a different probability and thus the final state is a different superposition of the eigenstates and therefore will, generally, correspond to a different physical state.

1.1 Diffraction Without QCD

Diffractive scattering naturally implies low momentum transfers between colliding particles, i.e. the region of Mandelstam variable $t \approx 0$. The discovery of diffractive events (along with many others) predates QCD and so necessarily a theory was developed to describe and make predictions about them. The pre-QCD theory of strong interactions is based upon remarkably simple postulates about the scattering matrix (S-matrix): it should be Lorentz invariant (frame independent), unitary (probability conservation), and analytic (causal). The reader interested in a thorough treatise on S-matrix theory is referred elsewhere [3], we shall only reproduce the relevant points here.

The scattering amplitude from an in state $|a>$ to an out state $|b>$ is related to the S-matrix element S_{ab} by the relationship

$$S_{ab} = \delta_{ab} + i(2\pi)^4 \delta^{(4)} \left(\sum_a p_a - \sum_b p_b \right) \mathcal{A}_{ab}. \tag{1.1.1}$$

The unitarity of the S-Matrix then gives

$$2\Im m \mathcal{A}_{ab} = (2\pi)^4 \delta^{(4)} \left(\sum_a p_a - \sum_b p_b \right) \sum_c \mathcal{A}_{ac} \mathcal{A}^{\dagger}_{bc} \tag{1.1.2}$$

where $\sum_c$ implies a sum over particle numbers and types. The relation (1.1.2) may be visualised with unitarity diagrams as shown in figure (1.1). Unitarity diagrams

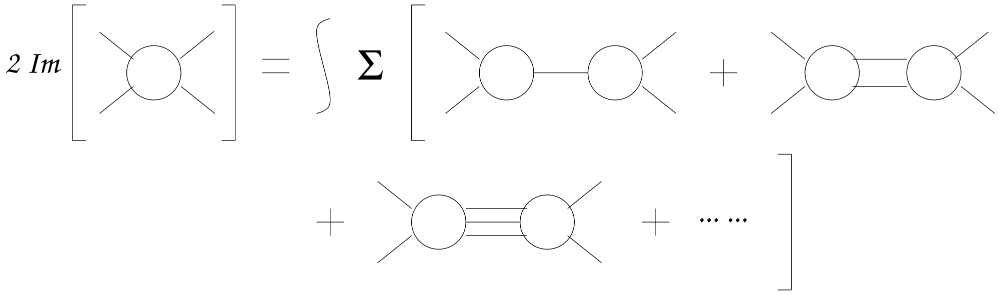

Figure 1.1: Unitarity expressed through unitarity diagrams.

are quite different from Feynman diagrams as all internal particle states are placed on-shell. Such diagrams are said to be cut. An important case of the Cutkosky rules, which are the rules for calculating cut diagrams, is the optical theorem which relates the imaginary part of the forward scattering amplitude to the total cross section

$$2\Im m\mathcal{A}_{aa}(s,0) = (2\pi)^4\delta^{(4)}\left(\sum_f p_f - \sum_a p_a\right)\sum_n |\mathcal{A}_{an}|^2 = F\sigma_{tot} \tag{1.1.3}$$

where F is the flux factor. To define the $a \to b$ scattering amplitude completely its real part must still be determined and experimentally this may be done with knowledge of the forward elastic differential cross section. However, experimental results from the diffractive region indicate that the real part of the scattering amplitude is small.

It is possible to write the amplitude in a particularly interesting form. We start by considering the partial wave decomposition of a particular $2 \to 2$ scattering in the cross channel:

$$A(s,t) = \sum_l (2l+1)a_l(t)P_l\left(1 + \frac{2s}{t}\right) \tag{1.1.4}$$

where $P_l(z)$ is a Legendre polynomial of order l, $a_l(t)$ is the partial wave amplitude and we have neglected all masses. Sommerfeld and Watson rewrote the partial wave expansion (1.1.4) as a contour integral in the angular momentum plane (l) i.e.

$$A(s,t) = \oint_C dl\,(2l+1)\frac{a(l,t)}{\sin(\pi l)}P\left(l, 1 + \frac{2s}{t}\right) \tag{1.1.5}$$

where the contour C surrounds the positive real axis as shown in figure (1.2). The functions $a(l,t)$ and $P(l, 1+2s/t)$ are the analytic continuations of the partial wave amplitude and the Legendre polynomial. The denominator $\sin(\pi l)$ gives rise to the poles at integer l which reproduce (1.1.4). However, it is obvious that the function

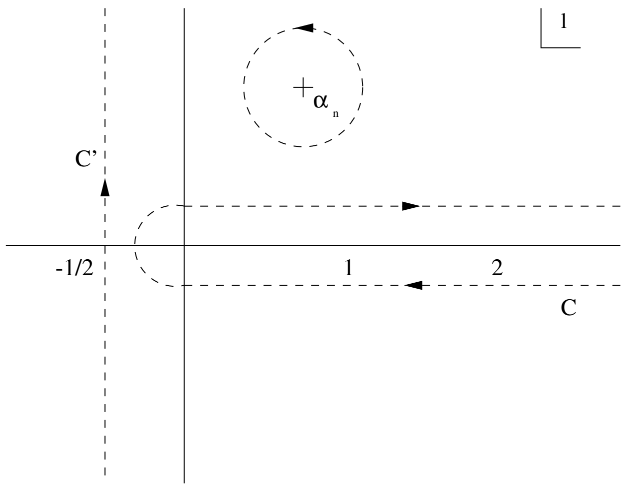

Figure 1.2: The Sommerfeld-Watson transform.

$a(l,t)$ isn't uniquely defined by (1.1.5); one could add any function that vanishes at integer values of πl and still reproduce (1.1.4). Carlson's theorem states that $a(l,t)$ is unique provided that $a(l,t) < \exp(\pi|l|)$ as $|l| \to \infty$; but as $a(l,t)$ contains terms that alternate in sign, i.e. proportional to $(-1)^l$, Carlson's theorem is violated along the imaginary axis. This ambiguity is solved by introducing two analytic functions $a^{(+)}(l,t)$ and $a^{(-)}(l,t)$ which are analytic continuations of the even and odd partial wave amplitudes. We now must modify (1.1.5) to read

$$A(s,t) = \int_C dl \, \frac{(2l+1)}{\sin(\pi l)} \sum_{\eta=\pm 1} \frac{(\eta + e^{-i\pi l})}{2} a^{(\eta)}(l,t) P\left(l, 1 + \frac{2s}{t}\right) \tag{1.1.6}$$

where η takes the values ± 1 and is called the signature of the partial wave and $a^{(+)}(l,t)$ and $a^{(-)}(l,t)$ are the even and odd partial wave amplitudes. The function $(\eta + e^{-i\pi l})/2$ is called the signature factor.

1.1.1 Regge Poles

The next step is to deform the contour to the one C' as shown in figure (1.2), which runs parallel to the imaginary axis with $\mathcal{R}e\, l < 0$. We must be careful to encircle any poles that the functions $a^{(\eta)}(l,t)$ may have at $l = \alpha_{n_\eta}(t)$ and pick up the residue from those poles. In the case of simple poles only we have

$$\begin{aligned} A(s,t) &= \frac{1}{2i}\int_{1/2-i\infty}^{1/2+i\infty} dl \left[\frac{(2l+1)}{\sin(\pi l)} \sum_{\eta=\pm1} \frac{(\eta + e^{-i\pi l})}{2} a^{(\eta)}(l,t) P\left(l, 1+\frac{2s}{t}\right)\right] \\ &+ \sum_{\eta=\pm1}\sum_{n_\eta} \frac{\eta + e^{-i\pi\alpha_{n_\eta}}}{2} \frac{\tilde{\beta}_{n_\eta}(t)}{\sin(\pi\alpha_{n_\eta}(t))} P(\alpha_{n_\eta}(t), 1+2s/t). \end{aligned} \tag{1.1.7}$$

The simple poles $\alpha_{n_\eta}(t)$ are called the even-($\eta = +1$) and odd-($\eta = -1$) signature Regge poles and $\tilde{\beta}_{n_\eta}(t)$ is the residue of the pole multiplied by $\pi(2\alpha_{n_\eta} + 1)$. In the diffractive limit we have $s \gg |t|$ and we may replace the Legendre polynomial by its asymptotic form

$$\lim_{s\gg|t|} P\left(l, 1+\frac{2s}{t}\right) = \frac{\Gamma(2l+1)}{\Gamma^2(l+1)} \left(\frac{s}{t}\right)^l . \tag{1.1.8}$$

In this limit the contribution from the contour C' of figure (1.2) becomes negligible. We go further by only keeping the contribution from the Regge pole with the largest value of the real part of $\alpha_{n_\eta}(t)$. This is referred to as the leading Regge pole analysis and the amplitude in the Regge region is then written as

$$A(s,t) = \frac{(\eta + e^{-\pi\alpha_{n_\eta}(t)})}{2\sin(\alpha_{n_\eta}(t))} \frac{\gamma_a(t)\gamma_b(t)}{\Gamma(\alpha_{n_\eta}(t))} s^{\alpha_{n_\eta}(t)} \tag{1.1.9}$$

and we have extracted a factor of $1/\Gamma(\alpha_{n_\eta}(t))$ to cancel the so-called nonsense poles at $\alpha_{n_\eta}(t) = 0, -1, -2, \cdots$. Regge factorisation is characterised by the scattering amplitude factorising into three distinct terms: $\gamma_a(t)$, $\gamma_b(t)$ account for the coupling of hadronic states to the Reggeon, itself described by the remainder of (1.1.9). Regge factorisation implies that there is a universal process which is responsible for scattering in the high energy limit and which contains all the s dependence of the scatter.

1.1.2 Regge Trajectories

Chew and Frautschi plotted the spins of low lying mesons against squared mass and noticed that they lie on a straight line, i.e. $\alpha(t)$ is a linear function of t

$$\alpha(t) = \alpha(0) + \alpha^{'} t \tag{1.1.10}$$

at least for positive values of t. From (1.1.9) we deduce that the differential cross section in the asymptotic limit behaves as

$$\frac{d\sigma}{dt} \propto s^{2(\alpha(0)-\alpha^{'} t-1)} \tag{1.1.11}$$

and from the optical theorem we get the asymptotic dependence of the total cross section

$$\sigma_{tot} \propto s^{\alpha(0)-1}. \tag{1.1.12}$$

From the Regge trajectory for the isospin, $I = 1$ mesons we get the values of

$$\begin{aligned} \alpha(0) &= 0.55 \\ \alpha^{'} &= 0.86\mathrm{GeV}^{-2}. \end{aligned} \tag{1.1.13}$$

As $\alpha(0) < 1$ we conclude from (1.1.12) that the cross section for the transfer of an $I = 1$ state decreases as s increases and it becomes vanishingly small in the asymptotic limit.

1.1.3 The Pomeron

Experimentally it is observed that total cross sections rise as s is increased, i.e the Regge trajectory responsible for the high energy behaviour has an intercept, $\alpha(0)$, greater than one. Pomeranchuk noticed that if a trajectory carries quantum numbers then the total cross section must fall as s increases. Later this statement was rephrased in the positive sense. The total cross section which rises with s must be dominated by a trajectory with the same quantum numbers as the vacuum, i.e none at all. The "vacuum" trajectory is called the Pomeron after Pomeranchuk and is denoted $\alpha_P(t)$. Recall that in the high energy limit it is determined experimentally that the amplitude is imaginary. Using (1.1.9) we write the ρ parameter (the ratio of the real and imaginary part of the amplitude) as

$$\rho = \frac{\Re e\mathcal{A}}{\Im m\mathcal{A}} = \frac{(\eta + \cos(\pi\alpha_{n_\eta}(t)))}{\sin(\pi\alpha_{n_\eta})(t)}. \tag{1.1.14}$$

We can see from (1.1.14) that the Pomeron must have even signature and that its intercept must be ≈ 1. Donnachie and Landshoff (DL) [4] have made fits to both total and differential cross sections using the Regge pole model of the Pomeron. The total cross section fits for proton-proton and antiproton-proton are

$$\begin{aligned} \sigma_{PP} &= 21.7\, s^{0.08} + 56.1\, s^{-0.45}\ \text{mb} \\ \sigma_{P\overline{P}} &= 21.7\, s^{0.08} + 98.4\, s^{-0.45}\ \text{mb}. \end{aligned} \tag{1.1.15}$$

The first term is the contribution from the Pomeron pole with a fitted intercept of 1.08. This is identical for both PP and $P\overline{P}$ as the Pomeron carries the vacuum quantum numbers and hence cannot distinguish between particles and antiparticles. The second term is derived from including the exchange of the $I = 1$ meson trajectory with an intercept of 0.55, as given in (1.1.13). The Reggeon trajectory has a different coupling to particle and anti-particle states, displayed by the different parameterisations in (1.1.15). The fact that the fits (1.1.15) have an intercept slightly above one tells us that they will eventually violate the Froissart-Martin bound, which states from unitarity that in the extreme high energy limit the amplitude cannot grow any faster than $s\log^2(s)$. Using the optical theorem this translates into the upper bound for the total cross section

$$\sigma_{tot} = C\ \log^2(s). \tag{1.1.16}$$

Where C is a constant derived from the pion mass and has a value of approximately 60 mb. However, due to the DL Pomeron intercept being so close to one, we can neglect the restriction imposed by the Froissart-Martin bound as it is only violated at energies close to the Planck scale. Presumably some other physics will come into play in order to tame the DL cross section a long time before those energies are achieved. This is indeed the case when one considers the plausible mechanism of the exchange of multiple DL Pomerons.

One is able to obtain further information about the Pomeron from observing different variables apart from just the total cross section. It has been determined from the ISR experiment at CERN and the TEVATRON collider that the differential cross section, $d\sigma/dt$, data are consistent with the Pomeron having a linear trajectory with a gradient of

$$\alpha^{'} = 0.25\text{GeV}^{-2}. \tag{1.1.17}$$

This provides us with a possible candidate for the first bound state that lies on such a trajectory. From (1.1.17) we discover that when $\alpha_P = 2$ at $t = 3.7\,\text{GeV}^2$ there should be a resonance state with the quantum numbers of the vacuum and with a mass of 1.9 GeV. The WA91 collaboration at CERN have indeed discovered evidence for a glueball at this energy and this could well be the first evidence for a bound state to lie on the Pomeron trajectory.

The differential cross section at fixed s also gives a probe into the functions $\gamma_{(a,b)}$ which describe the coupling of hadrons to the Pomeron. It turns out that the Pomeron couples to hadrons in the same way as photons do, i.e. $\gamma_{(a,b)}$ are proportional to the electromagnetic form factor. A consequence of this is that the Pomeron couples to on-shell quarks as though it is a point particle. This is born out by the quark counting rule as the coupling strengths of the Pomeron to baryons and mesons are experimentally determined to be in the ratio $1.6 : 1$, slightly higher than one would naively expect from considering the $3 : 2$ ratio of the numbers of valence quarks in the baryon and meson states.

At high energies elastic scattering events are difficult to detect as both particles are scattered at too low an angle to make identification possible. However, if one of the particles receives sufficient energy in the collision to break up into its constituent partons, which subsequently hadronise and are detected, and the other remains intact, scattering through a small angle, we have the processes of diffractive dissociation. This class of events is often viewed as though the Pomeron has been emitted by the hadron which remains intact and then undergoes an inelastic scattering event with the other hadron, producing a final state hadronic system, X. This class of event is characterised by a large rapidity gap between the two final state systems. Rapidity, y_i, of particle i

is defined as

$$y_i = \frac{1}{2}\log\left(\frac{E_i + p_{zi}}{E_i - p_{zi}}\right) \tag{1.1.18}$$

where the z-axis is the direction of the incident beams. The intact particle remains travelling largely in the forward direction and thus has a large positive rapidity whilst the hadronic system is clustered around the backward direction and has a large negative rapidity. Events characterised by such a large rapidity gap have been observed by the UA8 collaboration at CERN, the D0 [5] and CDF [6] collaborations at Fermilab, and the H1 [7] and ZEUS [8] collaborations at DESY. The idea of emitting a Pomeron has lead people to define Pomeron structure functions in the same way as is done for hadrons [9]. Although the Pomeron is not a hadron, we can nevertheless think of diffraction dissociation events probing the quark and gluon content of the Pomeron. The data from HERA on the Pomeron structure function strongly indicate that it is a gluon dominated object.

The Pomeron has a further role to play in the description of deep inelastic events (DIS). When measurement is made of the DIS structure functions $F_1(x, Q^2)$ and $F_2(x, Q^2)$ one views the measurement as the total cross section of a virtual photon with squared momentum $-Q^2$ and a proton. The centre of mass energy for the photon-proton collision is given by

$$s = \frac{Q^2(1-x)}{x}, \tag{1.1.19}$$

and as we are in the Regge limit ($s \gg Q^2$) we are also working in the limit of low Bjorken x ($x \ll 1$). At very small x we expect that the total hadronic cross section should be governed by Pomeron exchange: using the DL parameterisation we expect that the structure function $F_2(x, Q^2)$ should behave as

$$F_2(x, Q^2) = A\, x^{-0.08} + B\, x^{0.45}, \tag{1.1.20}$$

which is very good fit for $10^{-2} < x < 10^{-1}$. However, at the HERA collider x values as low as 10^{-6} have been reached and the data indicate that there is a much steeper x dependence of about $x^{-0.3}$, which clearly deviates from the behaviour (1.1.20). Recently DL have discussed the possibility that there might be more than one Pomeron

[10]. They supposed the existence of a second, harder, simple Regge pole Pomeron that can describe the HERA low x data. It was also introduced because of the failure of the soft Pomeron to describe the high Q^2 diffractive dissociation and diffractive vector meson data. The DL fit to the proton structure function is now of the form

$$F_2(x, Q^2) = \sum_{i=0}^{2} f_i(Q^2) x^{-\epsilon_i} \tag{1.1.21}$$

where the new parametrisation for the hard Pomeron comes from the $i = 0$ term. (The soft Pomeron and the Reggeon are $i = 1, 2$ respectively). The new fits for large Q^2 data are

$$\begin{aligned} f_0(x) &= A_0 \left(\frac{Q^2}{Q^2 + a_0}\right)^{1+\epsilon_0} \left(1 + X \log\left(1 + \frac{Q^2}{Q_0^2}\right)\right) \\ f_1(x) &= A_1 \left(\frac{Q^2}{Q^2 + a_1}\right)^{1+\epsilon_1} \frac{1}{1 + \sqrt{Q^2/Q_1^2}} \\ f_2(x) &= A_2 \left(\frac{Q^2}{Q^2 + a_2}\right) \end{aligned} \tag{1.1.22}$$

where the intercept of the soft Pomeron is still fitted to be $1 + \epsilon_1 = 1.0808$ and the intercept for the new hard Pomeron is $\epsilon_0 = 1.418$. The crucial point is that because of the introduced, by necessity, Q^2 dependence of the soft Pomeron it now becomes a higher twist $\approx 1/Q$ term, which surprised DL and forced them to rethink earlier parametrisations. The new parameterisation (1.1.22) still needs to be tested with the high Q^2 dissociative and vector meson production data.

It has been shown that the Pomeron is a valuable concept in the discussion of high energy phenomena in the Regge limit. By using the ideas of Regge theory, DL have built up a powerful, and simple, picture that is very accurate in comparison with a wide variety of data. For the most part their ideas have also successfully weathered the scrutiny of new data as it became available. However, hadronic events are understood today as being governed by the underlying interactions of the quarks and gluons within the hadrons, that is to say that we now believe that QCD is the correct theory of the strong interaction and as such should offer a description of all classes of hadronic events including those in the Regge region.

1.2 Diffraction Within QCD

The strong nuclear interaction was brought into step with the quantum field theoretical ideas of electrodynamics with the invention of QCD in 1973 based on the non-Abelian gauge group $SU(3)$. Today it represents our most complete description of hadronic states and interactions. However, due to asymptotic freedom and the value of the fundamental QCD constant, $\Lambda_{QCD} \sim 100\,\mathrm{MeV}$, the applicability of perturbation theory is restricted to a small class of states and interactions where all scales are greater than the infra-red scale(Λ). There is a huge amount of QCD physics where the interaction kinematics force the problem to be treated non perturbatively. The description of the structure of hadrons and nuclei in terms of their constituent quarks and gluons, the low energy nucleon-nucleon interaction, and the structure of exotic states of matter, such as the quark-gluon plasma found in neutron stars or in the early universe, are all examples of physics that lie within the non-perturbative sector of QCD.

The picture of diffraction presented so far also must be viewed as an essentially non-perturbative process as the energy transfer, t, involved in diffractive processes is almost always substantially smaller than the QCD infra-red scale. Almost all diffractive events fall into this category and it is because of their essential non perturbative nature that the DL Pomeron is known as the soft Pomeron. However, with the advancement of accelerator technology, particularly the commissioning of the HERA ring at DESY and the TEVATRON ring at FNAL, it became feasible to study a new class of diffractive events, still in the Regge region, but with all scales being sufficiently hard to allow a description in the language of perturbative QCD. Thus it is currently believed that the theoretical description [11] of hard diffractive events lies within the successful knitting together of perturbative QCD and Pomeranchuk's theorem into a QCD composite object known as the perturbative Pomeron (pP).

1.2.1 Partons, Perturbative QCD and the Regge Limit

The discovery that electrons can recoil with large momenta from a proton target, which subsequently breaks up, suggests that there is structure to the proton with the charge and mass being concentrated in highly localised regions within the proton. This is analogous to Rutherford's discovery of substructure within the atom by the observation of the large recoil of α particles off the central nucleus. The angular and energy distributions of the scattered electrons indicates that the scattering centres, termed partons, exhibit a property called scaling which allows the identification of the partons as point like particles similar to the electron. We consider that the partons are free within the bounds of the proton and all scattering events take place with just single parton participation. This is justified when one looks at the interaction with the impulse approximation, where it is found that the partons may be considered as free for the duration of the scatter because the forces which constrain the partons inside the hadron work over much larger time and distance scales relative to the duration of the interaction.

The parton model introduces the concept of a parton distribution function (pdf), with the distributions of the various types of partons to be determined from data, e.g. on the proton structure functions. Parton distribution functions are universal, i.e. they do not depend on the particular experimental situation under discussion, only the type of hadron. The scaling, or point-like, property of partons is implicitly stated in the parton model as the pdfs are to first approximation only functions of the longitudinal momentum fraction (x) of the parent hadron which they carry. Stated differently: a point is always infinitely smaller than any finite sized probe.

It was not long before the quark degrees of freedom of the fledgling QCD were identified as the partons. However, we must also consider the gluon degrees of freedom when making predictions using QCD. In DIS scattering experiments we are looking deep into the structure of the proton and so the use of perturbative QCD becomes valid. Indeed, the results of calculations of DIS from tree level QCD are in agreement with the parton model. The first order corrections to the parton model are derived from gluon Bremsstrahlung and self energy diagrams and are found to give corrections of order $\alpha_s \log(Q^2/\mu^2)$ to the virtual photon-quark cross section (μ^2 is a cut off necessary to regulate infra-red divergences). The presence of the $\log(Q^2)$ indicates that the structure functions are now a function of the size ($\approx 1/\sqrt{(Q^2)}$) of the probe and the point like nature of the partons is lost and scaling is violated. Moreover, the presence of the logarithm counteracts the diminishing value of $\alpha_s(Q^2)$ as we turn up the virtuality of the photon. This means that as we proceed in the perturbation series the higher order terms, which contain higher powers of $\alpha_s \log(Q^2/\mu^2)$, do not become negligible at a finite order and we need to sum the series to infinity. As we tune the virtuality of the photon up we first see the constituent quarks that have been associated with the parton model and if the quarks were non-interacting then this would be the case no matter how hard we made our photon probe and the parton model would hold. But as the photon becomes harder and harder we begin to see the quark as a dressed object with a finite size. The density of partons becomes greater as we go to smaller and smaller x because quarks with high momentum fractions lose energy by radiating gluons. As a consequence of the largeness of the coupling, α_s, the quark and gluon distributions inside the proton are undetermined in pQCD at values of Q^2 that are less than the infra-red scale. However, we can use pQCD to determine the distributions at given Q^2 provided than we can extract an experimental distribution at some lower (higher) value Q_0^2. The equations which sum the perturbative series and tell us the quark and gluon distributions in the high Q^2 kinematic region are the Dokshitzer-Gribov-Lipatov-Altarelli-Parisi (DGLAP) [12] equations:

$$\frac{\partial q_i(x,Q^2)}{\partial \log Q^2} = \frac{\alpha_s}{2\pi}\int_x^1 \frac{dy}{y}\left[q_i(y,Q^2)P_{qq}\left(\frac{x}{y}\right) + g(y,Q^2)P_{qg}\left(\frac{x}{y}\right)\right] \tag{1.2.23}$$

for the quark distribution, and

$$\frac{\partial g(x,Q^2)}{\partial \log Q^2} = \frac{\alpha_s}{2\pi}\int_x^1 \frac{dy}{y}\left[\sum_i q_i(y,Q^2)P_{gq}\left(\frac{x}{y}\right) + g(y,Q^2)P_{gg}\left(\frac{x}{y}\right)\right] \tag{1.2.24}$$

for the gluon distribution. The sum runs over quark and antiquark types and the splitting functions P are independent of i if all quarks are considered to be massless.

As well as considering processes where Q^2 is the only large scale we can also use perturbation theory to make predictions about scattering events in the Regge limit. This has become more relevant in recent years due to leaps in accelerator technology. We can now access kinematic regions which can be considered to be firmly within the Regge region and where the scales are still hard enough to justify the use of perturbation theory.

As an example, quark-quark scattering in the Regge limit is considered at tree level. The relevant Feynman rules are

$$\frac{-i\delta_{ab}g^{\mu\nu}}{q^2}$$

for the gluon propagator (in Feynman gauge) and

$$-ig(\tau^a)_{ij}(\gamma^\mu)_{\alpha\beta}$$

for the qqg vertex. These two expressions are illustrated in diagrams (1.3) and (1.4). With information on the gluon propagator, the qqg vertex and the quark spinors we

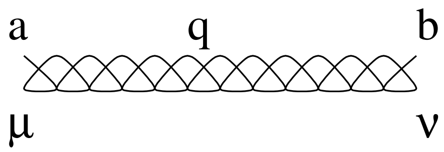

Figure 1.3: The gluon propagator in Feynman gauge.

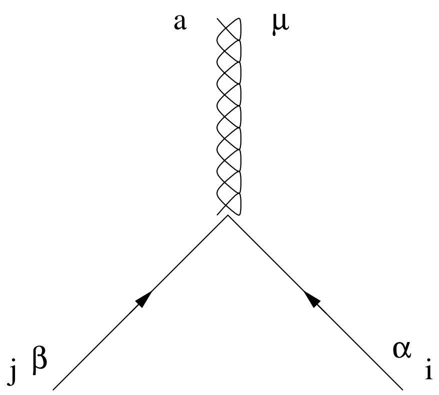

Figure 1.4: The quark-quark-gluon vertex.

may write the $qq \to qq$ amplitude at tree level:

$$A^{tree}_{qq\to qq} = -ig\overline{u}(\lambda_1^{'}, p_1)\gamma^\mu u(\lambda_1, p_1 - q)\tau^a_{ij} \ \frac{-i\delta_{ab}g_{\mu\nu}}{q^2} \ - ig\overline{u}(\lambda_2^{'}, p_2)\gamma^\nu u(\lambda_2, p_2 + q)\tau^b_{kl}. \tag{1.2.25}$$

As we are working in the Regge limit we may simplify the spinors associated with the upper and lower lines by disregarding the momenta transfer. This is the eikonal approximation, which is valid when the momentum transfer is small relative to other momenta in the problem. We now write (1.2.25) as

$$A^{tree}_{qq\to qq} = -ig\overline{u}(\lambda_1^{'}, p_1)\gamma^{\mu}u(\lambda_1, p_1)\tau^a_{ij} \; \frac{-i\delta_{ab}g_{\mu\nu}}{q^2} \; - ig\overline{u}(\lambda_2^{'}, p_2)\gamma^{\nu}u(\lambda_2, p_2)\tau^b_{kl} \quad (1.2.26)$$

which allows us to use the normalisation of the spinors

$$u(\lambda_i, p_i)u^{\dagger}(\lambda_i^{'}, p_i) = 2E_i\delta_{\lambda_i\lambda_i^{'}} \quad (1.2.27)$$

and replace (1.2.26) with

$$A^{tree}_{qq\to qq} = 4g^2\frac{(p_1.p_2)}{q^2}\delta_{\lambda_1^{'}\lambda_1}\delta_{\lambda_2^{'}\lambda_2}\tau^a_{ij}\tau^a_{kl}, \quad (1.2.28)$$

where $\tau^a_{ij}\tau^a_{kl}$ is the octet exchange colour factor. We make the replacements $s = 2p_1.p_2$, $t = q^2$ and $\alpha_s = g^2/(4\pi)$ and arrive at the simple form for the tree level $qq \to qq$ amplitude in the Regge limit

$$A^{tree}_{qq\to qq} = 8\pi\alpha_s\frac{s}{t}\tau^a_{ij}\tau^a_{kl}\delta_{\lambda_1\lambda_1^{'}}\delta_{\lambda_2\lambda_2^{'}}. \quad (1.2.29)$$

The $qq \to qq$ amplitude at one loop level is calculated from the diagrams where two gluons are exchanged. There are two diagrams that contribute; one where the two gluons cross (u channel) and one where they don't (t channel). The Cutkosky rules are applied to the calculation and the result for octet exchange is proportional to the tree level amplitude but multiplied by a factor

$$\epsilon_G(t)\log(\frac{s}{t})$$

where $\epsilon_G(t)$ is a factor introduced by the loop integration and includes the extra power of the coupling constant. One immediately sees that at the one loop level there is a single power of

$$\alpha_s\log(\frac{s}{t})$$

introduced. This number is approximately equal to unity and so we conclude that the one loop correction to $qq \to qq$ is of the same order of magnitude as the tree level amplitude. At subsequent orders we only keep those terms which generate the logarithms in s/t, the so called leading logarithm approximation (LLA), and disregard all others which are sub leading. Progressing to two loops the topology of the gluon configurations means that there are 25 diagrams that have to taken into consideration, simplified to five on either side of the cut by the Cutkosky rules. If we wish to progress to include the three and higher loop calculations then the number of different ways in which we can couple the gluons effectively means that the calculation becomes impossible. Lipatov et al. [13] solved this problem by introducing an effective three gluon vertex which accounts for all the different gluon configurations that contribute. Readers interested in the details of the construction of the Lipatov vertex are referred to a more detailed text on the subject [14], we only reproduce the result here:

$$\begin{aligned}\Gamma^{\sigma}_{\mu\nu}(k_1,k_2) &= \frac{2p_{1\nu}p_{2\mu}}{s}\left[\left(\rho_1+\frac{2\mathbf{k_1}^2}{\lambda_2 s}\right)p_1^{\sigma}+\left(\lambda_2+\frac{2\mathbf{k_2}^2}{\rho_1 s}\right)p_2^{\sigma}\right. \\ &\left. - (k_1+k_2)^{\sigma}_{\perp}\right], \qquad (1.2.30)\end{aligned}$$

where we have Sudakov [15] decomposed the gluon momenta

$$k_i^{\mu} = \rho_i p_1^{\mu} + \lambda_i p_2^{\mu} + k_{i\perp}^{\mu}$$

and all boldface momenta are two (transverse) dimensional. One amplitude for the two loop contribution is shown in figure (1.5). There is also a contribution from non-ladder

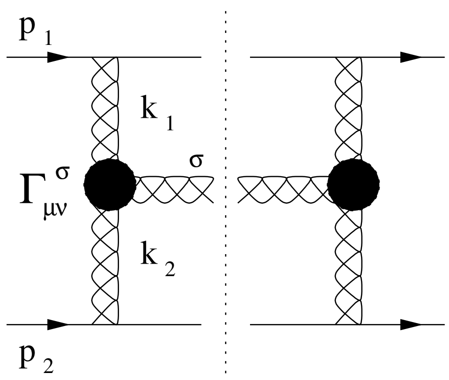

Figure 1.5: The two loop contribution to $qq \to qq$ illustrating the Lipatov vertex.

graphs where 3 gluons are exchanged in the t-channel. At three loop and beyond terms involving fermion loops and the four gluon vertex need to be considered. Such terms are subleading in the LLA and are therefore not included. Subsequent progression is achieved by increasing the number of s-channel gluons by one at each order building up a ladder structure and by carefully accounting for the virtual corrections (which ultimately do not spoil the ladder like structure). The LLA means that we impose the strong ordering of the Sudakov momenta down the ladder

$$\rho_{i-1} \gg \rho_i \gg \rho_{i+1},$$

$$|\lambda_{i-1}| \ll |\lambda_i| \ll |\lambda_{i+1}|,$$

which greatly simplifies the calculation.

Skipping all the details it can be shown that at each order we generate a power of $\epsilon_G(t)\log(s/t)$ and a numerical factor. For colour octet exchange the numerical factors are those of the exponential series, which allows us to write the full amplitude to infinite order as the tree level amplitude multiplied by an exponential factor:

$$A^{\infty}_{qq\to qq} = A^{tree}_{qq\to qq}\left(\frac{s}{t}\right)^{\epsilon_G(t)}. \tag{1.2.31}$$

This emulates Regge factorisation. The infinite perturbation series for colour octet exchange has lead to a Reggeised gluon.

1.2.2 The Perturbative Pomeron

One can use perturbation theory to build up a model of the Pomeron in exactly the same way as the Reggeised gluon is built up. Exceptions are that we start the series an order in perturbation theory higher than the Reggeised gluon and, because of the different colour factors for singlet exchange, the numerical factors at subsequent orders don't produce the coefficients of the exponential series. What is generated is an integral equation where the iteration of the kernel adds an extra rung to the gluon ladder.

To write the integral equation we first take a Mellin transform and write the colour singlet $qq \to qq$ scattering amplitude as

$$\int_1^{\infty} d\left(\frac{s}{\mathbf{k}^2}\right)\left(\frac{s}{\mathbf{k}^2}\right)^{-\omega-1}\frac{A^{(1)}(s,t)}{s} = 4i\alpha_s^2\delta_{\lambda_1'\lambda_1}\delta_{\lambda_2'\lambda_2}G_0^{(1)}\int\frac{d^2\mathbf{k_1}d^2\mathbf{k_2}}{\mathbf{k_1}^2(\mathbf{k_2}-\mathbf{q})^2}f(\omega,\mathbf{k_1},\mathbf{k_2},\mathbf{q}), \tag{1.2.32}$$

where $G_0^{(1)}$ is the colour factor for singlet exchange, ω is the Mellin conjugate variable to s and $f(\omega, \mathbf{k_1}, \mathbf{k_2}, \mathbf{q})$ is related to a 4-point gluon Green's function (see (1.2.48) for the precise definition). The kernel of the integral equation then acts on the function $f(\omega, \mathbf{k_1}, \mathbf{k_2}, \mathbf{q})$, with each iteration of the kernel adding a rung to the gluon ladder. The full integral equation is written explicitly as

$$\begin{aligned}
\omega f(\omega, \mathbf{k_1}, \mathbf{k_2}, \mathbf{q}) &= \delta^2(\mathbf{k_1} - \mathbf{k_2}) \\
&+ \frac{\alpha_s N_c}{2\pi^2} \int d^2\mathbf{k}' \Bigg[\frac{-\mathbf{q^2}}{(\mathbf{k}' - \mathbf{q})^2 \mathbf{k_1^2}} f(\omega, \mathbf{k}', \mathbf{k_2}, \mathbf{q}) \\
&+ \frac{1}{(\mathbf{k}' - \mathbf{k_1})^2} \left(f(\omega, \mathbf{k}', \mathbf{k_2}, \mathbf{q}) - \frac{\mathbf{k_1^2} f(\omega, \mathbf{k_1}, \mathbf{k_2}, \mathbf{q})}{[\mathbf{k}'^{\mathbf{2}} + (\mathbf{k}' - \mathbf{k_1})^2]} \right) \\
&+ \frac{1}{(\mathbf{k}' - \mathbf{k_1})^2} \left(\frac{(\mathbf{k_1} - \mathbf{q^2}) \mathbf{k}'^{\mathbf{2}} f(\omega, \mathbf{k}', \mathbf{k_2}, \mathbf{q})}{(\mathbf{k}' - \mathbf{q})^2 \mathbf{k_1}^{\mathbf{2}}} \right. \\
&- \left. \frac{(\mathbf{k_1} - \mathbf{q})^2 f(\omega, \mathbf{k_1}, \mathbf{k_2}, \mathbf{q})}{(\mathbf{k}' - \mathbf{q})^2 + (\mathbf{k_1} - \mathbf{k}')^2} \right) \Bigg]. \qquad (1.2.33)
\end{aligned}$$

This is the Balitski-Fadin-Kuraev-Lipatov (BFKL) equation [13], which sums up all the leading log diagrams for colour singlet exchange building up the picture of the Pomeron in QCD as a pair of Reggeised gluons exchanged in the t channel, which interact with each other by the exchange of normal gluons in the s channel.

For the case of zero momentum transfer the BFKL equation becomes solvable in the momentum space representation. It reduces to an inhomogenous Green's function equation that is solved by finding the eigenfunctions, and the corresponding eigenvalues, of the kernel. The eigenfunctions are

$$\phi_\nu^n(\mathbf{k}) = \frac{1}{\pi\sqrt{2}} (k^2)^{-1/2+i\nu} e^{in\theta}, \qquad (1.2.34)$$

with corresponding eigenvalues of

$$\chi_n(\nu) = 2(-\gamma_E - \Re e[\psi((n+1)/2 + i\nu)]), \qquad (1.2.35)$$

and the full result is [14, 16]

$$f(\omega, \mathbf{k_1}, \mathbf{k_2}, \mathbf{0}) = \sum_{n=-\infty}^{\infty} \int_{-\infty}^{\infty} d\nu \left(\frac{k_1}{k_2} \right)^{i\nu} \frac{e^{in(\theta_1 - \theta_2)}}{2\pi^2 k_1 k_2} \frac{1}{\omega - \overline{\alpha}_s \chi_n(\nu)}, \qquad (1.2.36)$$

where $\overline{\alpha}_s \equiv N_c \alpha / \pi$. Using the saddle point method we are able to find an analytic expression for the $qq \to qq$ amplitude via BFKL Pomeron exchange. From the optical theorem the total qq total cross section has an s dependence of

$$\sigma_{tot} \propto s^{\omega_0} \tag{1.2.37}$$

where ω_0 is determined by the dominant $(n = \nu = 0)$ eigenvalue and is explicitly given by

$$\omega_0 = \frac{N_c \alpha_s}{\pi} 4 \ln 2 = \chi_0(0). \tag{1.2.38}$$

This value (≈ 0.5 for $\alpha_s = 0.2$) is to be contrasted with the phenomenological fits of the DL Pomeron ($= 0.08$). The high value of the BFKL intercept is of concern as the BFKL Pomeron violates the Froissart-Martin bound much more strongly than the DL Pomeron. One process that tames the growth of the total cross section involves the exchange of multiple BFKL Pomerons [17, 18].

There are several other points of concern with the $t = 0$ solution to the BFKL equation, mainly the validity of the use of perturbation theory. When the $t = 0$ BFKL equation is solved in the asymptotic region the solution is also the solution of the diffusion equation. What is produced is a cigar shaped distribution in the $y - \mathbf{k}^2$ plane, due to Bartels and Lotter [19], of gluon momenta along the ladder as shown in figure 1.6. The ends of the ladder are fixed by the virtualities of the external particles and of major concern is the possibility that the diffusion of the gluon momenta along the ladder may take us into the non-perturbative region. This process of diffusion

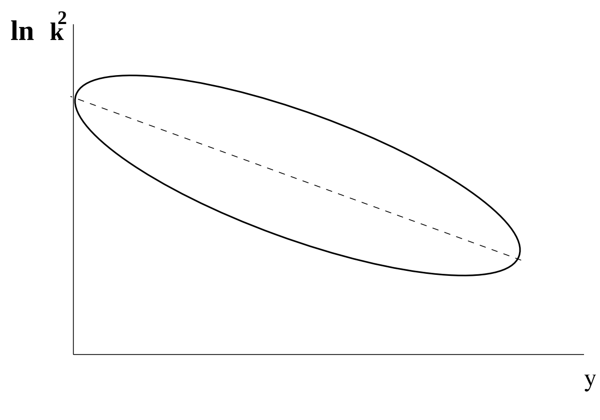

Figure 1.6: Bartels' Cigar.

means that we are wrong in our assumption of a fixed value of α_s in the derivation of the BFKL equation. A more sensible value would be to take $\alpha_s(\mathbf{k}'^2)$ where $\mathbf{k}'$ is the transverse momenta of a typical gluon within the ladder, but allowing the coupling constant to run in this manner is strictly going beyond the validity of the LLA and forms part of the next to leading log (NLO) [20] corrections to the BFKL equation.

1.2.3 The Solution to the BFKL Equation for Finite t

The solution of the BFKL equation for non zero momentum transfer avoids the infra-red problems associated with diffusion by fixing a minimum scale which acts as a cut off and inhibits diffusion into the infra-red region [21]. The solution becomes more complicated and is unknown in the momentum space representation of the BFKL equation. In order the solve the BFKL equation we are forced to take a Fourier transform to impact parameter space, ie perform the following transformation:

$$\tilde{f}(\omega,\mathbf{b_1},\mathbf{b_1'},\mathbf{b_2},\mathbf{b_2'}) = \int d^2\mathbf{k_1} d^2\mathbf{k_2} d^2\mathbf{q} \left[e^{i(\mathbf{k_1}.\mathbf{b_1}+(\mathbf{q}-\mathbf{k_1}).\mathbf{b_1'}-\mathbf{k_2}.\mathbf{b_2}-(\mathbf{q}-\mathbf{k_2}).\mathbf{b_2'})} \frac{f(\omega,\mathbf{k_1},\mathbf{k_2},\mathbf{q})}{\mathbf{k_2}^2(\mathbf{k_1}-\mathbf{q})^2} \right]. \tag{1.2.39}$$

The BFKL equation in impact parameter space now becomes solvable as it is invariant under the conformal (Möbius) transformations represented by the mapping

$$b \to \frac{a+cb}{d+eb} \tag{1.2.40}$$

where a, c, d, e are complex numbers ($ae - cd \neq 0$) and we have written the transverse vectors as complex coordinates

$$b = b_x + ib_y, \quad b^* = b_x - ib_y. \tag{1.2.41}$$

The conformal invariance allows the identification of a solution of the $t \neq 0$ BFKL equation in terms of eigenfunctions that are representations of the two dimensional conformal group. The eigenvalues are identical to the $t = 0$ solution and the full solution to the BFKL equation becomes [14, 16]

$$\tilde{f}(\omega,\mathbf{b_1},\mathbf{b_1'},\mathbf{b_2},\mathbf{b_2'}) = \sum_{n=-\infty}^{\infty} \int_{-\infty}^{\infty} d\nu d^2\mathbf{b_0}$$
$$\frac{16\nu^2+4n^2}{(4\nu^2+1-n^2)^2+16n^2\nu^2} \frac{\overline{E}_{\nu,n}(\mathbf{b_1},\mathbf{b_1}',\mathbf{b_0})\overline{E}^*_{\nu,n}(\mathbf{b_2},\mathbf{b_2}',\mathbf{b_0})}{\omega-\overline{\alpha}_s\chi_n(\nu)}. \tag{1.2.42}$$

where

$$\overline{E}_{\nu,0}(\mathbf{b},\mathbf{b}^{'},\mathbf{b_0}) = \left(\frac{(\mathbf{b}-\mathbf{b}^{'})^2}{(\mathbf{b}-\mathbf{b_0})^2(\mathbf{b}'-\mathbf{b_0})^2}\right)^{1/2+i\nu} \tag{1.2.43}$$

for a general transverse vector $\mathbf{b_0}$.

1.2.4 Impact Factors

We must now concern ourselves with the coupling of the Pomeron to external hadronic states. This has already been done for the case of quark-quark scattering in the build up of BFKL equation. Taking (1.2.32) as our base we can represent the scattering amplitude for the scattering of two general hadronic states as

$$A^{(1)}(s,t) = \frac{isG}{(2\pi)^4}\int d^2\mathbf{k_1}d^2\mathbf{k_2}\frac{\Phi_1(\mathbf{k_1},\mathbf{q})\Phi_2(\mathbf{k_2},\mathbf{q})}{\mathbf{k_2}(\mathbf{k_1}-\mathbf{q})^2}f(s,\mathbf{k_1},\mathbf{k_2},\mathbf{q}) \tag{1.2.44}$$

where the functions $\Phi_i(\mathbf{k_i},\mathbf{q})$ are the impact factors which describe the coupling to the external states and G is the process dependent colour factor. (1.2.44) is the QCD Pomeron factorisation formula. Unlike the gluon, where Regge factorisation takes place, the factorised form of the QCD Pomeron amplitude remains as a convolution and is referred to as high energy factorisation. This is illustrated diagramatically in figure (1.7). We may simply read the quark impact factor from (1.2.32):

$$\Phi_q = 8\pi^2\alpha_s\delta_{\lambda\lambda'}. \tag{1.2.45}$$

The most general form for an impact factor is shown in figure (1.7). The only stipulation about its actual construction is that it must involve the emission of the two gluons that form the head (tail) of the BFKL ladder. When constructing impact factors we must take account all of the different Feynman diagrams which account for the transition from the “in” state to the “out” state with the emission of the two gluons.

In order to determine the relationship between Feynman amplitudes and the impact factor we write

$$A(s,t) = iG\int d(PS)_1 B_1^{\mu\nu}G_{\mu\nu\alpha\beta}B_2^{\alpha\beta}d(PS)_2 \tag{1.2.46}$$

where $G_{\mu\nu\alpha\beta}$ is a four point gluon Green function and the phase space associated with the impact factor is

$$d(PS)_i = \prod_j \frac{d^4l_j}{(2\pi)^3}\delta(l_j^2). \tag{1.2.47}$$

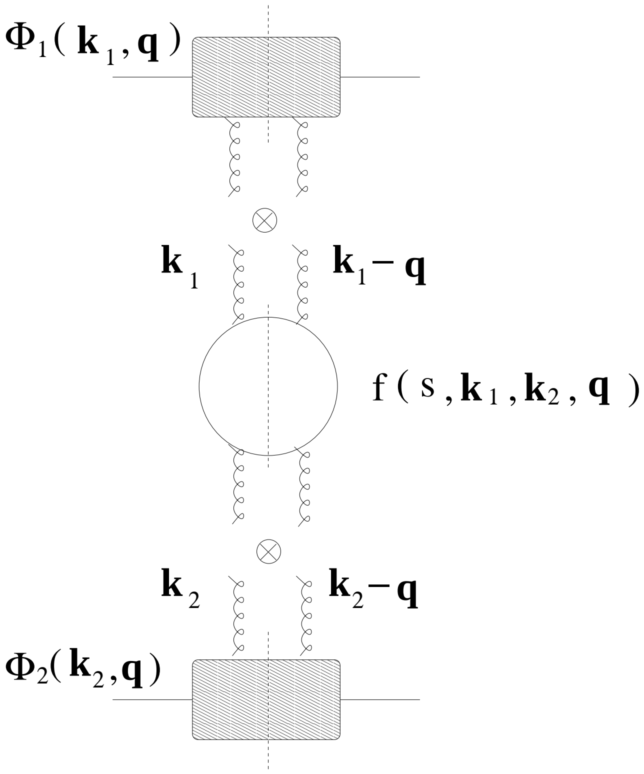

Figure 1.7: High energy factorisation.

The product runs over all the cut lines in the impact factor i. $B_i^{\mu\nu}$ are the amplitudes obtained from Feynman rules with all the cut lines placed on shell. $f(s, \mathbf{k_1}, \mathbf{k_2}, \mathbf{q})$ defined earlier is such that

$$\frac{f(s, \mathbf{k_1}, \mathbf{k_2}, \mathbf{q})}{\mathbf{k_2}^2(\mathbf{k_1} - \mathbf{q})^2} \equiv \frac{s}{(2\pi)^4} \int d\rho_1 d\lambda_2 \frac{4p_1^\mu p_1^\nu p_2^\alpha p_2^\beta}{s^2} \, G_{\mu\nu\alpha\beta}(s, \mathbf{k_1}, \mathbf{k_2}, \mathbf{q}) \tag{1.2.48}$$

which leaves

$$\int d\lambda_1 B_1^{\mu\nu} \quad = \quad \frac{2p_1^\mu p_1^\nu}{(2\pi)^4} \Phi_1(\mathbf{k_1}, \mathbf{q}) \tag{1.2.49}$$

and

$$\int d(PS)_1 B_1^{\mu\nu} = A_1^{\mu\nu}. \tag{1.2.50}$$

Thus we have defined the relationship between the Feynman amplitude and the impact factor, with a similar expression for $B_2^{\alpha\beta}$ under the replacement $d\rho_1 \to d\lambda_2$. Placing (1.2.49) into (1.2.48) we arrive at (1.2.44) and (1.2.49) is the rule for extracting the impact factor.

As an example of how to construct impact factors from cut Feynman diagrams we explicitly show how the quark impact factor (1.2.45) may be constructed. The relevant cut amplitude is illustrated in figure (1.8) We use the eikonal approximation

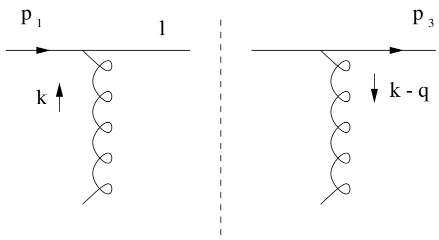

Figure 1.8: The amplitude used to construct the quark impact factor.

for the qqg vertex to give

$$\begin{aligned} A^{\mu\nu} &= -\int \frac{d^4k_1}{(2\pi)^3}\delta[(p_1+k_1)^2]2g^2 2p_1^\mu p_1^\nu \delta_{\lambda\lambda'}\delta'_{\lambda\lambda'} \\ &= 2\pi g^2 \frac{2p_1^\mu p_1^\nu}{(2\pi)^4}\delta_{\lambda\lambda'}\int d^2\mathbf{k_1} d\rho_1. \end{aligned} \tag{1.2.51}$$

which, using (1.2.49), gives the desired form for the quark impact factor ($4\pi\alpha_s = g^2$).

1.2.5 Issues Surrounding the BFKL Pomeron

In the previous section we have shown how the concept of the Pomeron has been transcribed into the modern language of pQCD, how the model was built up from the Reggeised gluon and how external hadronic states are coupled to the universal four point gluon Green's function.

Recently the BFKL equation has been solved in the next to leading log (NLO) regime [20], where all terms of order $\alpha_s^2 \log(s/s_0)$ are included in the iterations of the kernel. The resummation of all the NLO terms took many years to perform. The kernel separates into two pieces; one which remains conformally invariant and one which breaks the conformal invariance and accounts for the running of the coupling. At first there was great concern about the stability of the perturbative expansion [22] which threatened to swamp the LO result, putting the whole theoretical programme in jeopardy. These concerns were in part due to the presence of spurious and unphysical logarithms which were introduced at NNLO and beyond. This concern was later arrested by considering physically realistic situations [23] which reduced the higher order corrections and re-validated the whole programme. However, from the point of view of phenomenology there is little that can be done at present with the higher order corrections to BFKL as work has mostly concentrated on the corrections to the kernel itself. The impact factors for the NLO Pomeron have yet to be calculated and the solution for the NLO kernel for finite t has yet to be understood.

1.2.6 High $|t|$ Diffraction

It has been shown [21] that at high enough values of $|t|$ the gluon momenta along the BFKL ladder do not diffuse into the non perturbative region. Viewed differently, the BFKL mechanism at high $|t|$ acts over sufficiently short distances regardless of the size of the external particles. Furthermore, the soft Pomeron contribution is suppressed due to shrinkage. Consequently these two effects make high $|t|$ diffraction an excellent testing ground for the BFKL dynamics. With virtually all diffractive data coming from the $|t| \approx 0$ region it is important to carefully pick processes where there is as large a contribution from the large $|t|$ region, or ones where the large $|t|$ contribution may be easily extracted [24]. One such process is gaps between jets [25, 26], where one looks for events where a pair of jets are separated by a large rapidity gap. Such events are observed at both HERA [27] and the TEVATRON [28]. Unfortunately, the restriction to observe a pair of high p_t jets within the detectors places severe restrictions on the experimental reach in rapidity. It has been suggested that at HERA [29] double diffractive dissociation (DDD) events offer a less demanding method for isolating the BFKL pomeron. But, a reliable calculation of the expected rate for DDD is made difficult because there is the possibility of additional strong interactions between the diffracting systems which could result in the loss of gaps. Processes which avoid the 'gap survival' problem are diffractive semi-exclusive vector meson production in photon-hadron collisions: $\gamma p \to VX$ [30, 31, 32, 33, 34] and exclusive vector meson production in photon-photon collisions: $\gamma\gamma \to VV$ [30, 36]. The meson(s) is(are) produced with a high p_t relative to the incoming photon(s), and the largeness of this momentum transfer typically leads to the dissociation of the hadron ($\gamma p \rightarrow VX$). A principal challenge in computing the rate for meson production lies in determining how the meson is produced. The meson wave function is intrinsically a non perturbative object in origin.

Data [27, 28, 34] from the gaps between jets process, DDD at HERA and vector meson production all exhibit behaviour which is consistent with the BFKL prediction and support a value of $\alpha_s \approx 0.2$ [35].

Therefore, in order to make a clean appraisal of the application of the BFKL Pomeron at high $|t|$, one is forced to look for physically measurable quantities where the calculation of the cross section requires a minimum of input from non-perturbative physics. As indicated above, non perturbative form factors, wavefunctions, hadronisation effects and final state interactions are all sources of uncertainty when testing a perturbative theory. Processes entirely calculable in perturbation theory which avoid these complications and the associated uncertainties are the semi-exclusive and exclusive diffractive production of photons at high $|t|$.

At HERA one can look for $\gamma p \rightarrow \gamma X$ where the photon is produced with a high p_t and the proton dissociates into the hadronic system X and at LEP or a future linear collider (LC) one may look for the related process $\gamma\gamma \rightarrow \gamma X$. The signals of these processes are identical, modulo leptons, and very clear. At HERA a low angle photon is observed close to the backward direction separated by a large rapidity gap from the hadronic system produced in the dissociation of the proton, which need not be detected. At an e^+e^- machine the same final state is observed (plus the extra final state lepton). Also the study of the exclusive reaction $\gamma\gamma \rightarrow \gamma\gamma$ in the Regge limit is also feasible at an ee machine. This class of process has long been proposed as a test of perturbative QCD close to the Regge limit. Studies conducted prior to the HERA age [30, 31] have concentrated on the lowest non trivial order of perturbation theory, i.e. two gluon exchange, to determine general features of the perturbative expansion in the Regge region. The authors of this early work recognised that in such semi-hard processes the largeness of the expansion parameter, $\alpha_s \log(s/\mathbf{k}^2) \approx 1$, demands that the perturbative series be summed to all orders. Recently, and in parallel with the

the course of the work presented in this thesis, this summation has been performed for the process $\gamma q(g) \to \gamma q(g)$, the common hard scatter in the proton and photon dissociation processes, in the case of photoproduction [37] (the other $Q^2 = 0$ photon diffracts into final state photon for $\gamma\gamma \to \gamma X$ scattering) where it shown that the LO BFKL scatter is much larger than the two gluon exchange term. In [37] the largeness of the LO BFKL result was compared to a VDM inspired model for low $|t|$ diffraction and found to give a much larger contribution to the cross section making it difficult to match the results from the perturbative to the non perturbative regions. It was indicated in [37] that this imbalance is most probably the result of the dynamics of the BFKL equation and that the NLO corrections are likely to tame the cross section and a better match would be achieved. What is clear is that we should be examining data that have already been collected to determine to what extent there is evidence for the BFKL Pomeron.

Closely related studies may be made at LEP2 or a future LC , both high $|t|$ double diffractive photon production and, at $|t| = 0$ for photons with sufficient virtuality, the total $\gamma\gamma$ cross section [36, 38, 39, 40, 41] may be investigated in the Regge region.

We can see from (1.2.44) that the calculation of any of the above processes stems from knowledge of the $\gamma^*\gamma$ impact factor, the parton line impact factor, as given by (1.2.45), and the relevant colour factor, which we previously factorised out from the impact factors into the amplitude (1.2.44).

In the remainder of this thesis we calculate the rates for the processes $e^+e^- \to e^+e^-\gamma\gamma$ and $e^+e^- \to e^+e^-\gamma X$ at LEP and a future LC and $\gamma^* P \to \gamma X$ at HERA. This work involves the calculation of the $\gamma^*\gamma$ impact factor, its convolution with the BFKL eigenfunctions, and the rates for the hard subprocesses and has been published [42].

Chapter 2

$\gamma^* q \to \gamma q$ and $\gamma^*\gamma^* \to \gamma\gamma$

2.1 The $\gamma^*\gamma$ Impact Factor

The relevant Feynman diagrams for the computation of the γ^*-γ impact factor are shown in figure 2.1. Dispersive techniques are used to calculate the imaginary part of the amplitude, all that is required in the LLA. The study of the photon impact factor is not new and for QED processes dates back to [43, 44]. In this thesis we extend previous studies to include a non-zero momentum transfer and the possibility of virtual incoming photons.

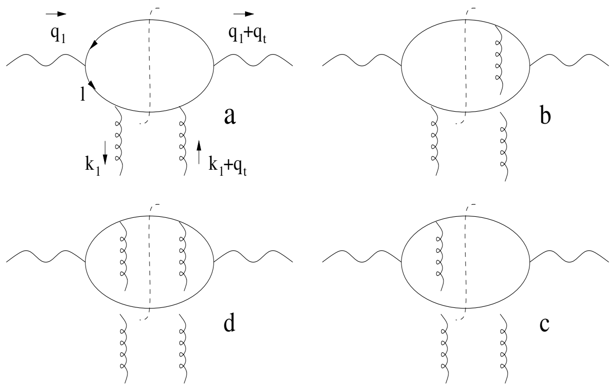

Figure 2.1: The four diagrams that contribute to the photon impact factor.

We detail the calculation of the contribution to the impact factor arising from the amplitude of figure 2.1(a). The same techniques apply to all diagrams.

$$(A^{jk}_{(a)})^{\mu\nu} = -(4\pi)^2 \alpha_s \alpha \sum_q e_q^2 \int d(PS) \, \frac{\mathrm{Tr}(\not{l}\gamma^\mu(\not{l}-\not{k}_1)\gamma^\nu(\not{l}+\not{q}) \not{\epsilon}^k_{(f)}(\not{l}-\not{q}_1) \not{\epsilon}^j_{(i)})}{l^2(l+q)^2}. \tag{2.1.1}$$

The photon polarisation states are labelled by j and k and $d(PS)$ refers to the two body phase space of the cut quark lines shown in figure 2.1. We define two light like and mutually orthogonal vectors, p_1 and p_2:

$$\begin{aligned} p_1 &= (\sqrt{s}/2, 0, 0, \sqrt{s}/2) \\ p_2 &= (\sqrt{s}/2, 0, 0, -\sqrt{s}/2). \end{aligned} \tag{2.1.2}$$

All momenta are then Sudakov decomposed [15] into components proportional to p_1, and p_2 and a third perpendicular vector:

$$\begin{aligned} q_1^\mu &= p_1^\mu - \frac{Q^2}{s} p_2^\mu \\ l^\mu &= \rho p_1^\mu + \lambda p_2^\mu + l_\perp^\mu \\ k_1^\mu &= \rho_1 p_1^\mu + \lambda_1 p_2^\mu + k_{1\perp}^\mu \\ q^\mu &= \rho_t p_1^\mu + \lambda_t p_2^\mu + q_\perp^\mu, \end{aligned} \tag{2.1.3}$$

q_1 is the incoming photon momentum ($Q^2 = -q_1^2$), l the quark momentum, $k_1 + q$ and $-k_1$ are the momenta of the gluon legs. The momentum transfer is $q^2 = t < 0$.

The LLA part of the impact factor is projected out by only keeping those terms in the numerator of (2.1.1) that are proportional to $p_1^\mu p_1^\nu$, which is equivalent to using the eikonal approximation for the internal spinors. The amplitude now becomes

$$(A^{jk}_{(a)})^{\mu\nu} = -(4\pi)^2 \frac{4}{s^2} \alpha_s \alpha \sum_q e_q^2 \int d(PS) \frac{\mathrm{Tr}(\not{l}\,\not{p}_2(\not{l}-\not{k}_1)\,\not{p}_2(\not{l}+\not{q})\,\not{\epsilon}^k_{(f)}(\not{l}-\not{q}_1)\,\not{\epsilon}^j_{(i)})}{l^2(l+q)^2} \, p_1^\mu p_1^\nu. \tag{2.1.4}$$

The two body phase space integration over the cut lines may be reformulated to one over two loop momenta. Under the Sudakov decomposition

$$\begin{aligned} \int d(PS) &= \int \frac{d^4 l}{(2\pi)^3} \frac{d^4 k_1}{(2\pi)^3} \, \delta((l-k_1)^2)\, \delta((q_1-l)^2) \\ &= \left(\frac{s}{2}\right)^2 \int d\rho \, d\lambda \, d\rho_1 \, d\lambda_1 \int \frac{d^2\mathbf{l}}{(2\pi)^3} \frac{d^2\mathbf{k}_1}{(2\pi)^3} \, \frac{-1}{\rho(1-\rho)s^2} \, \delta\left(\lambda - \lambda_1 - \frac{(\mathbf{l}-\mathbf{k}_1)^2}{s\rho}\right) \\ &\times \; \delta\left(\lambda + \frac{Q^2}{s} + \frac{\mathbf{l}^2}{s(1-\rho)}\right). \end{aligned} \tag{2.1.5}$$

The strong ordering of the longitudinal momenta in the BFKL ladder allows us to disregard terms proportional to ρ_1 and ρ_t which are suppressed with respect to terms proportional to ρ by a power of $\mathbf{k}^2/s$. We have also transfered from the Minkowski metric to the Euclidean one:

$$-(k_{1\perp}^\mu)^2 = \mathbf{k}_1^2. \tag{2.1.6}$$

The δ functions are used to absorb the λ and λ_1 integrals and lead to a redefinition of the momenta

$$\begin{aligned}
q_1^\mu &= p_1^\mu - Q^2\frac{p_2^\mu}{s} \\
l^\mu &= \rho p_1^\mu - \left(\frac{\mathbf{l}^2}{(1-\rho)} + Q^2\right)\frac{p_2^\mu}{s} + l_\perp^\mu \\
k_1^\mu &= -\left(\frac{(\mathbf{k}_1 - \mathbf{l})^2}{\rho} + Q^2 + \frac{\mathbf{l}^2}{(1-\rho)}\right)\frac{p_2^\mu}{s} + k_{1\perp}^\mu \\
q^\mu &= (Q^2 + \mathbf{q}^2)\frac{p_2^\mu}{s} + q_\perp^\mu.
\end{aligned} \tag{2.1.7}$$

Our notation follows that of [14] and we can readily extract the corresponding impact factor by removing the

$$\frac{2p_1^\mu p_1^\nu}{(2\pi)^4}\int d\rho_1 d^2\mathbf{k}_1$$

from (2.1.4) and reabsorbing it to form part of the definition of the universal 4 point gluon Green function as shown in (1.2.49):

$$\Phi_{(a)}^{jk}(\mathbf{k}_1, \mathbf{q}) = -\frac{2\alpha\alpha_s}{s^2}\sum_q e_q^2 \int d^2\mathbf{l}\int_0^1 d\rho \frac{T_{(a)}^{jk}}{\rho(1-\rho)}, \tag{2.1.8}$$

where $T_{(a)}^{jk}$ is given by

$$T_{(a)}^{jk} = \frac{\mathrm{Tr}(\not{l}\ \not{p}_2(\not{l} - \not{k}_1)\ \not{p}_2(\not{l} + \not{q})\ \not{\epsilon}_{(f)}^k(\not{l} - \not{q}_1)\ \not{\epsilon}_{(i)}^j)}{l^2(l+q)^2}. \tag{2.1.9}$$

It is not necessary to calculate the contributions to the impact factor from all four diagrams explicitly since they are related to each other, as a consequence of gauge invariance, by the momentum transformations shown in figure 2.2. Thus, the full impact factor is given by

$$\Phi_{\gamma\gamma}^{jk}(\mathbf{k}_1, \mathbf{q}) = -\alpha\alpha_s\left(\frac{2}{s}\right)^2\sum_q e_q^2\int d^2\mathbf{l}\int_0^1 d\rho\frac{1}{\rho(1-\rho)}\left[T_{(c)}^{jk} - T_{(c)}^{jk}|_{\mathbf{k}_1=0}\right] \tag{2.1.10}$$

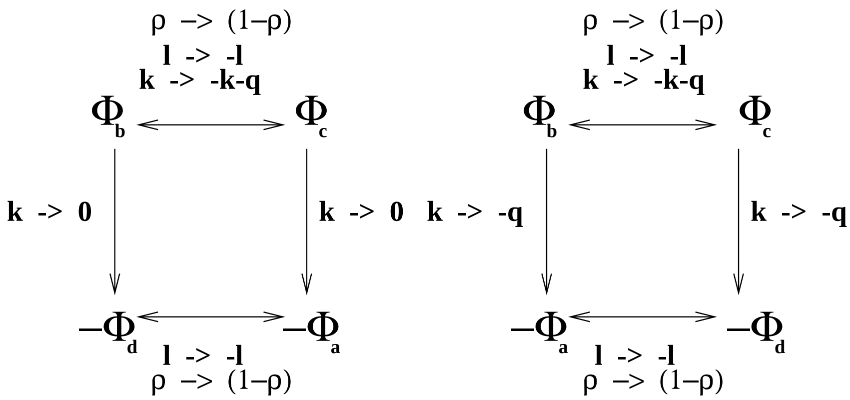

Figure 2.2: The relationship between the four diagrams of figure 2.1.

where

$$T^{jk}_{(c)} = \frac{\mathrm{Tr}(\not{l}\ \not{p}_2(\not{l}+\not{k}_1+\not{q})\ \not{\epsilon}^k_{(f)}(\not{l}-\not{q}_1+\not{k}_1)\ \not{p}_2(\not{l}-\not{q}_1)\ \not{\epsilon}^j_{(i)})}{(l-q_1)^2(l+k_1+q)^2}. \tag{2.1.11}$$

As all of the information necessary for the construction of the full impact factor is contained within the contributions from either diagrams (b) or (c) and we simplify the discussion by concentrating only on diagram (c) from now on.

2.1.1 Photon Polarisation

The transverse polarisation vectors of the incoming photon lie in the transverse plane by definition. However, as the final state photon gets a kick its polarisation vector has components in the non-transverse directions. In the Lorentz gauge, the most general polarisation vectors for the incoming and outgoing photons are

$$\begin{aligned} \epsilon^{k\,\mu}_{(f)} &= \epsilon^{k\,\mu}_{\perp} - \frac{2\,q_\perp\cdot\epsilon^k_\perp}{s}\,p_2^\mu, \\ \epsilon^{j\,\mu}_{(i)} &= \epsilon^{j\,\mu}_{\perp}. \end{aligned} \tag{2.1.12}$$

The details of the explicit calculation of these polarisation vectors is given in appendix A. The polarisation vectors are placed into the amplitude (2.1.4) and the trace is taken with the FORM [45] program. The full FORM code is listed in the ultimate section of this chapter. The result for the impact factor is

$$\Phi^{jk}_{(x)}(\mathbf{k}_1,\mathbf{q}) \;=\; \pm\, 4\alpha_s\alpha\sum_q e_q^2\int_0^1 d\rho\int d^2\mathbf{l}\,\frac{1}{(\mathbf{l}^2+\overline{Q}^2)}$$

$$\frac{\boldsymbol{\Delta}_{(x)} \cdot \boldsymbol{\epsilon}^{*k}\, \mathbf{l} \cdot \boldsymbol{\epsilon}^{j} (1-2\rho)^2 - \boldsymbol{\epsilon}^{*k} \cdot \boldsymbol{\epsilon}^{j}\, \mathbf{l} \cdot (\mathbf{l} - \boldsymbol{\Delta}_{(x)}) + 4\mathbf{l} \cdot \boldsymbol{\epsilon}^{*k}\, \mathbf{l} \cdot \boldsymbol{\epsilon}^{j} \rho(1-\rho) - \mathbf{l} \cdot \boldsymbol{\epsilon}^{*k}\, \boldsymbol{\Delta}_{(x)} \cdot \boldsymbol{\epsilon}^{j}}{(\boldsymbol{\Delta}_{(x)} - \mathbf{l})^2}, \tag{2.1.13}$$

where $x = a, b, c, d$ labels the diagram in figure 2.1. We are focusing on diagram (c), in which case

$$\boldsymbol{\Delta}_{(c)} = \mathbf{k}_1 + \rho \mathbf{q}.$$

The contributions to the impact factor arising from diagrams a, b and d may be obtained by making the momentum tranformations outlined in figure 2.2. In the limit of photoproduction, $Q^2 \to 0$, the expression (2.1.13) reduces to the impact factor calculated by Ginzburg et al. [30] in their earlier two gluon exchange work. The following substitutions relate the notation that we have used here to that which they used:

$$\begin{aligned}
\mathbf{k} &= -\mathbf{k_1} \\
\mathbf{n} &= \frac{\mathbf{q}}{|\mathbf{q}|} \\
\mathbf{r} &= \frac{-(2\mathbf{k_1} + \mathbf{q})}{|\mathbf{q}|} \\
\mathbf{v} &= \frac{\mathbf{q}^2 \mathbf{k_1} - (\mathbf{k_1}.\mathbf{q})\mathbf{q}}{|\mathbf{q}|\sqrt{\mathbf{k_1}^2 \mathbf{q}^2 - (\mathbf{k_1}.\mathbf{q})^2}} \\
\xi &= 2\rho - 1 \\
T &= \frac{2}{\mathbf{q}^2}\sqrt{\mathbf{k_1}^2 \mathbf{q}^2 - (\mathbf{k_1}.\mathbf{q})^2} \\
\mathbf{P} &= \frac{-2(\mathbf{k_1} + \rho\mathbf{q})}{|\mathbf{q}|}.
\end{aligned} \tag{2.1.14}$$

All boldface vectors are Euclidean and lie in the transverse plane, e.g. $\boldsymbol{\epsilon}^{j\,2} = -\epsilon_\perp^{j\;2}$. We have also introduced $\overline{Q}^2 \equiv Q^2 \rho(1-\rho)$.

The longitudinal polarisation vector of the incoming photon is given by

$$\epsilon^{0\mu} = \frac{1}{\sqrt{Q^2}} p_1^\mu + \frac{\sqrt{Q^2}}{s} p_2^\mu. \tag{2.1.15}$$

After substituting this expression into the amplitude and taking the trace:

$$\Phi^{0i}_{(x)}(\mathbf{k}_1, \mathbf{q}) = \frac{\pm 4\alpha_s \alpha}{Q} \sum_q e_q^2 \int_0^1 d\rho\ (2\rho - 1) \int d^2\mathbf{l} \frac{(\mathbf{l}^2 - \overline{Q}^2)}{(\mathbf{l}^2 + \overline{Q}^2)} \frac{(\boldsymbol{\Delta}_{(x)} - \mathbf{l}) \cdot \boldsymbol{\epsilon}_i}{(\boldsymbol{\Delta}_{(x)} - \mathbf{l})^2} \tag{2.1.16}$$

which vanishes since it is antisymmetric under the transformation $\rho \to (1-\rho)$. Thus in the LLA longitudinally polarised photons do not scatter into real photons.

2.1.2 Impact Factor in Position Space

The four gluon amplitude, $f(s, \mathbf{k}_1, \mathbf{k}_2, \mathbf{q})$ of (1.2.44), can be written [16]:

$$f(s, \mathbf{k}_1, \mathbf{k}_2, \mathbf{q}) = \frac{1}{(2\pi)^6} \int d^2\boldsymbol{\rho}_1\, d^2\boldsymbol{\rho}_2\, d^2\boldsymbol{\rho}_3\, d^2\boldsymbol{\rho}_4\; e^{-i(\mathbf{k}_1\cdot\boldsymbol{\rho}_1 - (\mathbf{k}_1+\mathbf{q})\cdot\boldsymbol{\rho}_2 - \mathbf{k}_2\cdot\boldsymbol{\rho}_3 + (\mathbf{k}_2+\mathbf{q})\cdot\boldsymbol{\rho}_4)}$$
$$\int_{-\infty}^{\infty} d\nu\, \frac{\nu^2}{(\nu^2+1/4)^2} e^{z\chi(\nu)} E^{\nu}(\boldsymbol{\rho}_1, \boldsymbol{\rho}_2) E^{*\nu}(\boldsymbol{\rho}_3, \boldsymbol{\rho}_4). \tag{2.1.17}$$

We have neglected the contributions with conformal spin $n > 0$ since they give rise to sub-leading contributions at high energies. The eigenfunctions of the kernel are given explicitly by

$$E^{\nu}(\boldsymbol{\rho}_1, \boldsymbol{\rho}_2) \;=\; \left| \frac{\boldsymbol{\rho}_1 - \boldsymbol{\rho}_2}{\boldsymbol{\rho}_1 \boldsymbol{\rho}_2} \right|^{1+2i\nu}, \tag{2.1.18}$$

and the eigenvalue is

$$\chi(\nu) = 2\Psi(1) - \Psi(1/2 + i\nu) - \Psi(1/2 - i\nu), \tag{2.1.19}$$

($\Psi(x)$ is the digamma function) and

$$z = \frac{N_c \alpha_s}{\pi} \ln\left(\frac{s}{s_0}\right). \tag{2.1.20}$$

The choice of scale s_0 and μ^2, the scale at which one evaluates α_s, are arbitrary in the LLA. The number of colours, $N_c = 3$. The scattering amplitude (1.2.44) can now be written [16]

$$A(s,t) = \frac{is\, G}{(2\pi)^{10}} \int_{-\infty}^{\infty} d\nu \frac{\nu^2}{(\nu^2+1/4)^2} e^{z\chi(\nu)}\; I_1^{\nu}(t)\; I_2^{*\nu}(t) \tag{2.1.21}$$

and we have introduced the functions

$$I_i^{\nu}(t) = \int d^2\mathbf{k}_1\; \Phi_i(\mathbf{k}_1, \mathbf{q}) \int d^2\boldsymbol{\rho}_1 d^2\boldsymbol{\rho}_2\; E^{\nu}(\boldsymbol{\rho}_1, \boldsymbol{\rho}_2)\; e^{-i\mathbf{k}_1\cdot(\boldsymbol{\rho}_1 - \boldsymbol{\rho}_2) + i\mathbf{q}\cdot\boldsymbol{\rho}_2}. \tag{2.1.22}$$

For photon production we need to calculate (2.1.22) using $\Phi^{jk}_{\gamma\gamma}$. We work in the helicity basis:

$$\boldsymbol{\epsilon}^{\pm} = -\frac{1}{\sqrt{2}}(1, \pm i). \tag{2.1.23}$$

There are four amplitudes to consider: $(j,k) = (+,+), (+,-), (-,+), (-,-)$ and we are concentrating on the $(-,-)$ amplitude

$$\Phi^{(-,-)}_{(x)}(\mathbf{k}_1, \mathbf{q}) = 4\alpha\alpha_s \sum_q e_q^2 \int_0^1 d\rho\, (\rho^2 + (1-\rho)^2) \int d^2\mathbf{l}\; \frac{1}{(\mathbf{l}^2 + \overline{Q}^2)} \frac{\Delta^*_{(x)} l - \mathbf{l}^2}{(\boldsymbol{\Delta}_{(x)} - \mathbf{l})^2}. \tag{2.1.24}$$

From now on, non boldface momenta are understood to be complex numbers, e.g. $l = l_x + il_y$. To compute $I^{\nu}_{(-,-)}$ we first take the Fourier transform of the impact factor:

$$\Phi^{(-,-)}_{(x)}(\boldsymbol{\rho}_1, \boldsymbol{\rho}_2) = \mathrm{e}^{i\mathbf{q}\cdot\boldsymbol{\rho}_2} \int d^2\mathbf{k}_1 \, \Phi^{(-,-)}_{(x)}(\mathbf{k}_1, \mathbf{q}) \, \mathrm{e}^{-i\mathbf{k_1}\cdot(\boldsymbol{\rho_1}-\boldsymbol{\rho_2})}. \tag{2.1.25}$$

Summing over all four diagrams and inserting two delta functions of momentum variables $\mathbf{k}_2, \mathbf{l}'$ gives

$$\begin{aligned}\Phi_{(-,-)}(\boldsymbol{\rho}_1, \boldsymbol{\rho}_2) \;&=\; 4\alpha\alpha_s \sum_q e_q^2 \int_0^1 d\rho \, (\rho^2 + (1-\rho)^2) \int \mathrm{d}^2\mathbf{k}_1 \, \mathrm{d}^2\mathbf{k}_2 \, \mathrm{e}^{-i\mathbf{k}_1\cdot\boldsymbol{\rho}_1} \, \mathrm{e}^{i\mathbf{k}_2\cdot\boldsymbol{\rho}_2} \\ &\delta^2(\mathbf{k}_2 - \mathbf{k}_1 - \mathbf{q}) \int \mathrm{d}^2\mathbf{l} \, \mathrm{d}^2\mathbf{l}' \, \frac{l'^* \, l}{(\mathbf{l}^2 + \overline{Q}^2)\mathbf{l}'^2} \Big[\delta^2(\mathbf{l}' + \mathbf{l} - \mathbf{k}_1 - \rho\mathbf{q}) \\ &-\delta^2(\mathbf{l}' - \mathbf{l} - \mathbf{k}_1 - (1-\rho)\mathbf{q}) - \delta^2(\mathbf{l}' + \mathbf{l} - \rho\mathbf{q}) + \delta^2(\mathbf{l}' - \mathbf{l} - (1-\rho)\mathbf{q})\Big] . \end{aligned} \tag{2.1.26}$$

Equivalently, we absorb the delta functions by introducing Fourier transforms over the two position variables $\mathbf{r}_1, \mathbf{r}_2$, and drop for the time being the pre-factors and the integral over the momentum fraction ρ,

$$\begin{aligned}&\int \frac{d^2\mathbf{r}_1 \, d^2\mathbf{r}_2}{(2\pi)^4} \int \mathrm{d}^2\mathbf{k}_1 \, \mathrm{d}^2\mathbf{k}_2 \, \mathrm{e}^{-i\mathbf{k_1}\cdot\boldsymbol{\rho_1}} \, \mathrm{e}^{i\mathbf{k_2}\cdot\boldsymbol{\rho_2}} \, \mathrm{e}^{i\mathbf{r}_1\cdot(\mathbf{k_2}-\mathbf{k_1}-\mathbf{q})} \int d^2\mathbf{l} \, d^2\mathbf{l}' \, \frac{l'^* \, l}{(\mathbf{l}^2 + \overline{Q}^2) \, \mathbf{l}'^2} \\ &\quad\Big[\mathrm{e}^{-i\mathbf{r}_2\cdot(\mathbf{l}'+\mathbf{l}-\mathbf{k}_1-\rho\mathbf{q})} - \mathrm{e}^{i\mathbf{r}_2\cdot(\mathbf{l}'-\mathbf{l}-\mathbf{k}_1-(1-\rho)\mathbf{q})} - \mathrm{e}^{i\mathbf{r}_2\cdot(\mathbf{l}'+\mathbf{l}-\rho\mathbf{q})} + \mathrm{e}^{i\mathbf{r}_2\cdot(\mathbf{l}'-\mathbf{l}-(1-\rho)\mathbf{q})}\Big]. \end{aligned} \tag{2.1.27}$$

After some algebra, this becomes

$$\begin{aligned}&\epsilon_a^- \epsilon_b^+ \int \frac{d^2\mathbf{r}_1 \, d^2\mathbf{r}_2}{(2\pi)^4} \, \mathrm{e}^{-i\mathbf{r}_1\cdot\mathbf{q}} \int \mathrm{d}^2\mathbf{k}_1 \, \mathrm{d}^2\mathbf{k}_2 \left[\mathrm{e}^{i\mathbf{k_1}\cdot(\mathbf{r_1}+\mathbf{r_2}+\boldsymbol{\rho_1})} - \mathrm{e}^{-i\mathbf{k_1}\cdot(\mathbf{r_1}+\boldsymbol{\rho_1})}\right] \mathrm{e}^{i\mathbf{k_2}\cdot(\mathbf{r_1}+\boldsymbol{\rho_2})} \\ &\left[\mathrm{e}^{-i\mathbf{r}_2\cdot\rho\mathbf{q}} \left(\frac{\nabla^a_{\mathbf{r}_2}}{i} \int d^2\mathbf{l} \, \frac{\mathrm{e}^{i\mathbf{r}_2\cdot\mathbf{l}}}{\mathbf{l}^2 + \overline{Q}^2}\right) - \mathrm{e}^{-i\mathbf{r}_2\cdot(1-\rho)\mathbf{q}} \left(\frac{\nabla^a_{\mathbf{r}_2}}{-i} \int d^2\mathbf{l} \, \frac{\mathrm{e}^{-i\mathbf{r}_2\cdot\mathbf{l}}}{\mathbf{l}^2 + \overline{Q}^2}\right)\right] \frac{\nabla^b_{\mathbf{r}_2}}{i} \int d^2\mathbf{l}' \, \frac{\mathrm{e}^{-i\mathbf{r}_2\cdot\mathbf{l}'}}{\mathbf{l}'^2} \end{aligned} \tag{2.1.28}$$

where a and b are vector indices in the transverse space. Performing the angular parts of the $\mathbf{l}$ and $\mathbf{l}'$ integrals and the $\mathbf{k}_1$ and $\mathbf{k}_2$ integrals yields

$$\begin{aligned}&-\epsilon_a^- \epsilon_b^+ \, (2\pi)^2 \int d^2\mathbf{r}_1 \, d^2\mathbf{r}_2 \left[\mathrm{e}^{-i\mathbf{r}_2\cdot\rho\mathbf{q}} + \mathrm{e}^{-i\mathbf{r}_2\cdot(1-\rho)\mathbf{q}}\right] \mathrm{e}^{-i\mathbf{r}_1\cdot\mathbf{q}} \left(\nabla^a_{\mathbf{r}_2} \int d|\mathbf{l}| \, \frac{|\mathbf{l}| J_0(|\mathbf{r}_2||\mathbf{l}|)}{\mathbf{l}^2 + \overline{Q}^2}\right) \\ &\left(\nabla^b_{\mathbf{r}_2} \int d|\mathbf{l}'| \, \frac{J_0(|\mathbf{r}_2||\mathbf{l}'|)}{|\mathbf{l}'|}\right) \left[\delta^2(\mathbf{r}_1 + \mathbf{r}_2 + \boldsymbol{\rho}_1) - \delta^2(\mathbf{r}_1 + \boldsymbol{\rho}_1)\right] \delta^2(\mathbf{r}_1 + \boldsymbol{\rho}_2). \end{aligned} \tag{2.1.29}$$

Using

$$\nabla_{\mathbf{r}_2} J_0(|\mathbf{r}_2||\mathbf{l}|) = -|\mathbf{l}| \; J_1(|\mathbf{r}_2||\mathbf{l}|) \; \hat{\mathbf{r}}_2, \tag{2.1.30}$$

$$\boldsymbol{\epsilon}^{+} \cdot \hat{\mathbf{r}}_2 \; \boldsymbol{\epsilon}^{-} \cdot \hat{\mathbf{r}}_2 = 1, \tag{2.1.31}$$

completing the radial $\mathbf{l}$ integral and rearranging leads to the result:

$$\begin{aligned}\Phi_{(-,-)}(\boldsymbol{\rho}_1,\boldsymbol{\rho}_2) \;&=\; 16\pi^2\alpha\alpha_s \sum_q e_q^2 \int_0^1 d\rho\; [\rho^2+(1-\rho)^2] \int d^2\mathbf{r}_1 d^2\mathbf{r}_2 \;\frac{1}{|\mathbf{r}|}\; \mathrm{e}^{i\rho\mathbf{q}\cdot\mathbf{r}_1} \\ &\mathrm{e}^{i(1-\rho)\mathbf{q}\cdot\mathbf{r}_2}\;\; \overline{Q}K_1(|\mathbf{r}|\overline{Q})\; [\delta^2(\mathbf{r}_1-\boldsymbol{\rho}_1)-\delta^2(\mathbf{r}_2-\boldsymbol{\rho}_1)]\; [\delta^2(\mathbf{r}_1-\boldsymbol{\rho}_2)-\delta^2(\mathbf{r}_2-\boldsymbol{\rho}_2)],\end{aligned} \tag{2.1.32}$$

where $\mathbf{r}=\mathbf{r}_1-\mathbf{r}_2$. The impact factors for the other polarisation states are

$$\begin{aligned}\Phi_{(+,+)}(\boldsymbol{\rho}_1,\boldsymbol{\rho}_2) \;&=\; \Phi_{(-,-)}(\boldsymbol{\rho}_1,\boldsymbol{\rho}_2) \\ \Phi_{(+,-)}(\boldsymbol{\rho}_1,\boldsymbol{\rho}_2) \;&=\; 32\pi^2\alpha\alpha_s \sum_q e_q^2 \int_0^1 d\rho \int d^2\mathbf{r}_1 d^2\mathbf{r}_2\; \rho(1-\rho)\; \frac{r^2}{|\mathbf{r}|^3}\; \mathrm{e}^{i\rho\mathbf{q}\cdot\mathbf{r}_1}\; \mathrm{e}^{i(1-\rho)\mathbf{q}\cdot\mathbf{r}_2} \\ &\quad K_1(|\mathbf{r}|\overline{Q})\;\overline{Q}\; [\delta^2(\mathbf{r}_1-\boldsymbol{\rho}_1)-\delta^2(\mathbf{r}_2-\boldsymbol{\rho}_1)]\; [\delta^2(\mathbf{r}_1-\boldsymbol{\rho}_2)-\delta^2(\mathbf{r}_2-\boldsymbol{\rho}_2)] \\ \Phi_{(-,+)}(\boldsymbol{\rho}_1,\boldsymbol{\rho}_2) \;&=\; 32\pi^2\alpha\alpha_s \sum_q e_q^2 \int_0^1 d\rho \int d^2\mathbf{r}_1 d^2\mathbf{r}_2\; \rho(1-\rho)\; \frac{r^{*2}}{|\mathbf{r}|^3}\; \mathrm{e}^{i\rho\mathbf{q}\cdot\mathbf{r}_1}\; \mathrm{e}^{i(1-\rho)\mathbf{q}\cdot\mathbf{r}_2} \\ &\quad K_1(|\mathbf{r}|\overline{Q})\;\overline{Q}\; [\delta^2(\mathbf{r}_1-\boldsymbol{\rho}_1)-\delta^2(\mathbf{r}_2-\boldsymbol{\rho}_1)]\; [\delta^2(\mathbf{r}_1-\boldsymbol{\rho}_2)-\delta^2(\mathbf{r}_2-\boldsymbol{\rho}_2)].\end{aligned} \tag{2.1.33}$$

2.2 Projection on Conformal Eigenstates

We must now project the position space impact factors onto the conformal eigenfunctions of the BFKL kernel, i.e. we must perform the following convolution:

$$I^{\nu}_{(h^*_\gamma,h_\gamma)}(Q^2,q^2) = \int d^2\boldsymbol{\rho}_1 d^2\boldsymbol{\rho}_2\; \Phi_{(h^*_\gamma,h_\gamma)}(\boldsymbol{\rho}_1,\boldsymbol{\rho}_2)\; E^{\nu}(\boldsymbol{\rho}_1,\boldsymbol{\rho}_2). \tag{2.2.34}$$

This part of the calculation follows very closely that of [37]. For completeness, we reproduce the steps here, extending the calculation to finite Q^2. In two of the terms of (2.1.33) the δ-functions force $\boldsymbol{\rho}_1=\boldsymbol{\rho}_2$ which results in a vanishing contribution due to the vanishing of E^{ν}. Hence,

$$\begin{aligned}I^{\nu}_{(+,+)}(Q^2,q^2) &= -32\pi^2\alpha_s\alpha \sum_q e_q^2 \int_0^1 d\rho\; [\rho^2+(1-\rho)^2]\;\overline{Q} \\ &\int d^2\mathbf{r}_1 d^2\mathbf{r}_2\; \frac{1}{|\mathbf{r}|}\; K_1(|\mathbf{r}|\overline{Q})\; e^{i\rho\mathbf{q}\cdot\mathbf{r}_1}\; e^{i(1-\rho)\mathbf{q}\cdot\mathbf{r}_2}\; \left|\frac{\mathbf{r}}{\mathbf{r}_1\mathbf{r}_2}\right|^{1+2i\nu}\end{aligned} \tag{2.2.35}$$

i.e.

$$I^{\nu}_{(+,+)}(Q^2,q^2) = -32\pi^2\alpha_s\alpha \sum_q e_q^2 \int_0^1 d\rho\ [\rho^2+(1-\rho)^2]\ \overline{Q}$$
$$\int d^2\mathbf{r}\ d^2\mathbf{r}_2\ \mathrm{e}^{i\rho\mathbf{q}\cdot\mathbf{r}}\ \mathrm{e}^{i\mathbf{q}\cdot\mathbf{r}_2}|\mathbf{r}|^{2i\nu}\ K_1(|\mathbf{r}|\overline{Q})\ |(\mathbf{r}+\mathbf{r}_2)\ \mathbf{r}_2|^{-1-2i\nu}\ . \tag{2.2.36}$$

We next shift $\mathbf{r}_2$ by $-\rho\mathbf{r}$ to eliminate the $\mathbf{r}$ dependent phase factor:

$$I^{\nu}_{(+,+)}(Q^2,q^2) = -32\pi^2\alpha_s\alpha \sum_q e_q^2 \int_0^1 d\rho\ [\rho^2+(1-\rho)^2]\ \overline{Q}\ \int d^2\mathbf{r}\ d^2\mathbf{r}_2\ \mathrm{e}^{i\mathbf{q}\cdot\mathbf{r}_2}$$
$$K_1(|\mathbf{r}|\overline{Q})\ |\mathbf{r}|^{2i\nu}\ |[\mathbf{r}_2+(1-\rho)\mathbf{r}]\ [\mathbf{r}_2-\rho\mathbf{r}]|^{-1-2i\nu}. \tag{2.2.37}$$

We now switch to the complex notation, i.e from $\mathbf{r}=(r_1,r_2)$ to $a=r_1+i\ r_2$ and $b=r_1-i\ r_2$, and use the freedom to choose q to be real:

$$I^{\nu}_{(+,+)}(Q^2,q^2) = -8\pi^2\alpha_s\alpha \sum_q e_q^2 \int_0^1 d\rho\ [\rho^2+(1-\rho)^2]\ \overline{Q}\ \int da\ db\ da_2\ db_2\ \mathrm{e}^{iq/2(a_2+b_2)}$$
$$(ab)^{i\nu}K_1(\sqrt{ab\ \overline{Q}^2})\ \{[a_2+(1-\rho)a]\ [b_2+(1-\rho)b]\ [a_2-\rho a][b_2-\rho b]\}^{-1/2-i\nu}. \tag{2.2.38}$$

To proceed we factorise the integration in a,b and a_2,b_2 by writing the Bessel function as a Mellin transform:

$$K_1(x) = \frac{1}{8\pi}\int_{-\infty}^{\infty} d\lambda\ \left(\frac{x}{2}\right)^{-\gamma-i\lambda}\Gamma(\frac{i\lambda+\gamma-1}{2})\ \Gamma(\frac{i\lambda+\gamma+1}{2}) \qquad [\Re e\ \gamma>1], \tag{2.2.39}$$

and re-scaling a & b by a_2 & b_2 respectively:

$$I^{\nu}_{(+,+)}(Q^2,q^2) = -2\pi\alpha_s\alpha\ \sum_q e_q^2 \int_0^1 d\rho\ [\rho^2+(1-\rho)^2]\ \int_{-\infty}^{\infty} d\lambda\ (\overline{Q}^2)^{\frac{-\gamma-i\lambda+1}{2}}$$
$$2^{\gamma+i\lambda-1}\Gamma\left(\frac{i\lambda+\gamma-1}{2}\right)\ \Gamma\left(\frac{i\lambda+\gamma+1}{2}\right)\ \int da_2\ db_2\ \mathrm{e}^{iq/2(a_2+b_2)}\ (a_2b_2)^{\frac{-\gamma-i\lambda}{2}-i\nu}$$
$$\int da\ db\ (ab)^{\frac{-\gamma-i\lambda}{2}+i\nu}\ \{[1+(1-\rho)a]\ [1+(1-\rho)b]\ [1-\rho a][1-\rho b]\}^{-1/2-i\nu}. \tag{2.2.40}$$

Re-scaling a_2 and b_2 by $2i/q$ gives

$$I^{\nu}_{(+,+)}(Q^2,q^2) = 2\pi\alpha_s\alpha\ \sum_q e_q^2 \left(\frac{2}{q}\right)^{1-2i\nu} \int_0^1 d\rho\ [\rho^2+(1-\rho)^2]\ \int_{-\infty}^{\infty} d\lambda\ \left(\frac{\overline{Q}^2}{q^2}\right)^{\frac{-\gamma-i\lambda+1}{2}}$$
$$\Gamma\left(\frac{i\lambda+\gamma-1}{2}\right)\ \Gamma\left(\frac{i\lambda+\gamma+1}{2}\right)\ \int da_2\ db_2\ \mathrm{e}^{-(a_2+b_2)}\ (-a_2b_2)^{\frac{-\gamma-i\lambda}{2}-i\nu}$$
$$\int da\ db\ (ab)^{\frac{-\gamma-i\lambda}{2}+i\nu}\ \{[1+(1-\rho)a]\ [1+(1-\rho)b]\ [1-\rho a][1-\rho b]\}^{-1/2-i\nu}. \tag{2.2.41}$$

Attention must now be drawn to the analytic structure of the integrand and the corresponding paths of integration. For the a_2, b_2 integrals we proceed by keeping b_2 quasi-fixed, which we are allowed to do, and consider the analytic structure of the a_2 plane. When b_2 is kept positive the minus sign gives a cut on the positive real axis, and the cut appears on the negative real axis when b_2 is negative, this is illustrated in figure 2.3. The negative sign in the exponential means that we close the contour

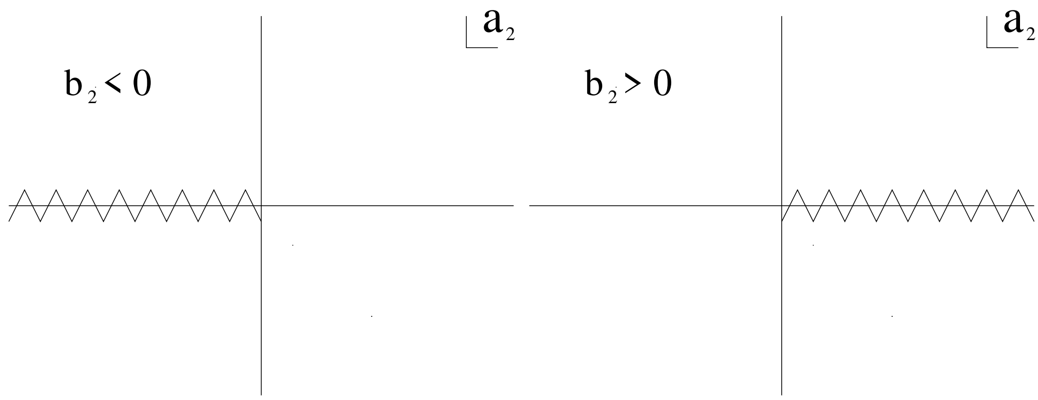

Figure 2.3: The analytic structure of the a_2 plane for $b_2 > 0$ and $b_2 < 0$.

to the right. The integral is non zero if a singularity is encountered, i.e. b_2 must be positive. Closing the contour around the cut means taking the discontinuity across the real axis and integrating a_2 over the real axis. This most easily computed if we switch to polar coordinates for a_2

$$a_2 = re^{i\theta} \quad , \quad -\pi < \theta \leq \pi. \tag{2.2.42}$$

The integral is found by considering the path just above and below the real axis, i.e. $\theta = \pm\delta$ and taking the limit of $\delta \to 0$ to get the discontinuity. If we define our integrand as a function of angle, $I(\delta)$,

$$\begin{aligned} \int da_2 db_2 I(0) &= \lim_{\delta\to 0}\int_0^\infty db_2 dr[I(\delta) - I(-\delta)] \\ &= \lim_{\delta\to 0}\int_0^\infty db_2 dr I^{'}(0)[e^{i(\delta-\pi)z} - e^{i(-\delta+\pi)z}] \\ &= -2i\sin(z\pi)\int_0^\infty db_2 dr I^{'}(0) \end{aligned} \tag{2.2.43}$$

where $(-1)^z I'(0) = I(0)$ and $z = \frac{-\gamma - i\lambda}{2} - i\nu$. Thus the a_2, b_2 integrals are completed as follows:

$$\begin{aligned}
&\int da_2\ db_2\ \mathrm{e}^{-(a_2+b_2)} (-a_2\ b_2)^{\frac{-\gamma-i\lambda}{2}-i\nu} \\
&= 2i\ \sin[(\frac{\gamma+i\lambda}{2}+i\nu)\pi] \int_0^\infty da_2\ a_2^{\frac{-\gamma-i\lambda}{2}-i\nu}\ \mathrm{e}^{-a_2} \int_0^\infty db_2\ b_2^{\frac{-\gamma-i\lambda}{2}-i\nu}\ \mathrm{e}^{-b_2} \\
&= 2i\ \sin[(\frac{\gamma+i\lambda}{2}+i\nu)\pi]\ \Gamma^2\left(\frac{-\gamma-i\lambda}{2}-i\nu+1\right)
\end{aligned} \tag{2.2.44}$$

The a, b integrations are performed in a similar way; b is fixed and we consider the integration over a. There are three cuts in the a plane; one running along the real axis starting at the origin and ending at $-\infty$ when $b > 0$ or $+\infty$ when $b < 0$. The other cuts are on either side of the origin when $-1/(1-\rho) < b < 1/\rho$, going from $-1/(1-\rho)$ to $-\infty$ and $1/\rho$ to $+\infty$ respectively. Figure 2.4 shows the analytic structure of the a plane for all values of b. As we have no exponential, or any other factor which is

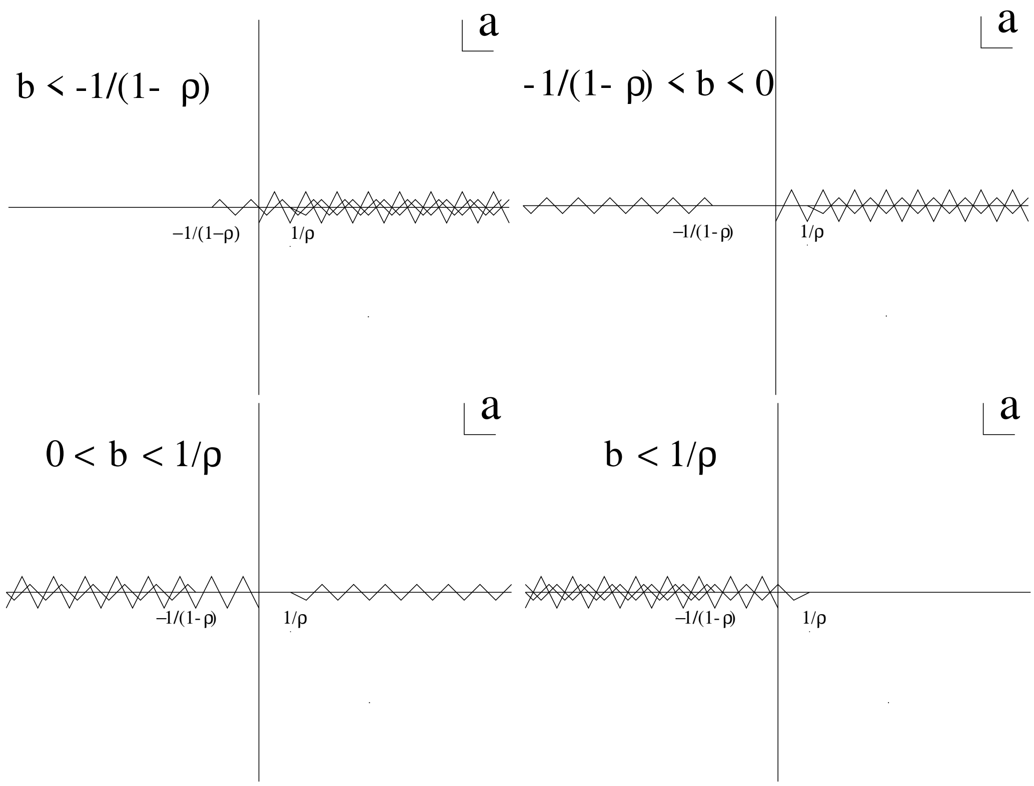

Figure 2.4: The analytic structure of the a plane for all values of b.

singular at infinity, we are free to close the contour on either side of the a plane and hence the integral will only be non-vanishing when the cut appear on opposite sides of the a plane. We have two cases to consider; $-1/(1-\rho) < b < 0$ when we have two cuts on the positive real axis, and $0 < b < 1/\rho$ where we have two cuts on the negative real axis. For each case we close the contour on the side which has the single cut. The discontinuity is found using the same method as for the previous integration and is the same for both cases. Thus the a, b integrals are completed as follows:

$$\begin{aligned}
&\int da\ db\ (ab)^{\frac{-\gamma-i\lambda}{2}+i\nu}\{[1+(1-\rho)a][1+(1-\rho)b][1-\rho a][1-\rho b]\}^{-1/2-i\nu} \\
&= 2i\sin[(-1/2-i\nu)\pi]\left\{\int_{-1/(1-\rho)}^{0} db\ \int_{-\infty}^{-1/(1-\rho)} da + \int_0^{1/\rho} db\ \int_{1/\rho}^{\infty} da\right\} \\
&\quad (ab)^{\frac{-\gamma-i\lambda}{2}+i\nu}\{-[1+(1-\rho)a][1+(1-\rho)b][1-\rho a][1-\rho b]\}^{-1/2-i\nu} \\
&= 2i\ \sin(x_2\pi)\ [\rho(1-\rho)]^{x_2}(1-\rho)^{-2(1+x_1+x_2)}\int_0^1 db\ b^{x_1}\left\{(1-b)\left(1+\frac{\rho}{1-\rho}b\right)\right\}^{x_2} \\
&\quad \int_1^{\infty} da\ a^{x_1}\left\{(a-1)\left(a+\frac{1-\rho}{\rho}\right)\right\}^{x_2} + [\rho \to (1-\rho)]
\end{aligned} \tag{2.2.45}$$

and we have defined

$$\begin{aligned}
x_1 &= \frac{-\gamma-i\lambda}{2}+i\nu \\
x_2 &= -1/2-i\nu.
\end{aligned} \tag{2.2.46}$$

The above integrals are representations of the hypergeometric function [46], i.e. (2.2.45) can be written

$$\begin{aligned}
&= 4i\ \sin(x_2\pi)[\rho(1-\rho)]^{x_2}(1-\rho)^{-2(1+x_1+x_2)}\frac{\Gamma(x_1+1)\Gamma(x_2+1)}{\Gamma(x_1+x_2+2)} \\
&\quad \frac{\Gamma(-x_1-2x_2-1)\Gamma(x_2+1)}{\Gamma(-x_1-x_2)}\,{}_2F_1\left(-x_2, x_1+1; x_1+x_2+2; \frac{\rho}{\rho-1}\right) \\
&\quad {}_2F_1\left(-x_2, -x_1-2x_2-1; -x_1-x_2; \frac{\rho-1}{\rho}\right)
\end{aligned} \tag{2.2.47}$$

and we have anticipated the symmetry between ρ and $(1-\rho)$ when performing the ρ integral. We can further simplify the hypergeometric functions to reach

$$\begin{aligned}
&= -4i\ \sin((1/2+i\nu)\pi)(1-\rho)^{-1+\gamma+i\lambda}\frac{\Gamma(\frac{-\gamma-i\lambda}{2}+i\nu+1)\,\Gamma(\frac{\gamma+i\lambda}{2}+i\nu)}{\Gamma(\frac{\gamma+i\lambda+1}{2})\Gamma(\frac{-\gamma-i\lambda+3}{2})} \\
&\quad \Gamma^2(1/2-i\nu)\,{}_2F_1\left(1/2+i\nu, 1/2-i\nu; \frac{-\gamma-i\lambda+3}{2}; \rho\right) \\
&\quad {}_2F_1\left(1/2+i\nu, 1/2-i\nu; \frac{\gamma+i\lambda+1}{2}; 1-\rho\right).
\end{aligned} \tag{2.2.48}$$

Using these integrals, (2.2.41) reduces to

$$I^{\nu}_{(+,+)}(Q^2,q^2) = 16\pi^3\alpha_s\alpha\sum_q e_q^2\left(\frac{2}{q}\right)^{1-2i\nu}\frac{\Gamma(1/2-i\nu)}{\Gamma(1/2+i\nu)}$$
$$\int_{-\infty}^{\infty} d\lambda\,\left(\frac{Q^2}{q^2}\right)^{\frac{-\gamma-i\lambda+1}{2}}\frac{\Gamma(\frac{i\lambda+\gamma-1}{2})}{\Gamma(\frac{-i\lambda-\gamma+3}{2})}\Gamma(\frac{-\gamma-i\lambda}{2}-i\nu+1)\Gamma(\frac{-\gamma-i\lambda}{2}+i\nu+1)$$
$$\int_0^1 d\rho\,[\rho^2+(1-\rho)^2]\,\left(\frac{\rho}{1-\rho}\right)^{\frac{-\gamma+1-i\lambda}{2}}{}_2F_1\left(1/2+i\nu,1/2-i\nu;\frac{-\gamma-i\lambda+3}{2};\rho\right)$$
$${}_2F_1\left(1/2+i\nu,1/2-i\nu;\frac{\gamma+i\lambda+1}{2};1-\rho\right) \tag{2.2.49}$$

and we have used the identity

$$\Gamma(z)\Gamma(1-z) = \frac{\pi}{\sin(z\pi)}. \tag{2.2.50}$$

We define

$$I^{\nu}_{(+,+)}(Q^2,q^2) = 16\pi^3\alpha_s\alpha\sum_q e_q^2\left(\frac{2}{q}\right)^{1-2i\nu}\frac{\Gamma(1/2-i\nu)}{\Gamma(1/2+i\nu)} \tag{2.2.51}$$
$$\int_{-\infty}^{\infty} d\lambda\,\left(\frac{Q^2}{q^2}\right)^{\frac{-\gamma-i\lambda+1}{2}}\frac{\Gamma(\frac{i\lambda+\gamma-1}{2})}{\Gamma(\frac{-i\lambda-\gamma+3}{2})}\Gamma(\frac{-\gamma-i\lambda}{2}-i\nu+1)\Gamma(\frac{-\gamma-i\lambda}{2}+i\nu+1)\,W$$

and perform the ρ-integration by expanding the first hypergeometric function for the ρ^2 term and the second hypergeometric function for the $(1-\rho)^2$ term to give

$$W = \frac{1}{\Gamma(1/2+i\nu)\Gamma(1/2-i\nu)}\sum_{n=0}^{\infty}\frac{\Gamma(1/2+i\nu+n)\Gamma(1/2-i\nu+n)}{\Gamma(1+n)}$$
$$\left\{\frac{\Gamma(-\gamma/2-i\lambda/2+3/2)}{\Gamma(-\gamma/2-i\lambda/2+3/2+n)}\int_o^1 d\rho\rho^{-\gamma/2+5/2-i\lambda/2+n}(1-\rho)^{\gamma/2-1/2+i\lambda/2}\right.$$
$${}_2F_1\left(1/2+i\nu,1/2-i\nu;\frac{\gamma+i\lambda+1}{2};1-\rho\right)$$
$$+\quad\frac{\Gamma(\gamma/2+i\lambda/2+1/2)}{\Gamma(\gamma/2+i\lambda/2+1/2+n)}\int_0^1 d\rho\rho^{\gamma/2+3/2+i\lambda/2+n}(1-\rho)^{-\gamma/2+1/2-i\lambda/2}$$
$$\left.{}_2F_1\left(1/2+i\nu,1/2-i\nu;\frac{-\gamma-i\lambda+3}{2};1-\rho\right)\right\}. \tag{2.2.52}$$

The above integrals are computed using 7.512.4 of [46] and give ratios of Γ functions which we eliminate using the recurrence relation of the Γ function to give

$$W = \frac{\Gamma(-\gamma/2-i\lambda/2+3/2)\Gamma(\gamma/2+i\lambda/2+1/2)}{\Gamma(1/2+i\nu)\Gamma(1/2-i\nu)}$$
$$\sum_{n=0}^{\infty}\frac{(n+1)(n+2)(A+6n+2n^2)}{[(1/2+n)^2+\nu^2][(3/2+n)^2+\nu^2][(5/2+n)^2+\nu^2]} \tag{2.2.53}$$

where $A = 9/2 + \gamma^2/2 - \gamma - i\lambda + i\lambda\gamma - \lambda^2/2$. After some algebra the series can be reduced using a series form of the Ψ (digamma) function

$$\Psi(x+iy) - \Psi(x-iy) = \sum_{n=0}^{\infty} \frac{2yi}{y^2+(x+n)^2}. \tag{2.2.54}$$

Using the recurrence relation of the Ψ function and the relation

$$\Psi(1/2+z) - \Psi(1/2-z) = \pi\tan(\pi z) \tag{2.2.55}$$

we eliminate them to leave

$$W = \frac{\Gamma(-\gamma/2 - i\lambda/2 + 3/2)\Gamma(\gamma/2 + i\lambda/2 + 1/2)}{32\Gamma(1/2+i\nu)\Gamma(1/2-i\nu)} \frac{\pi^2(3+2A+12\nu^2)}{1+\nu^2} \frac{\tanh(\pi\nu)}{\pi\nu}. \tag{2.2.56}$$

Placing the result of (2.2.56) into (2.2.49) the final result for the non-flip amplitude takes the following form:

$$\begin{aligned} I^{\nu}_{(+,+)}(Q^2,q^2) = \alpha_s\alpha\pi^6 \sum_q e_q^2 \left(\frac{2}{q}\right)^{1-2i\nu} & \frac{1}{\Gamma^2(1/2+i\nu)} \frac{\tanh(\pi\nu)}{\pi\nu} \frac{1}{(1+\nu^2)} \\ \int_{\gamma-1-i\infty}^{\gamma-1+i\infty} \frac{dx}{2\pi i} \left(\frac{Q^2}{q^2}\right)^{-x/2} & \Gamma(1/2-i\nu-x/2)\ \Gamma(1/2+i\nu-x/2) \\ & \Gamma(x/2)\ \Gamma(x/2+1)\ (x^2+11+12\nu^2) \end{aligned} \tag{2.2.57}$$

and we have changed integration variables to $x = \gamma - 1 + i\lambda$. Of course the $(-,-)$ amplitude is equivalent. For the flip amplitudes we proceed in the same fashion. The final answer is

$$\begin{aligned} I^{\nu}_{(+,-)}(Q^2,q^2) &= I^{\nu}_{(-,+)}(Q^2,q^2) \\ &= 4\alpha_s\alpha\pi^6 \sum_q e_q^2 \left(\frac{2}{q}\right)^{1-2i\nu} \frac{1}{\Gamma^2(1/2+i\nu)} \frac{\tanh(\pi\nu)}{\pi\nu} \frac{1}{(1+\nu^2)} \\ & \qquad \int_{\gamma-1-i\infty}^{\gamma-1+i\infty} \frac{dx}{2\pi i} \left(\frac{Q^2}{q^2}\right)^{-x/2} \Gamma(3/2-i\nu-x/2) \\ & \qquad \Gamma(3/2+i\nu-x/2)\ \Gamma(x/2)\ \Gamma(x/2+1). \end{aligned} \tag{2.2.58}$$

The $n \neq 0$ Terms

Recently our calculation of $I^{\nu,n}_{\gamma^*\gamma}(Q^2,q^2)$ has been confirmed to be correct and extended to all values of n [47]. It was found that the only non-zero contributions are for $n = \pm 2$.

The n-odd terms are automatically zero and it was explained that no $n > 2$ terms contribute because of the spin-1 nature of the photon. We reproduce the results of [47] for completeness.

First the $n = 2$ components

$$\begin{aligned} I^{\nu,2}_{(+,+)}(Q^2,q^2) &= I^{\nu,2}_{(-,-)}(Q^2,q^2) \\ &= -i\alpha_s\alpha\pi^5 \sum_q e_q^2 \left(\frac{2}{q}\right)^{1-2i\nu} \frac{1}{\Gamma^2(1/2+i\nu)} \frac{\tanh(\pi\nu)}{\pi\nu} \frac{1}{(1+\nu^2)} \frac{1/2-i\nu}{1/2+i\nu} \\ &\qquad \int_{\gamma-1-i\infty}^{\gamma-1+i\infty} dx \left(\frac{Q^2}{q^2}\right)^{-x/2} \Gamma(3/2-i\nu-x/2) \\ &\qquad \Gamma(3/2+i\nu-x/2)\,\Gamma(x/2)\,\Gamma(x/2+1) \end{aligned} \tag{2.2.59}$$

$$\begin{aligned} I^{\nu,2}_{(+,-)}(Q^2,q^2) &= I^{\nu,2}_{(-,+)}(Q^2,q^2) \\ &= i\alpha_s\alpha\pi^5 \sum_q e_q^2 \left(\frac{2}{q}\right)^{1-2i\nu} \frac{1}{\Gamma^2(1/2+i\nu)} \frac{\tanh(\pi\nu)}{\pi\nu} \frac{1}{(1+\nu^2)} \frac{1/2-i\nu}{1/2+i\nu} \\ &\qquad \int_{\gamma-1-i\infty}^{\gamma-1+i\infty} dx \left(\frac{Q^2}{q^2}\right)^{-x/2} \Gamma(5/2-i\nu-x/2) \\ &\qquad \Gamma(1/2+i\nu-x/2)\,\Gamma(x/2)\,\Gamma(x/2+1). \end{aligned} \tag{2.2.60}$$

The authors of [47] then derived the $n = -2$ components from [16], which we do not explicitly show here. We have checked that the inclusion of these terms gives a negligible correction to the $n = 0$ result.

2.2.1 The Limits $Q^2 \gg q^2$ and $Q^2 \ll q^2$

In the limit $Q^2 \gg q^2$ we are able to complete the x integration. We must close the contour in the right half plane to give a positive power series in q^2/Q^2. The leading contribution is extracted by considering the left most poles. For the non-flip amplitude these are located at $x = 1 \pm 2i\nu$:

$$\begin{aligned} I^{\nu}_{(+,+)}(Q^2,q^2)\Big|_{Q^2\gg q^2} &= 2\alpha_s\alpha\pi^6 \sum_q e_q^2 \left(\frac{2}{q}\right)^{1-2i\nu} \frac{1}{\Gamma^2(1/2+i\nu)} \frac{\tanh(\pi\nu)}{\pi\nu} \frac{1}{(1+\nu^2)} \\ &\left\{ \left(\frac{Q^2}{q^2}\right)^{-1/2-i\nu} \Gamma(-2i\nu)\Gamma(1/2+i\nu)\Gamma(3/2+i\nu)[(1+2i\nu)^2+11+12\nu^2] \;+\; c.c. \right\}. \end{aligned} \tag{2.2.61}$$

For the flip amplitude, the left most poles are located at $x = 3 \pm 2i\nu$ giving

$$I^{\nu}_{(+,-)}(Q^2,q^2)\Big|_{Q^2 \gg q^2} = 8\alpha_s\alpha\pi^6 \sum_q e_q^2 \left(\frac{2}{q}\right)^{1-2i\nu} \frac{1}{\Gamma^2(1/2+i\nu)} \frac{\tanh(\pi\nu)}{\pi\nu} \frac{1}{(1+\nu^2)}$$
$$\left\{ \left(\frac{Q^2}{q^2}\right)^{-3/2-i\nu} \Gamma(-2i\nu)\Gamma(3/2+i\nu)\Gamma(5/2+i\nu) \ + \ c.c. \right\}. \qquad (2.2.62)$$

We see that, in the limit $Q^2 \gg q^2$, the flip amplitude is suppressed by a factor of q^2/Q^2.

In the limit $Q^2 \ll q^2$ we must close the contour in the left hand plane to give a positive power series in Q^2/q^2. The leading piece is found by considering the pole at $x = 0$. This gives the Q^2 independent contribution found in [37]. The first correction to this is found by considering the double pole located at $x = -2$. We find

$$I^{\nu}_{(+,+)}(Q^2,q^2)\Big|_{Q^2 \ll q^2} = 2\alpha_s\alpha\pi^6 \sum_q e_q^2 \left(\frac{2}{q}\right)^{1-2i\nu} \frac{\Gamma(1/2-i\nu)}{\Gamma(1/2+i\nu)} \frac{\tanh(\pi\nu)}{\pi\nu}$$
$$\frac{1}{(1+\nu^2)} \Bigg[(11+12\nu^2) - (\nu^2+1/4)\, \frac{Q^2}{q^2}\, (15+12\nu^2)$$
$$\left\{ \ln\frac{|t|}{Q^2} - \frac{8}{15+12\nu^2} - \Psi(3/2+i\nu) - \Psi(3/2-i\nu) \right\} \Bigg]. \qquad (2.2.63)$$

The analytic structure of the x plane is identical for the flip result and so

$$I^{\nu}_{(+,-)}(Q^2,q^2)\Big|_{Q^2 \ll q^2} = 8\alpha_s\alpha\pi^6 \sum_q e_q^2 \left(\frac{2}{q}\right)^{1-2i\nu} \frac{\Gamma(1/2-i\nu)}{\Gamma(1/2+i\nu)} \frac{\tanh(\pi\nu)}{\pi\nu} \frac{(\nu^2+1/4)}{(1+\nu^2)}$$
$$\left[1 - (\nu^2+9/4)\, \frac{Q^2}{q^2} \left\{ \ln\frac{|t|}{Q^2} - \Psi(5/2+i\nu) - \Psi(5/2-i\nu) \right\} \right]. \qquad (2.2.64)$$

2.3 $\gamma^*\gamma^* \to \gamma\gamma$

The cross section for $\gamma^*\gamma^* \to \gamma\gamma$ scattering can be computed by substituting the results for I^ν given by (2.2.57) and (2.2.58) into (2.1.21). The colour factor for this process is given by

$$G = \frac{N_c^2 - 1}{4} = 2. \qquad (2.3.65)$$

We must take account of all possible polarisation states when calculating the unpolarised cross section from the scattering amplitude. We take the average over initial and sum over final polarisation states to give:

$$\frac{d\sigma}{dt}^{\gamma^*\gamma^*\to\gamma\gamma} = \frac{1}{4}\sum_{h_1=\pm}\sum_{h_2=\pm}\sum_{h_3=\pm}\sum_{h_4=\pm}\frac{|A_{(h_1,h_2;h_3,h_4)}(s,t,Q^2)|^2}{16\pi s^2}. \tag{2.3.66}$$

The amplitudes are related to each other, e.g.

$$\begin{aligned} &A_{(+,+;+,+)}(s,t,Q_1^2,Q_2^2) = A_{(+,+;-,-)}(s,t,Q_1^2,Q_2^2) \\ &= A_{(-,-;+,+)}(s,t,Q_1^2,Q_2^2) = A_{(-,-;-,-)}(s,t,Q_1^2,Q_2^2) \end{aligned} \tag{2.3.67}$$

which cancels the polarisation average to leave

$$\begin{aligned} \frac{d\sigma}{dt}^{\gamma^*\gamma^*\to\gamma\gamma} &= \frac{|A_{(+,+;+,+)}(s,t,Q_1^2,Q_2^2)|^2}{16\pi s^2} + \frac{|A_{(+,+;+,-)}(s,t,Q_1^2,Q_2^2)|^2}{16\pi s^2} \\ &+ \frac{|A_{(+,-;+,+)}(s,t,Q_1^2,Q_2^2)|^2}{16\pi s^2} + \frac{|A_{(+,-;+,-)}(s,t,Q_1^2,Q_2^2)|^2}{16\pi s^2}. \end{aligned} \tag{2.3.68}$$

where the $(+,+;+,+)$ amplitude is explicitly:

$$\begin{aligned} A_{(+,+;+,+)}(s,t,Q_1^2,Q_2^2) &= \frac{-is}{64}\alpha_s^2\alpha^2\frac{s}{t}\left(\sum_q e_q^2\right)^2\int_{-\infty}^{\infty} d\nu e^{z\chi(\nu)}\left[\frac{\tanh(\pi\nu)}{(1+\nu^2)(\nu^2+1/4)}\right. \\ &\left.\frac{1}{\Gamma(1/2+i\nu)\Gamma(1/2-i\nu)}\right]^2\int_{\gamma-1-i\infty}^{\gamma-1+i\infty}\frac{dx}{2\pi i}\left(\frac{Q_1^2}{t}\right)^{-x/2}\Gamma(1/2-i\nu-x/2) \\ &\Gamma(1/2+i\nu-x/2)\Gamma(x/2)\Gamma(x/2+1)(11+12\nu^2-x^2)\int_{\gamma-1-i\infty}^{\gamma-1+i\infty}\frac{dx'}{2\pi i}\left(\frac{Q_2^2}{t}\right)^{-x'/2} \\ &\Gamma(1/2-i\nu-x'/2)\Gamma(1/2+i\nu-x'/2)\Gamma(x'/2)\Gamma(x'/2+1)(11+12\nu^2-x'^2), \end{aligned} \tag{2.3.69}$$

and z is given by (2.1.20). The amplitudes for the other helicity states have a very similar structure to (2.3.69).

2.3.1 The Low $|t|$ Limit

For this process we can study the $|t| \to 0$ region. The cross section will be greatest in this limit and, interestingly, we can study the behaviour of the amplitude in $|t| \to 0$ limit. We focus on the limit $Q_1^2 \sim Q_2^2 \gg |t|$ where Q_1^2 and Q_2^2 are the virtualities of the incoming photons. We shall find an analytic approximation for the $\gamma^*\gamma^* \to \gamma\gamma$ amplitude using the approximation to I^ν given by equation (2.2.61) and evaluating the

ν integration using an approximate method. Up to the desired accuracy we need only consider the non-flip amplitudes and we use the method of steepest descents (saddle point method) to evaluate the ν integration. The saddle point method is valid when integrals of the form

$$I = \int_{-\infty}^{+\infty} dx\, g(x)\, e^{-f(x)} \tag{2.3.70}$$

are to be evaluated and the integral is dominated by the exponential term i.e. in the dominant region of the integral the function $g(x)$ may be considered as smoothly varying compared to the exponential term and may be evaluated to $g(x_0)$ over the region of integration, or if that is zero then the first non vanishing even term in the Taylor series about x_0. The point x_0 is the saddle point in question and its location is defined by

$$f^{'}(x_0) = 0. \tag{2.3.71}$$

The function $f(x)$ is then approximated by the first two non vanishing terms in its Taylor series

$$f(x) \approx f(x_0) + \frac{1}{2} f^{''}(x_0)(x_0 - x)^2. \tag{2.3.72}$$

The integration is then Gaussian and the final result is

$$I \approx \frac{\sqrt{2\pi}}{(f''(x_0))^{1/2}} g(x_0) e^{-f(x_0)}. \tag{2.3.73}$$

When (2.2.61) is placed into (2.1.21) we find two distinct terms. One term is independent of $|t|$ and gives the limiting value of the amplitude when $|t| = 0$. The other term provides the leading $|t|$ dependence. Considering the saddle point integration of the $|t|$ dependent piece we find that the dominant term in the exponential is proportional to $\ln(Q_1^2 Q_2^2/t^2)$ and so we may make the assumption that the saddle point lies at $\nu \approx \pm i/2$ and approximate $\chi(\nu)$ by an expansion about $\nu = \pm i/2$: $\chi(\nu) \approx 1/(1/2 \pm i\nu)$. The saddle point is in fact at

$$\nu = \pm \frac{i}{2} \left(1 - \sqrt{\frac{4z}{\ln\left(Q_1^2 Q_2^2/t^2\right)}} \right) \approx \pm \frac{i}{2}. \tag{2.3.74}$$

For the $|t|$ independent piece we have a term proportional to $\ln(Q_1^2/Q_2^2)$ in the exponential. For $Q_1^2 \sim Q_2^2$ the saddle point is at

$$\nu = \pm \frac{i \ln(Q_1^2/Q_2^2)}{28\zeta(3) z} \approx 0 \tag{2.3.75}$$

and we can use $\chi(\nu) \approx 4\log 2 - 14\zeta(3)\nu^2$. Performing the integration over ν yields

$$A_{(+,+;+,+)}(s,t,Q_1^2,Q_2^2)\Big|_{Q_1^2\sim Q_2^2\gg|t|} \approx i\; 9\pi^2\alpha^2\alpha_s^2\left(\sum_q e_q^2\right)^2 \frac{s}{Q_1Q_2}$$
$$\left[\exp\left(4z\ln 2 - \frac{\ln^2\left(Q_1^2/Q_2^2\right)}{56\zeta(3)z}\right)\sqrt{\frac{\pi}{14\zeta(3)z}}\right.$$
$$\left. -\frac{4}{9\pi^{7/2}}\frac{|t|}{Q_1Q_2}\frac{\ln^{5/4}\left(Q_1^2Q_2^2/|t|^2\right)}{z^{7/4}}\exp\left(2\sqrt{z\ln(Q_1^2Q_2^2/|t|^2)}\right)\right]. \quad (2.3.76)$$

In the t dependent term we have regained the well known double leading log result [48]. There is a cusp in the cross-section at $-t = 0$, i.e. the slope is infinite.

At high energies the effective one Pomeron exchange amplitude is of the form

$$A(s,t) \approx A(s)e^{bt} \quad (2.3.77)$$

We emulate this factorisation by defining an effective b-parameter b_{eff} by

$$b_{\text{eff}} = \frac{2}{A(s,t)}\frac{\partial A(s,t)}{\partial t} \quad (2.3.78)$$

and using (2.3.76), we find that, in the vicinity of $-t = 0$,

$$b_{\text{eff}} = \frac{1}{A_0}\frac{4}{9\pi^{7/2}}\frac{1}{Q_1Q_2}\exp\left(2\sqrt{z\ln(Q_1^2Q_2^2/|t|^2)}\right)\frac{\ln^{5/4}\left(\frac{Q_1^2Q_2^2}{t^2}\right)}{z^{7/4}} \quad (2.3.79)$$

where

$$A_0 \approx e^{4z\ln 2}\sqrt{\frac{\pi}{14\zeta(3)z}}. \quad (2.3.80)$$

We can see from (2.3.79) that b decreases with energy. This means that the amplitude exhibits the property of "anti-shrinkage". This is in contrast to the soft Pomeron where the width of the diffraction peak shrinks as z is increased.

2.3.2 The High $|t|$ Limit

We now consider the limit $Q_1^2, Q_2^2 \ll |t|$. The saddle point is near $\nu = 0$ and after integration over ν we find that

$$A_{(+,+;+,+)}(s,t,Q_1^2,Q_2^2)\Big|_{|t|\gg Q_1^2,Q_2^2} = \frac{i}{4}\pi\frac{s}{|t|}\alpha^2\alpha_s^2\left(\sum_q e_q^2\right)^2 e^{4z\ln 2}$$
$$\left(\frac{\pi}{14\zeta(3)z}\right)^{3/2} C_1(Q_1)C_1(Q_2)$$

$$A_{(+,-;+,-)}(s,t,Q_1^2,Q_2^2)\Big|_{|t|\gg Q_1^2,Q_2^2} = \frac{i}{4}\pi\frac{s}{|t|}\alpha^2\alpha_s^2\left(\sum_q e_q^2\right)^2 e^{4z\ln 2} \left(\frac{\pi}{14\zeta(3)z}\right)^{3/2} C_2(Q_1)C_2(Q_2) \tag{2.3.81}$$

where

$$\begin{aligned} C_1(Q_1) &= 11+\frac{1}{4}\frac{Q_1^2}{|t|}\left(68-30\gamma_E-60\ln 2-15\ln\left(\frac{|t|}{Q_1^2}\right)\right) \\ C_2(Q_1) &= 1-\frac{9}{4}\frac{Q_1^2}{|t|}\left(-\frac{16}{3}+2\gamma_E+4\ln 2+\ln\left(\frac{|t|}{Q_1^2}\right)\right). \end{aligned} \tag{2.3.82}$$

The amplitudes $A_{(+,+;+,-)}$ and $A_{(+,-;+,+)}$ have a similar form, the final factors being replaced by $C_1(Q_1)C_2(Q_2)$ and $C_2(Q_1)C_1(Q_2)$ respectively.

We can see from the results for the $\gamma^*\gamma^* \to \gamma\gamma$ scattering amplitude in both the kinematic limits discussed that the $(+,+;+,+)$ amplitude is the dominant term in the calculation of the cross section. It is therefore safe to keep only this term in the subsequent calculation of the cross section.

2.4 $\gamma^* q \to \gamma q$

We may use the results (2.2.57) and (2.2.58) to compute $\gamma^* \to \gamma$ scattering off a hadronic state.

2.4.1 Coupling Conformal Eigenfunctions to Coloured States

Using the quark impact factor defined in (1.2.45) we naively find that the function I_ν^{q*} contains a delta function $\delta^{(2)}(\mathbf{b}_1 - \mathbf{b}_1')$ when the $\mathbf{k_1}$ integration is performed, rendering it zero. This is because in the original derivation of the conformal solution to the BFKL equation only colour neutral particle states were considered, and the conformal solution contains δ-function like contributions which are not present in perturbation theory. These do not give any contribution to physical amplitudes as they give zero contribution when convoluted with colour neutral external states. In the case of the

Pomeron coupling to single quark lines (coloured states) these δ-function contributions have to be subtracted using the Mueller-Tang subtraction prescription [26, 49]

$$\begin{aligned} E_\nu(\mathbf{b_1},\mathbf{b_1'}) &= \left(\frac{|\mathbf{b_1}-\mathbf{b_1'}|}{|\mathbf{b_1}||\mathbf{b_1'}|}\right)^{1+2i\nu} \rightarrow \\ E_\nu^{M-T}(\mathbf{b_1},\mathbf{b_1'}) &= \left(\frac{|\mathbf{b_1}-\mathbf{b_1'}|}{|\mathbf{b_1}||\mathbf{b_1'}|}\right)^{1+2i\nu} - \left(\frac{1}{\mathbf{b_1}^2}\right)^{1/2+i\nu} - \left(\frac{1}{\mathbf{b_1'}^2}\right)^{1/2+i\nu}. \end{aligned} \quad (2.4.83)$$

Using the Mueller-Tang subtraction the function $I_\nu^q(q)$ becomes

$$I_\nu^q(q) = 8\pi^2\alpha_s \int d^2\mathbf{b_1} d^2\mathbf{b_1'} d^2\mathbf{k_1} \left\{ -\left(\frac{1}{\mathbf{b_1}^2}\right)^{1/2+i\nu} - \left(\frac{1}{\mathbf{b_1'}^2}\right)^{1/2+i\nu} \right\} e^{-i[\mathbf{k_1}.\mathbf{b_1}-(\mathbf{k_1}+\mathbf{q}).\mathbf{b_1'}]} \quad (2.4.84)$$

where the impact factor for the coupling to the quarks and gluons in the proton is given by (1.2.45). The integration over $\mathbf{k_1}$ yields a delta function, $\delta^2(\mathbf{b_1}-\mathbf{b_2})$, which forms part of the impact parameter representation of the parton impact factor. The delta function cancels one of the impact parameter integrals and the remaining integrations are easily performed to give

$$I_q^\nu = -2(2\pi)^5\alpha_s \frac{\Gamma(1/2-i\nu)}{\Gamma(1/2+i\nu)} \left(\frac{2}{q}\right)^{1-2i\nu}. \quad (2.4.85)$$

2.4.2 The Full Amplitude

The colour factor for coupling to quarks is

$$G = \frac{N_c^2-1}{4N_c} = 2/3,$$

relative to which the coupling to gluons is enhanced by a factor $C_A/C_F = 9/4$. Putting the colour factor, along with (2.2.57), (2.2.58) and (2.4.85) into (2.1.21) yields

$$\begin{aligned} A_{(+,+)}(s,t,Q^2) &= i\,\alpha\alpha_s^2 \sum_q e_q^2 \,\frac{\pi}{6}\,\frac{s}{|t|} \int d\nu\, \frac{\nu^2}{(1/4+\nu^2)^2}\,\frac{1}{1+\nu^2}\,\frac{\tanh(\pi\nu)}{\pi\nu}\, e^{z\chi(\nu)} \\ &\int_{\gamma-1-i\infty}^{\gamma-1+i\infty} \frac{dx}{2\pi i}\left(\frac{Q^2}{|t|}\right)^{-x/2} \frac{\Gamma(1/2-i\nu-x/2)\,\Gamma(1/2+i\nu-x/2)}{\Gamma(1/2+i\nu)\,\Gamma(1/2-i\nu)} \\ &\qquad \Gamma(x/2)\,\Gamma(x/2+1)[x^2+11+12\nu^2] \end{aligned} \quad (2.4.86)$$

and

$$A_{(+,-)}(s,t,Q^2) = i\,\alpha\alpha_s^2 \sum_q e_q^2 \,\frac{2\pi}{3}\,\frac{s}{|t|} \int d\nu\, \frac{\nu^2}{(1/4+\nu^2)^2}\,\frac{1}{1+\nu^2}\,\frac{\tanh(\pi\nu)}{\pi\nu}\, e^{z\chi(\nu)}$$

$$\int_{\gamma-1-i\infty}^{\gamma-1+i\infty} \frac{dx}{2\pi i} \left(\frac{Q^2}{|t|}\right)^{-x/2} \frac{\Gamma(3/2-i\nu-x/2)\;\Gamma(3/2+i\nu-x/2)}{\Gamma(1/2+i\nu)\;\Gamma(1/2-i\nu)} \Gamma(x/2)\;\Gamma(x/2+1). \quad (2.4.87)$$

The $\gamma^* q \to \gamma q$ cross section is

$$\frac{d\sigma}{dt}^{\gamma^* q\to\gamma q} = \frac{1}{2}\sum_{h_1=\pm}\sum_{h_2=\pm} \frac{|A_{(h_1,h_2)}(s,t)|^2}{16\pi s^2} \quad (2.4.88)$$

which can be written

$$\frac{d\sigma}{dt}^{\gamma^* q\to\gamma q} \frac{|A_{(+,+)}(s,t)|^2+|A_{(+,-)}(s,t)|^2}{16\pi s^2}. \quad (2.4.89)$$

2.4.3 The Low $|t|$ Limit

The relevant saddle point is now at $\nu \approx \pm i/2$ and so

$$A_{(+,+)}(s,t,Q^2)\Big|_{Q^2\gg|t|} = \frac{8i}{3\sqrt{\pi}}\;\alpha\alpha_s^2\sum_q e_q^2\;\frac{s}{Q^2}\frac{\ln^{3/4}(Q^2/|t|)}{z^{5/4}}\exp\left(2\sqrt{z\ln(Q^2/|t|)}\right) \quad (2.4.90)$$

and

$$A_{(+,-)}(s,t,Q^2)\Big|_{Q^2\gg|t|} = \frac{16i}{9\sqrt{\pi}}\;\alpha\alpha_s^2\sum_q e_q^2\;\frac{s|t|}{Q^4}\frac{\ln^{3/4}(Q^2/|t|)}{z^{5/4}}\exp\left(2\sqrt{z\ln(Q^2/|t|)}\right) \quad (2.4.91)$$

The dominance of the non-flip amplitude over the flip amplitude is clear:

$$\frac{A_{(+,+)}}{A_{(+,-)}} = \frac{3Q^2}{2|t|}. \quad (2.4.92)$$

2.4.4 The High $|t|$ Limit

In the limit $-t \gg Q^2$ the saddle point integration about $\nu = 0$ yields

$$A_{(+,+)}(s,t,Q^2)\Big|_{Q^2\ll|t|} = \frac{8i}{3}\;\alpha\alpha_s^2\sum_q e_q^2\;\frac{s}{|t|}\;e^{4z\ln 2}\left(\frac{\pi}{14z\zeta(3)}\right)^{3/2} C_1(Q) \quad (2.4.93)$$

and

$$A_{(+,-)}(s,t,Q^2)\Big|_{Q^2\ll|t|} = \frac{8i}{3}\;\alpha\alpha_s^2\sum_q e_q^2\;\frac{s}{|t|}\;e^{4z\ln 2}\left(\frac{\pi}{14z\zeta(3)}\right)^{3/2} C_2(Q). \quad (2.4.94)$$

We follow the same method for calculating the $\gamma^* q \to \gamma$ cross section as we did for the $\gamma^*\gamma^* \to \gamma\gamma$ cross section and disregard the flip result as a small contribution in subsequent calculations.

2.5 Example FORM Program

Here we show the FORM code for the trace summation for diagram c

```
FORM by J.Vermaseren. Version 1.1 May 30 1995
Symbols lr,s,Q;
Vectors pg,l,p1,p2,q,k1,lt,k1t,qt,t1,t2,t3,e1,e3,e1t,pgf;
*
*compute traces for e+e->e+e-gamma,gamma
*diagram c
*NB:- MASSLESS QUARKS
*transverse incoming photons
Local A =
g_(1,l)*g_(1,p2)*g_(1,t1)*g_(1,e3)*g_(1,t2)*g_(1,p2)*g_(1,t3)*
g_(1,e1);
*
*Compute denominators
*
Local Denom1 = t1.t1;
Local Denom2 = t3.t3;
*
id t1 = l+k1+q;
id t2 = l+k1-pg;
id t3 = l-pg;
*
trace4,1;
*
*for on shell final state photons:-
*
id pgf.pgf = 0;
id pgf = pg + q;
*
*
*Sudakov parameterisation-high energy approximation
*
id k1 = (lt.lt)*p2/(s*lr) + (pg.pg)*p2/s
        -(lt.lt + 2*lt.k1t + k1t.k1t)*p2/((lr-1)*s)+ k1t;
id pg = p1 + ((pg.pg)/s)*p2;
id l = -(lt.lt)*p2/(s*lr)  + lr*p1 + lt;
id q = (-pg.pg-qt.qt)/s*p2 + qt;
*
id e1.p1 = 0;
id e1.p2 = 0;
id e3.p2 = 0;
id p1.p1 = 0;
```

```
id p2.p2 = 0;
id p1.lt = 0;
id p2.lt = 0;
id p1.qt = 0;
id p2.qt = 0;
id p1.k1t = 0;
id p2.k1t = 0;
id p1.p2 = s/2;
*
print Denom1;
print Denom2;
print A;
end

Time =       4.26 sec    Generated terms =      27121
                A        Terms in output =         18
                         Bytes used      =        622

Time =       4.28 sec    Generated terms =        116
           Denom1        Terms in output =         10
                         Bytes used      =        358

Time =       4.28 sec    Generated terms =         14
           Denom2        Terms in output =          3
                         Bytes used      =         72

A =
 8*p1.e3*lt.e1*lr^3*s^2 - 12*p1.e3*lt.e1*lr^2*s^2 + 4*p1.e3*lt.e1*
 lr*s^2 + 2*lt.lt*e1.e3*s^2 + 2*lt.k1t*e1.e3*s^2 - 2*lt.qt*e1.e3*
 lr*s^2 + 2*lt.qt*e1.e3*s^2 + 8*lt.e1*lt.e3*lr^2*s^2 - 8*lt.e1*
 lt.e3*lr*s^2 + 8*lt.e1*k1t.e3*lr^2*s^2 - 8*lt.e1*k1t.e3*lr*s^2
 + 2*lt.e1*k1t.e3*s^2 + 4*lt.e1*qt.e3*lr^2*s^2 - 6*lt.e1*qt.e3*
 lr*s^2 + 2*lt.e1*qt.e3*s^2 - 2*lt.e3*k1t.e1*s^2 + 2*lt.e3*qt.e1
 *lr*s^2-2*lt.e3*qt.e1*s^2;

Denom1 =
 lt.lt + 2*lt.k1t + 2*lt.qt + k1t.k1t + 2*k1t.qt + qt.qt - qt.qt*
 lr - 1/(lr*s - s)*lt.lt*lr*s - 2/(lr*s - s)*lt.k1t*lr*s - 1/
 (lr*s - s)*k1t.k1t*lr*s;

Denom2 =
 pg.pg - pg.pg*lr + lt.lt*lr^-1;
```

Chapter 3

Results

3.1 $\gamma^*\gamma^*$ and $\gamma^* q$ Cross Sections

Until we are able to produce a γq or a $\gamma\gamma$ collider, what has been calculated in the previous chapter must be thought of as subprocesses within a larger interaction. Canonically this is ee and ep physics, but there are exciting options being considered for the next generation of experiments. Obviously quark beams are currently out of the question, but a lot of variation can be pursued as to the method of photon production. Options being considered for the TESLA experiment, the European proposal for the next generation ee linear collider to be based at DESY, are to run the machine in $e\gamma$ and $\gamma\gamma$ modes [50], achievable by focusing a laser onto a lepton beam to produce a pure photon beam. Similar proposals are being considered in the Japanese and US designs for the NLC, which could be based at the KEK facility at Tsukuba in Japan or at an undecided site in the USA [51].

It is natural to consider the features of the universal subprocesses first before discussion of current and future experimental situations. We consider the exact results for the $\gamma^*\gamma^* \to \gamma\gamma$ and $\gamma^* q \to \gamma q$ differential cross sections obtained using (2.2.57): the solid lines in figures (3.1), (3.3), (3.4) and (3.5). Comparison is made with the results obtained using the approximation to $I^{\nu}_{(+,+)}$ given in (2.2.61) and (2.2.63): the dashed lines in figures (3.1), (3.3), (3.4) and (3.5). The choice of the s_0 parameter in (2.1.20) is the largest other scale in the problem apart from s, i.e. $\max(Q^2, |t|)$ for γq

scattering. For $\gamma\gamma$ scattering we choose a value for the z energy variable in (2.1.20), $z = 0.5$ is a suitable value for the energies under consideration at LEP, $z = 1$ and $z = 2$ reflect the higher values of s and similar values of $Q^2$and $|t|$ accessible at LEP2 and a future linear collider (LC) respectively. All ν integrals are computed numerically.

In figure (3.1) we show the γq cross section for centre of mass energies of 100 and 200 GeV, energies typical of the HERA collider. From figure (3.1) we can see that performing the x integration by keeping only the leading poles leads to accurate predictions for the cross section for a large range of values of $Q^2/|t|$ $(|t|/Q^2)$. We note that in the limit of $|t| \gg Q^2$ the cross section becomes insensitive to values of Q^2, as anticipated in the analytic expression (2.4.93).

The analytic expressions (2.4.90) and (2.4.93) produced by performing the ν integrations using the saddle method are shown in comparison with the exact result in figure (3.2). Answers obtained by the saddle point approximation are often only valid in extremely asymptotic limits, or in more modest limits, shifted by a logarithmic factor from the exact result. In figure (3.2) we have chosen a value of $s = 4 \times 10^5\,\mathrm{GeV}^2$ for both the exact and saddle point results. In the limit $|t| \gg \mathrm{Q}^2$ we have taken the photon to be almost on shell and have altered the scale in the logarithm of z, the BFKL energy variable, from $s/|t|$ to $5/6 * s/|t|$ to obtain agreement with the exact result. This is shown in the upper plot of figure (3.2). In the limit $|t| \ll \mathrm{Q}^2$ it was necessary to take a high value of $Q^2 = 10^4\,\mathrm{GeV}^2$ to match the saddle point result with the exact result with a shift of a similar magnitude: from s/Q^2 to $5/7 * s/Q^2$. This is shown in the lower plot of figure (3.2). We conclude that the saddle point method gives a more accurate result in the photoproduction limit than in the $|t| \to 0$ limit.

In figures (3.3), (3.4) and (3.5) we show the $\gamma\gamma$ cross section for three different values of z discussed above and compare the exact result with the leading pole analysis.

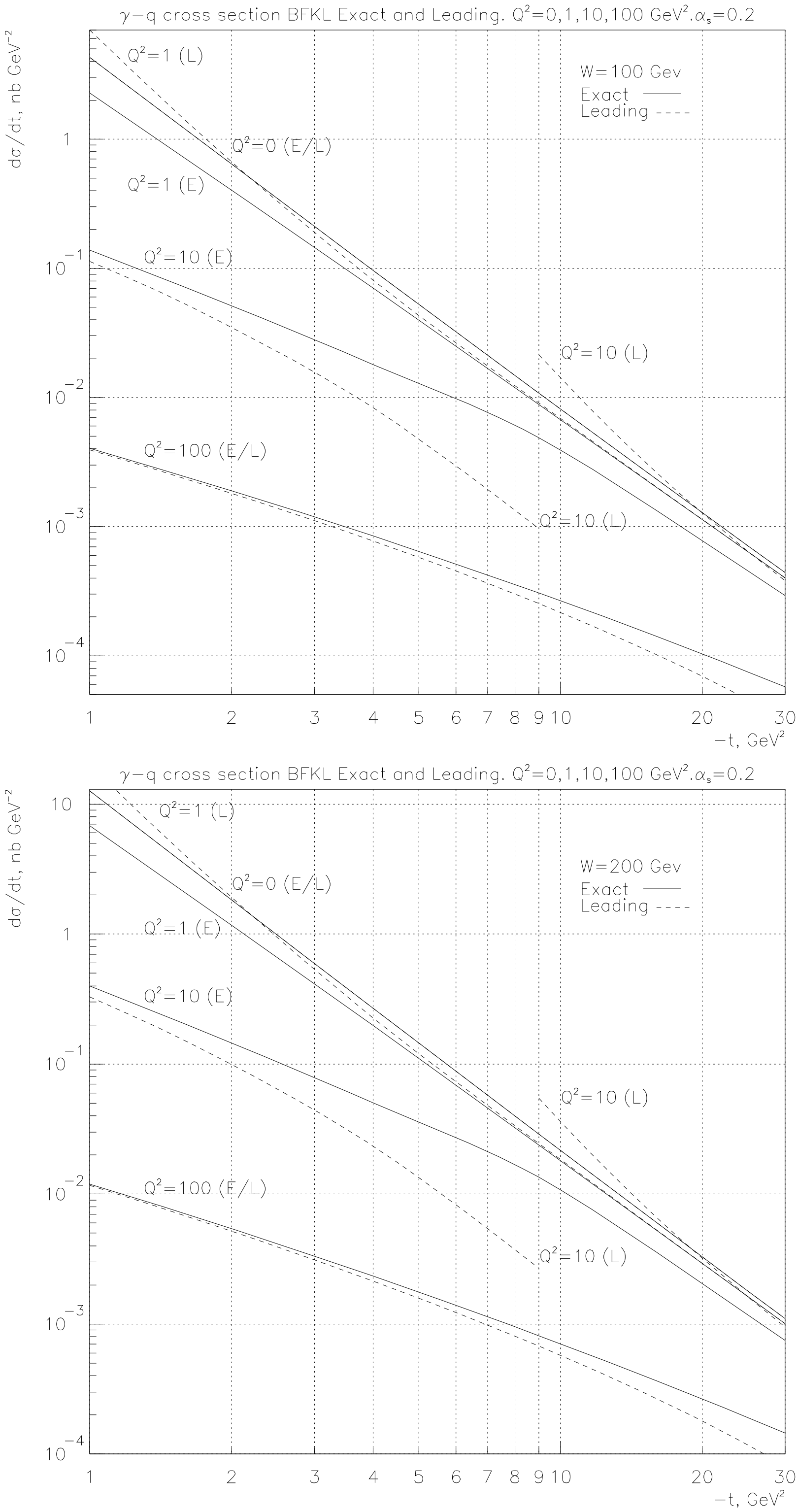

Figure 3.1: $\gamma^* q \to \gamma q$ cross section. Exact BFKL result (solid) compared with the leading pole approximation (dotted). $W = 100, 200\,\mathrm{GeV}$.

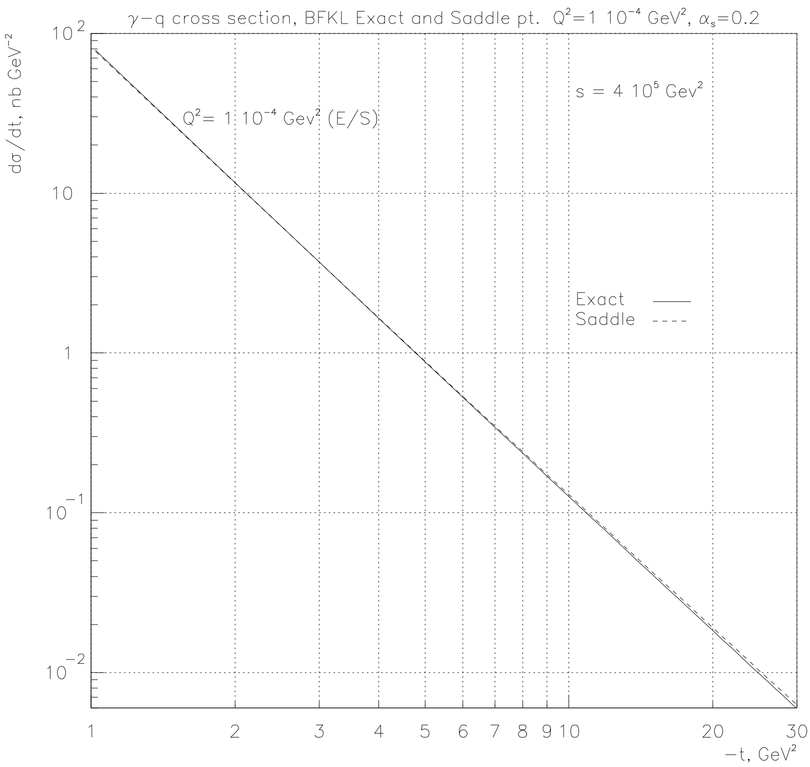

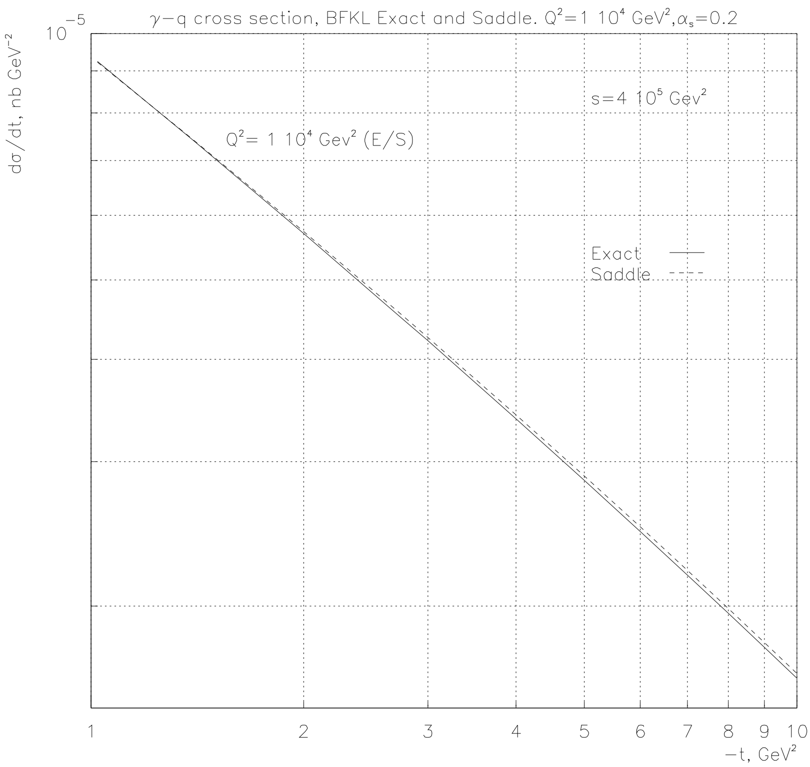

Figure 3.2: $\gamma^* q \to \gamma q$ cross section. Exact BFKL result (solid) compared with the saddle point approximation (dotted). $s = 4 \times 10^5\,\mathrm{GeV}^2$.

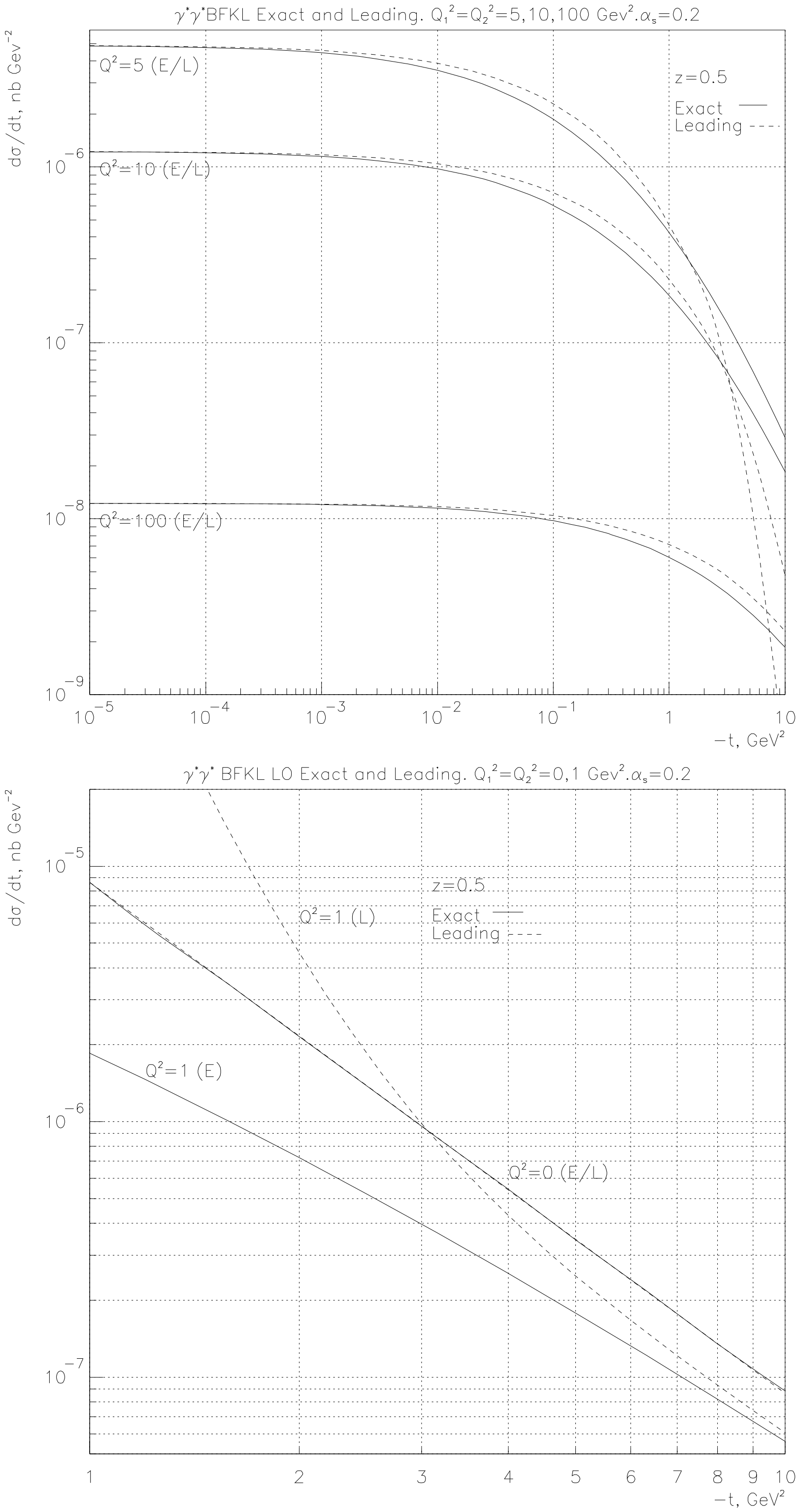

Figure 3.3: $\gamma^*\gamma^* \to \gamma\gamma$ cross section. Exact BFKL result (solid) compared with the leading pole approximation (dotted) at low and high $|t|/Q^2$, $z = 0.5$, $Q_1^2 = Q_2^2 = Q^2$.

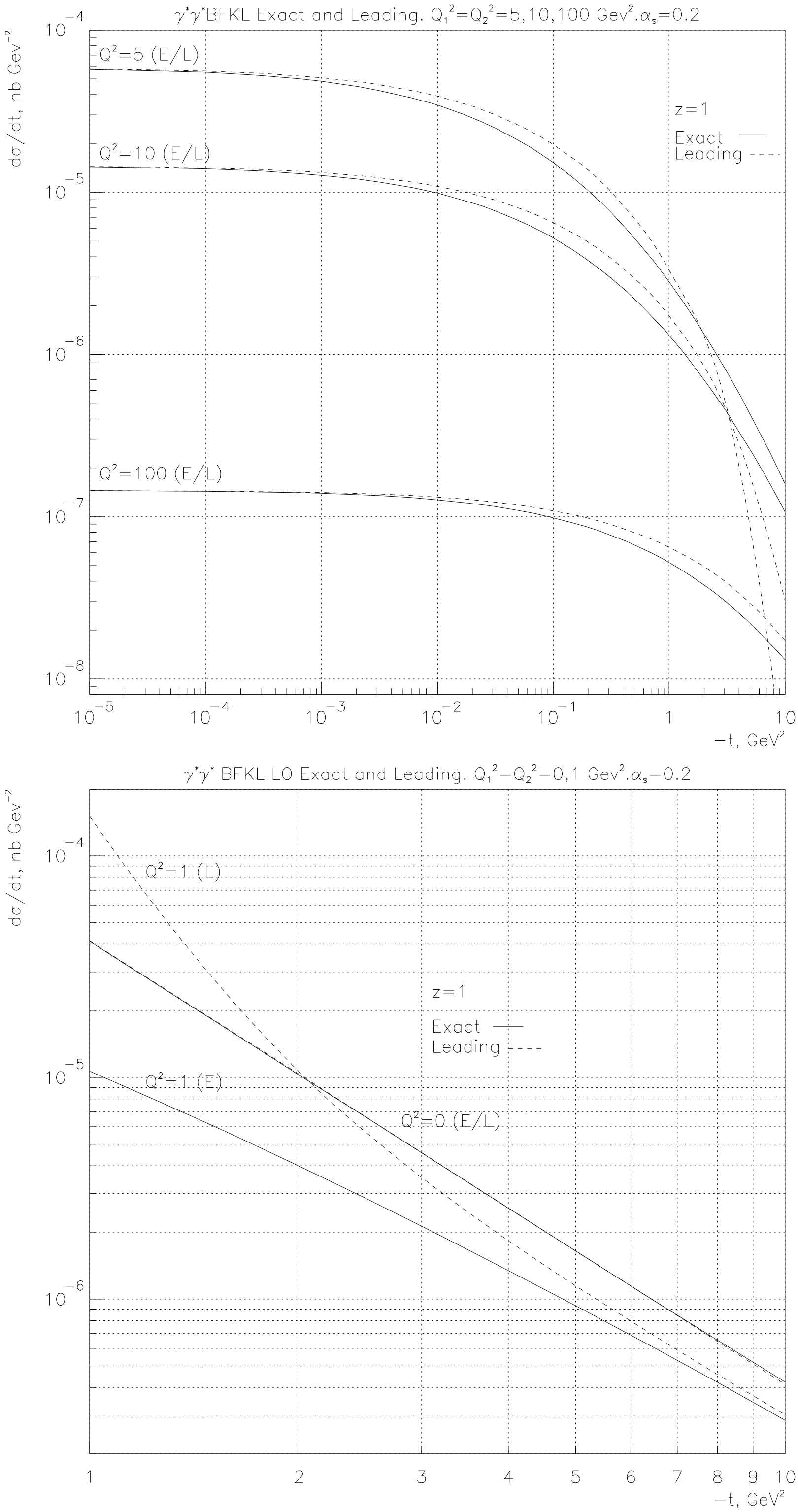

Figure 3.4: $\gamma^*\gamma^* \to \gamma\gamma$ cross section. Exact BFKL result (solid) compared with the leading pole approximation (dotted) at low and high $|t|/Q^2$, $z=1$, $Q_1^2 = Q_2^2 = Q^2$.

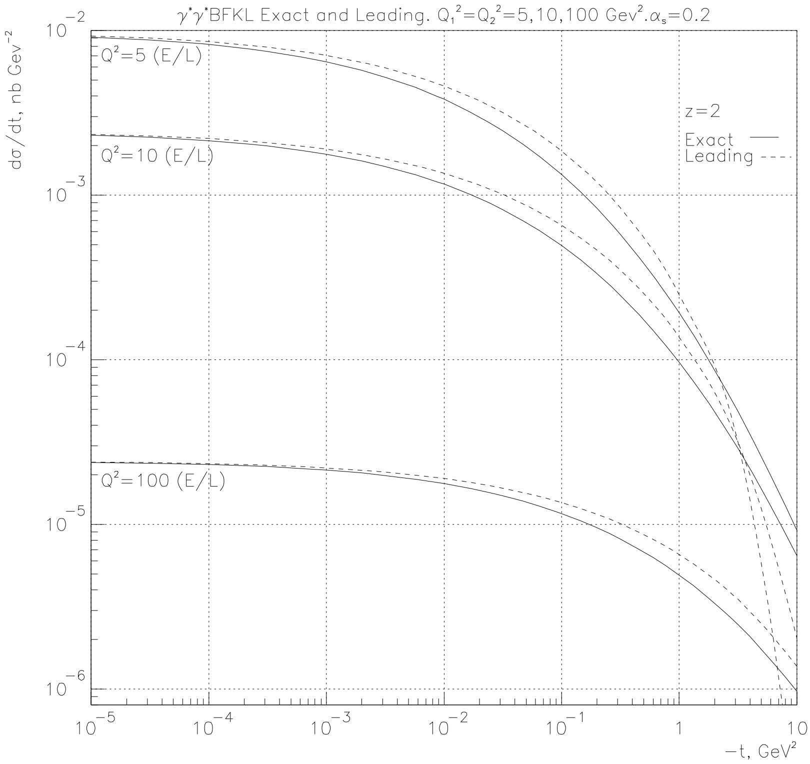

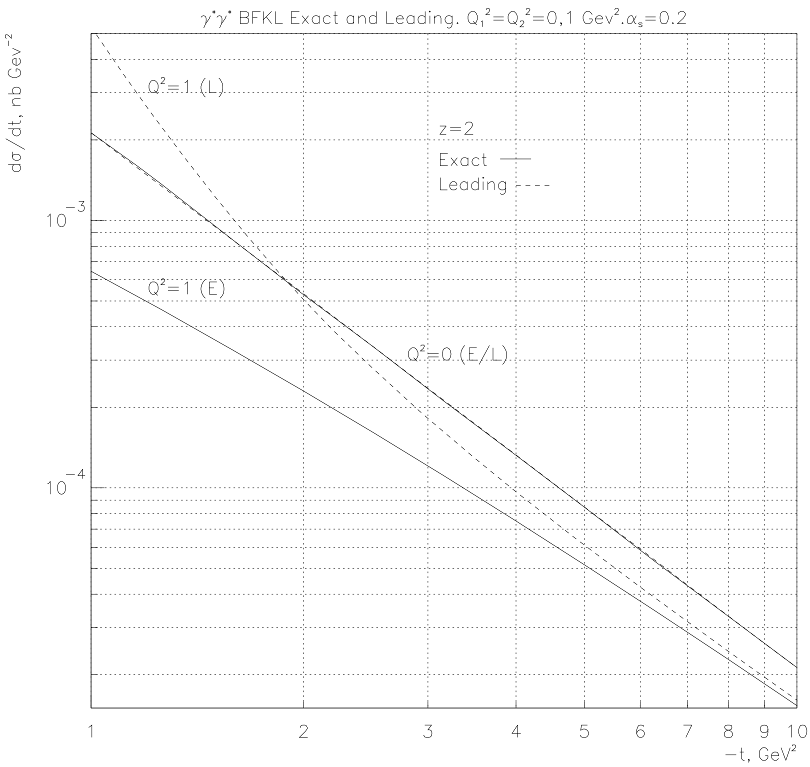

Figure 3.5: $\gamma^*\gamma^* \to \gamma\gamma$ cross section. Exact BFKL result (solid) compared with the leading pole approximation (dotted) at low and high $|t|/Q^2$, $z = 2$, $Q_1^2 = Q_2^2 = Q^2$.

3.2 $\gamma^* p \to \gamma X$ and $\gamma^*\gamma^* \to \gamma X$

The hadron level cross section is determined by the convolution of the γq cross section with a phenomenological parton density function (pdf) [52]. Using the appropriate pdf we are able to compute two single dissociative diffractive processes: $\gamma^*\gamma^* \to \gamma X$ and $\gamma^* p \to \gamma X$ [53], where X denotes the dissociative system. The cross section at hadron level is

$$\frac{d\sigma(\gamma H \to \gamma X)}{dt} = \int_{x_{\min}}^{1} dx \left(\frac{81}{16} g(x,t) + \sum_f (q(x,t) + \overline{q}(x,t)) \right)_H \frac{d\sigma(\gamma q \to \gamma q)}{dt}. \tag{3.2.1}$$

where $H = \gamma^*/P$. The lower limit of the x integral is determined by the on-shell condition for the struck quark in the hadron, i.e.

$$x_{\min} = \frac{1}{(\frac{M_X^2}{|t|} + 1)}, \tag{3.2.2}$$

where M_X is the maximum invariant mass of the hadron dissociation products. We choose $M_X = 10$ GeV, which is typical of the cuts imposed by the HERA experiments. We note that these cross sections for $\gamma^* p$ are large enough to make observation at HERA possible. In figure(3.6) we give the exact cross section for $\gamma^* p \to \gamma X$ and in figures (3.7) and (3.8) we give comparison between the exact and the leading pole analysis at low and high values of $|t|/Q^2$. In figure (3.9) we show the exact cross section for $\gamma^*\gamma^* \to \gamma X$ at $\sqrt{s} = 0.5, 1$ TeV, projected energies of a future LC and with the same maximum mass of the diffractive system i.e. less than 10 GeV. We note that the cross section at these energies is comparable to the $\gamma^* p \to \gamma X$ cross section at HERA energies.

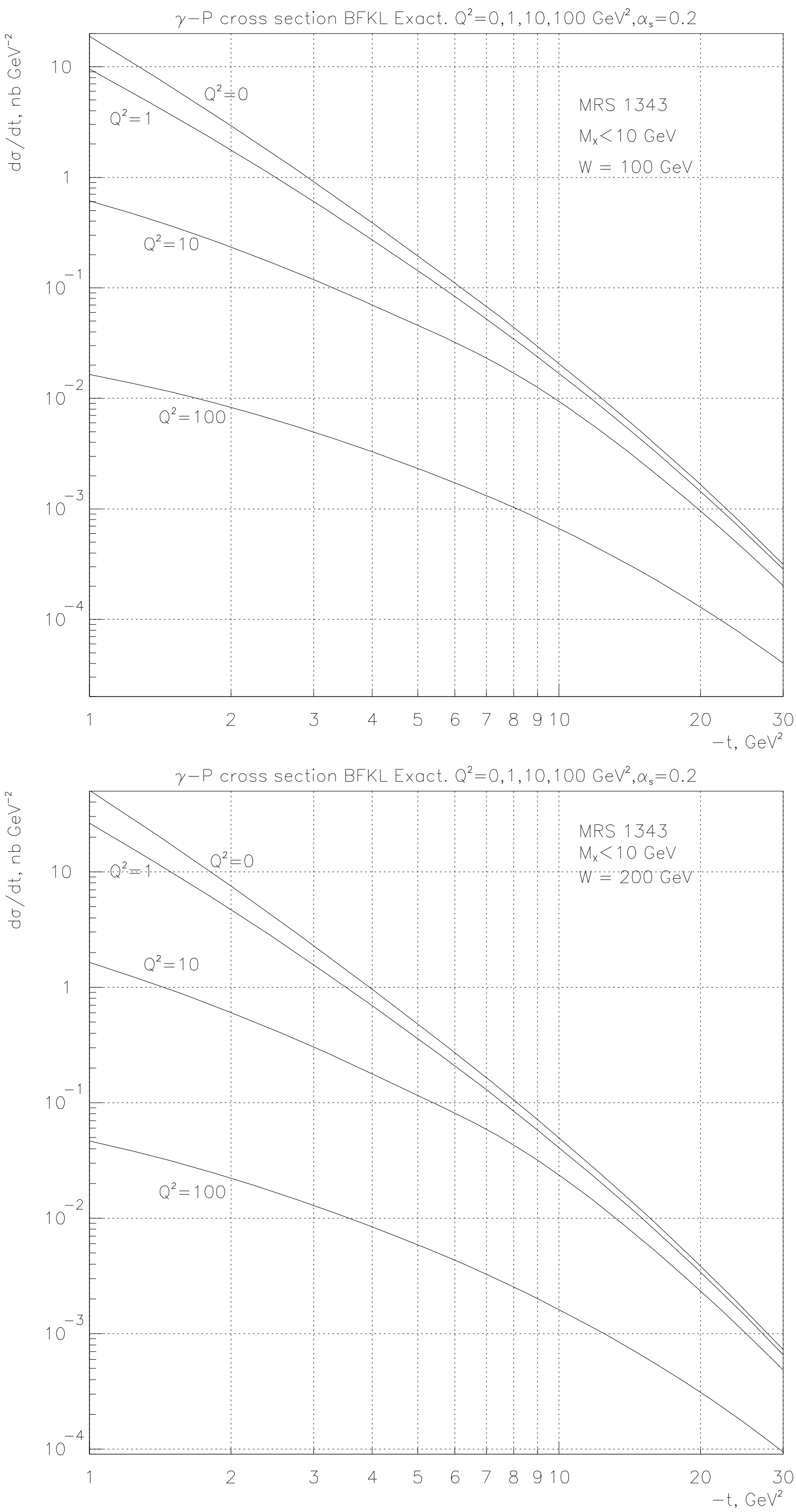

Figure 3.6: $\gamma^* p \to \gamma X$ cross section. Exact BFKL result. $W = 100, 200\,\mathrm{GeV}$.

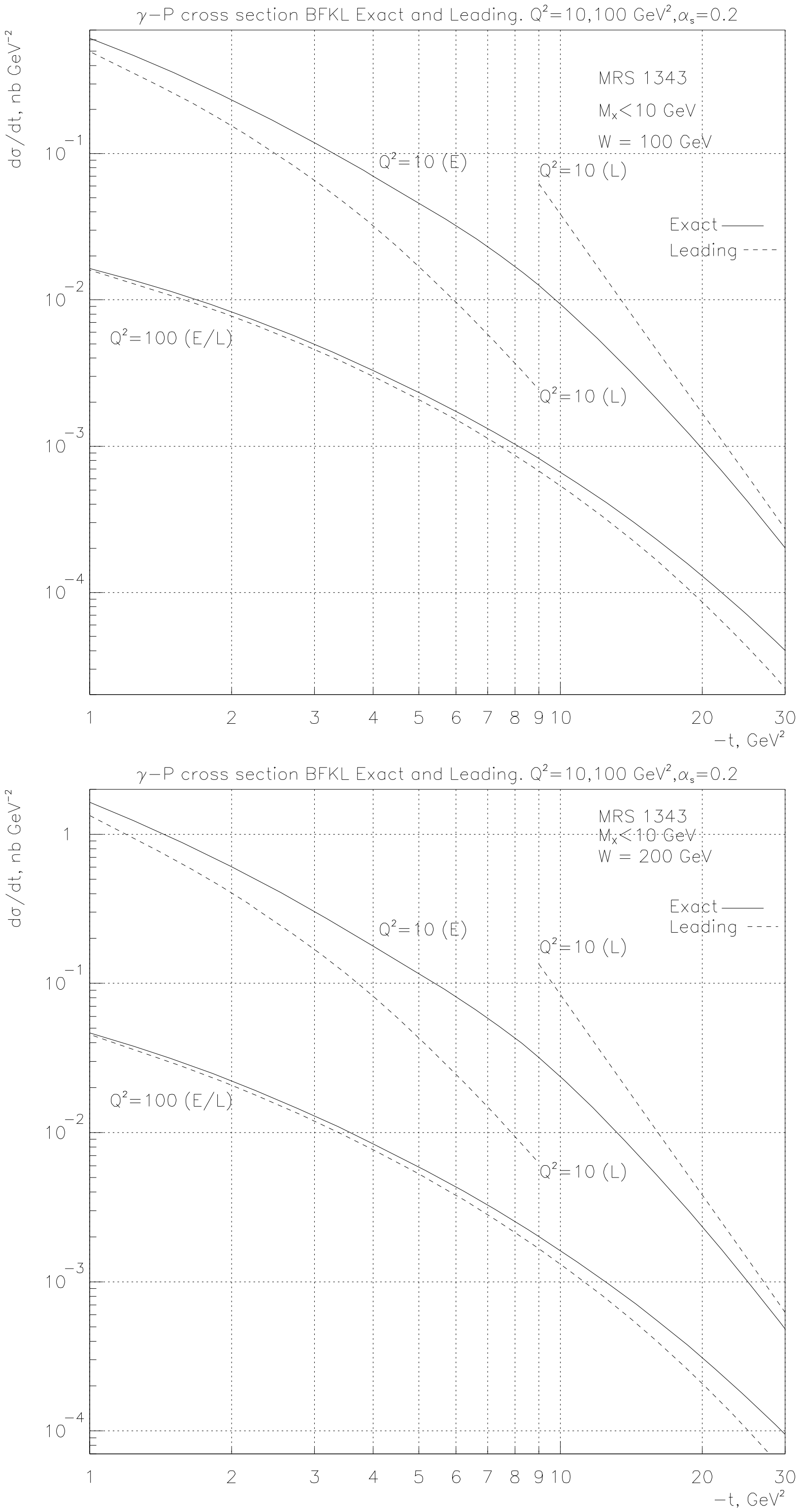

Figure 3.7: $\gamma^* p \to \gamma X$ cross section. Exact BFKL result (solid) compared with the leading pole approximations (dotted) at low and high $|t|/Q^2$. $W = 100, 200\,\mathrm{GeV}$.

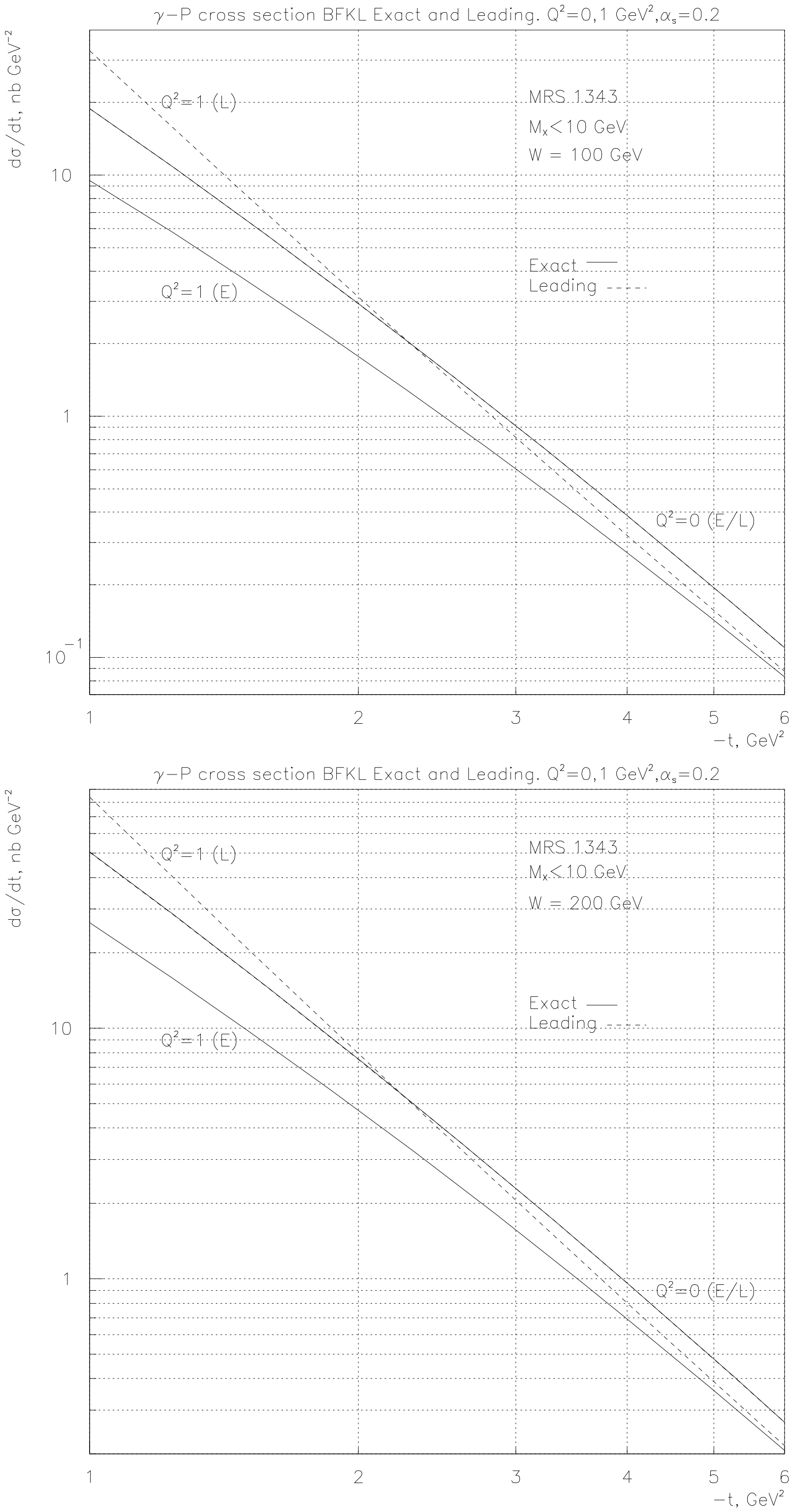

Figure 3.8: $\gamma^* p \to \gamma X$ cross section. Exact BFKL result (solid) compared with the leading pole approximation (dotted) at high $|t|/Q^2$. $W = 100, 200\,\mathrm{GeV}$.

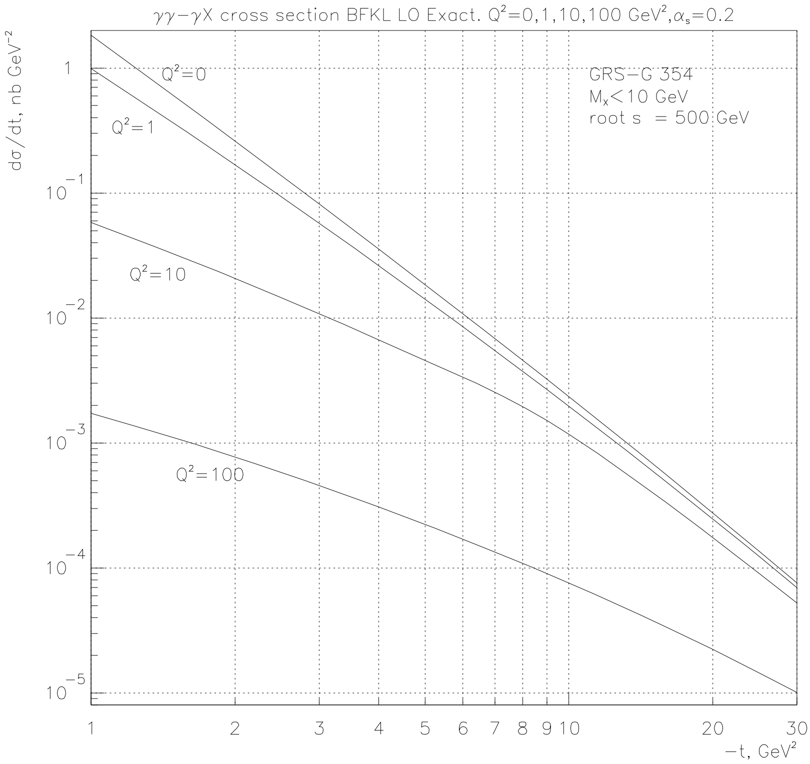

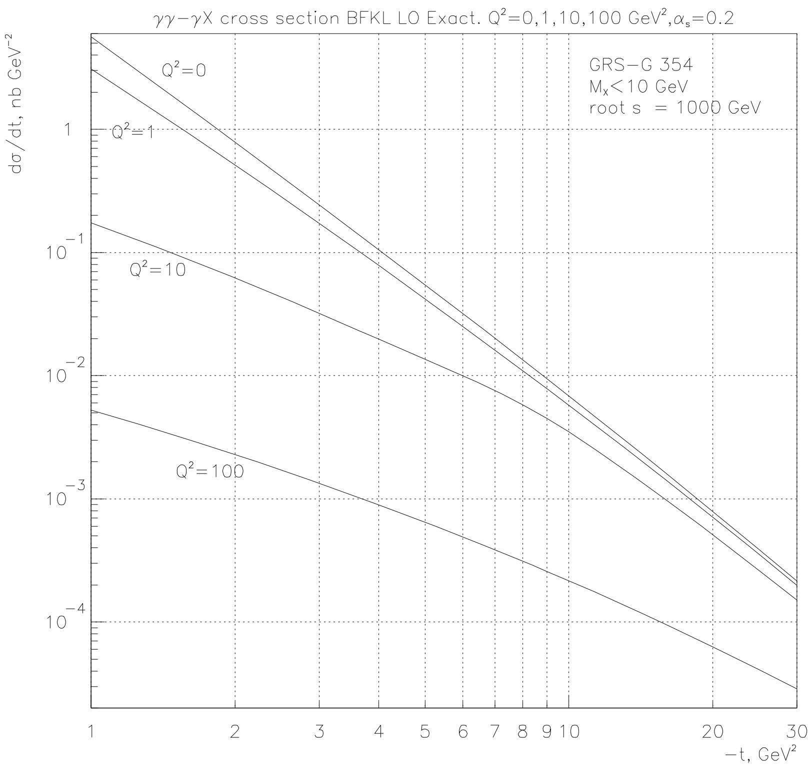

Figure 3.9: $\gamma^*\gamma^* \to \gamma X$ cross section. Exact BFKL result. $\sqrt{s} = 500, 1000\,\mathrm{GeV}$, $Q_1^2 = Q_2^2 = Q^2$.

3.2.1 The Effect of Different Pdfs

Figure (3.10) shows the effect of using different pdfs for the proton and the photon.

For the proton pdfs we chose MRS 1343 [53], CTEQ 144 [54] and GRV HO [55] distributions. We note that these pdfs give very similar results both for the shape and the normalisation of the cross section which is a reflection of the amount of data that is available to constrain parton distributions in the proton.

There are fewer data available on the partonic structure of the photon. This is reflected in the lower plot of figure (3.10) where there is an increased sensitivity of both the normalisation and the slope to the choice of distribution. This makes the choice of pdf more critical than for proton dissociation. We choose the GRS-G [56], SaS-G 1D v2 [57], DG-G [58] and GS-G-96 [59], where it may be used, LO distributions.

Strictly speaking, the use of virtual photon pdf's is wrong when considering values of $|t|$ which are less than the virtuality of the photon since one can no longer think of the photon as being probed by the momentum transfer $|t|$. The results of figure (3.9) should therefore be regarded with caution in the region $Q^2 \gg |t|$, and it is for this reason we have chosen to illustrate the ambiguities in the photon pdfs by only considering real photons on the lower plot of (3.10).

The idea of probe versus probed becomes a grey area when considering interactions of composite particles of similar invariant masses. The interaction between highly virtual photons and protons is a very challenging area theoretically due to this point and to date it remains an unsolved problem. What usually takes place in practice is that the assumption is made that we can distinguish between the probe and the probed.

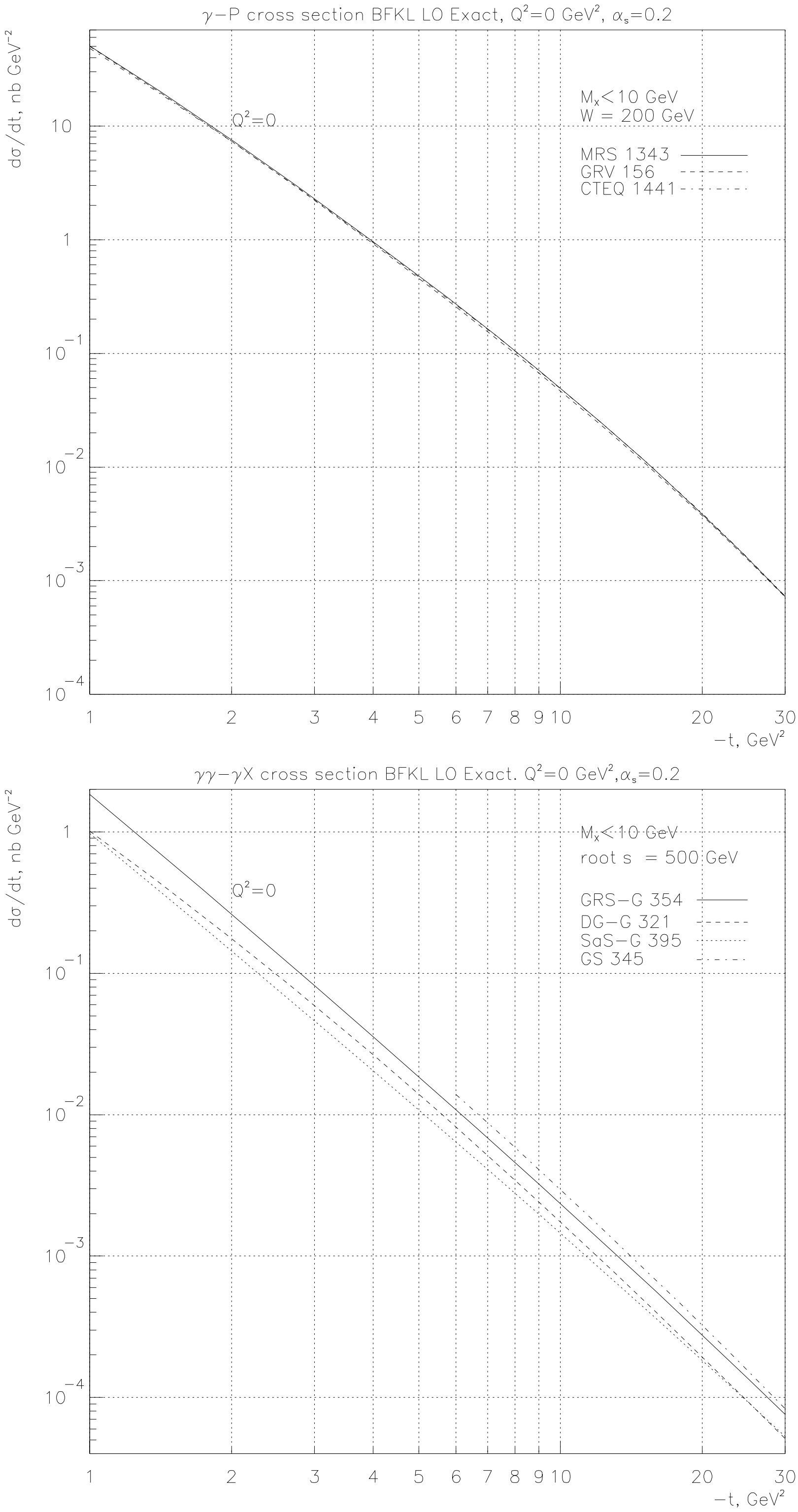

Figure 3.10: $\gamma^* P \to \gamma X$ and $\gamma^*\gamma^* \to \gamma X$ cross sections. Exact BFKL result showing the effect of different pdfs. $W = 200$GeV at HERA and $\sqrt{s} = 500$GeV at the future LC.

3.3 Electron Level Cross Sections

3.3.1 The Weizsäcker-Williams Formulation

At current experiments photon scattering is a subprocess of ee or ep scattering. However, it is satisfactory to leave the γp cross section in its current state. There is no need to fold in the photon flux as the rate is large enough to be seen at HERA, and HERA experimentalists often correct the measured cross sections for the photon flux to get γp cross sections. However, in order to make predictions about the number of events that will be seen at current and future ee experiments we need to fold in the flux of photons from each lepton. For $ee \to ee\gamma Y$, where Y is either a final state photon or the massive diffractive system X, the cross section is given by

$$\sigma_{ee\to ee\gamma Y} = \int dx_a dx_b \frac{dQ_a^2}{Q_a^2}\frac{dQ_b^2}{Q_b^2} dt f_{e\gamma}^{WW}(x_a) f_{e\gamma}^{WW}(x_b) \frac{d\sigma_{\gamma^*\gamma^*\to\gamma Y}}{dt}(x_a x_b s_{ee}, Q_a^2, Q_b^2). \tag{3.3.3}$$

Where, for the $ee \to ee\gamma X$ process (2.1.16), we have ignored any longitudinal polarisation as the integrand is strongly dominated by the $Q^2 = 0$ region. x_a and x_b denote the fractions of longitudinal momenta of the lepton a and b that are carried by the corresponding photons. The region of integration is determined by the geometry of the particular experiment. The Weizsäker and Williams(WW) [60] transverse flux factor is given by

$$f_{e\gamma}^{WW}(x) = \left(\frac{\alpha}{2\pi}\right)\frac{1+(1-x)^2}{x} \tag{3.3.4}$$

where $\alpha(\approx 1/137)$ is the electromagnetic fine structure constant. At first sight this formalism seems to be in contradiction with quantum mechanics. Cross sections are calculated from probability amplitudes, where the different amplitudes are added then the square taken to get the cross section. What is done here is to view the process as two sequential events. This is accurate in the limit of low Q^2 where the probabilities of the interaction $\propto \sigma_{\gamma^*\gamma^*\to\gamma\gamma}$ and the photon emission $f(x)$ can be separately calculated and multiplied.

Comment: Numerical Considerations

In calculating the integrated ee cross sections it would first seem appropriate to use the WW approximation as given in (3.3.3) and use the full expressions for photon-photon scattering derived from the expressions for $I^{\nu}_{\gamma^*\gamma}$ given by (2.2.57) and (2.2.58). All integrations then being performed numerically. Unfortunately, this is too excessive on computing time, yielding this method to be too unwieldy. In considering the single dissociation process we see from (3.2.1) that the conformal weight (ν) and the Fourier variable ($\gamma(z)$) integrations must be nested inside the momentum fraction (x) integration in order to calculate $\gamma^*\gamma^*$ cross section. Further levels of nesting are needed in the subsequent integrations and this overall depth of nesting ensures that the run time of any program to calculate ee cross sections becomes too large to make the use of (3.3.3) feasible. We therefore would like to approximate (3.3.3) to reduce the complexity of the numerical evaluations that have to be carried out without reducing the accuracy overtly.

3.3.2 Improved WW with Anti-Tagged Leptons

From (2.3.76), (2.4.90) and (3.3.3), setting $Q_a^2 = Q_b^2 = Q^2$, we deduce that in the limit of large Q^2 the $ee \to ee\gamma X$ and $ee \to ee\gamma\gamma$ cross sections depend on Q^2 as $1/Q^6$ and $1/Q^8$ respectively. We therefore concentrate our analysis on the photoproduction limit where the rate will be greatest, corresponding to anti-tagging the outgoing leptons at an angle θ_{tag} i.e. discounting events where the leptons are scattered at an angle greater than the tag angle. From (2.3.81), (2.4.93) and (2.4.94) we see that in the limit of $Q^2 \to 0$ that the photon subprocess becomes independent of Q^2. To first approximation we may make the replacement

$$\sigma_{\gamma^*\gamma^*\to\gamma X}(x_a x_b s_{ee}, Q_a^2, Q_b^2, t) \to \sigma_{\gamma^*\gamma^*\to\gamma X}(x_a x_b s_{ee}, 0, 0, t), \tag{3.3.5}$$

which allows us to perform the integrations over Q_a^2 and Q_b^2 to get

$$\sigma_{ee\to ee\gamma X} = \int dx_a dx_b dt \, \frac{d\sigma_{\gamma^*\gamma^*\to\gamma X}(x_a x_b s_{ee})}{dt} \\ f^{WW}_{e\gamma}(x_a) \log\left(\frac{Q^2_{a\,max}}{Q^2_{a\,min}}\right) f^{WW}_{e\gamma}(x_b) \log\left(\frac{Q^2_{b\,max}}{Q^2_{b\,min}}\right). \tag{3.3.6}$$

Care must be taken when using the above expression, at a critical value of Q_c^2 the approximation of using the real photon cross section breaks down and one must always ensure that the upper limit of integration in Q^2 is always below this critical value. Lebedev [61] carried out an analysis of the corrections to the above expression by considering the general vector dominance model (GVDM) [62] to introduce a Q^2 dependence to the real photon cross section. It was found at HERA that the corrections to the WW approximation were of the order of 2% for total hadronic photoabsorbtion cross section. Frixione et al. [63] examined the corrections to (3.3.3) for photoproduction by considering the first correction to the logarithmically enhanced flux factor whilst neglecting any corrections to the real photon cross section, GVDM or otherwise. At the energies accessible at HERA it was determined that the first correction to the photon distribution is of order 5 to 10%. We take these corrections into account and use the result of [63], which we reproduce the main features of here.

We consider the t, Q_b^2, x_b integrated cross section which is equivalent to the electroproduction process

$$e^-(p_1) + e^+(p_2) \to e^-(p_1^{'}) + H \tag{3.3.7}$$

where for us the H system is either $e^+\gamma\gamma$ or $e^+\gamma X$ but in principle could be a generic hadronic system. In terms of the variables x and Q^2 the differential cross section is given by

$$d\sigma = \frac{\alpha}{Q^4}\frac{W^{\mu\nu}T_{\mu\nu}}{16\pi s}dxdQ^2 \tag{3.3.8}$$

where $s = 2p_1 \cdot p_2, p_1^2 = p_1^{'2} = m_e^2, q = p_1 - p_1^{'}, q^2 = -Q^2$ and as usual $T_{\mu\nu}$ and $W^{\mu\nu}$ are the lepton and hadron tensors given by

$$T_{\mu\nu} = 4\left(p_{1\mu}p_{1\nu}^{'} + p_{1\mu}^{'}p_{1\nu} + \frac{q^2}{2}g_{\mu\nu}\right) \tag{3.3.9}$$

and

$$\begin{aligned} W^{\mu\nu} &= W_1(q^2, p_2\cdot q)\left(-g^{\mu\nu} + \frac{q^\mu q^\nu}{q^2}\right) \\ -\frac{q^2}{(p_2\cdot q)^2}&W_2(q^2, p_2\cdot q)\left(p_2^\mu - \frac{p_2\cdot q}{q^2}q^\mu\right)\left(p_2^\nu - \frac{p_2\cdot q}{q^2}q^\nu\right) \end{aligned} \tag{3.3.10}$$

As the hadron tensor may not be singular in the photoproduction limit the poles in

(3.3.10) must be fake. Under this restriction we obtain in the limit of vanishing Q^2

$$W_2(q^2, p_2 \cdot q) = W_1(0, p_2 \cdot q) + \mathcal{O}(q^2) \tag{3.3.11}$$

and we drop the terms of order q^2. After the contraction of the tensors and the simple integration over q^2 we arrive at the following expression

$$d\sigma_{e^-e^+\to eH} = f_{e\gamma}(x)\sigma_{\gamma e^+\to H}(0, p_2.q)dx \tag{3.3.12}$$

where the corrected photon distribution function $f_{e\gamma}(x)$ is given by

$$f^c_{e\gamma}(x) = -\frac{\alpha}{2\pi}\left[2m_e^2\left(\frac{1}{Q^2_{min}} - \frac{1}{Q^2_{max}}\right) + \frac{1+(1-x)^2}{x}\log\left(\frac{Q^2_{max}}{Q^2_{min}}\right)\right]. \tag{3.3.13}$$

We must now determine the two integration limits Q^2_{max} and Q^2_{min}. In terms of the lab frame variables E the energy of the incoming electron and $\theta(\ll 1)$, the angle of scatter of the electron, we get

$$Q^2 = \frac{m_e^2x^2}{1-x} + E^2(1-y)\theta + \mathcal{O}(E^2\theta^4, m_e^2\theta^2, m_e^4/E^2) \tag{3.3.14}$$

where we may freely drop the terms of order $E^2\theta^4, m_e^2\theta^2$ and m_e^4/E^2 with no loss of significant accuracy. The values of Q^2_{min} and Q^2_{max} obtained when $\theta = 0$ and $\theta = \theta_{tag}$ respectively. Thus the final expression for the corrected photon distribution function is given by

$$\begin{aligned} f^c_{e\gamma}(x) &= \frac{\alpha}{2\pi}\left\{2(1-x)\left[\frac{m_e^2x}{E^2(1-x)^2\theta^2_{tag} + m_e^2x^2} - \frac{1}{x}\right]\right. \\ &+ \left.\frac{1+(1-x)^2}{x}\log\left(\frac{E^2(1-x)^2\theta^2_{tag} + m_e^2x^2}{m_e^2x^2}\right)\right\} \end{aligned} \tag{3.3.15}$$

Our final expression for the ee cross section is thus

$$\sigma_{ee\to ee\gamma X} = \int dx_a dx_b dt\, \frac{d\sigma_{\gamma\gamma\to\gamma X}(x_a x_b s_{ee})}{dt} f^c_{e\gamma}(x_a) f^c_{e\gamma}(x_b) \tag{3.3.16}$$

3.3.3 Experimental Geometry and Event Number Predictions

In order to evaluate (3.3.16) it is necessary to determine the bounds of integration from the following pieces of information.

- The angle at which leptons are (anti-)tagged.
- The minimum acceptance angle for the detection of final state photons.
- The minimum acceptance energy for the detection of final state photons.

For anti-tagged leptons the relevant cuts may be easily extracted. Consider the frame where the z-axis is defined by the axis of the ee pair.

$$\begin{aligned} e^- &= E(1,0,0,1) \\ e^+ &= E(1,0,0,-1) \end{aligned} \tag{3.3.17}$$

where we have ignored the mass of the electron and $E = 0.5\sqrt{s_{ee}}$. As we are anti-tagging at a small angle we may approximate the 4-vector of photon $a(b)$ as real and collinear:

$$\begin{aligned} q_a &= x_a E(1,0,0,1) \\ q_b &= x_b E(1,0,0,-1) \end{aligned} \tag{3.3.18}$$

Remembering that this is exactly the frame that was used in the derivation of the photon-photon impact factor we recall (2.1.7) and approximate the 4-vector of the momentum transfer in the limit of small $|t|/s, Q^2/s$ as

$$q = \sqrt{|t|}(0,0,1,0) \tag{3.3.19}$$

The $x_{a(b)}$ limits for the production of a final state photon

Combining (3.3.17),(3.3.18) and (3.3.19) allows us to define the upper limit of the x integration in terms of the angle of acceptance of the final state photon, θ_γ,s and t,

$$x_{a(b)\,\max} = \frac{2\sqrt{|t|}}{\sqrt{s_{ee}}\tan\theta_\gamma} \tag{3.3.20}$$

The lower limit of the x integration is given by the acceptance of the detector on the energy of the photon, $E_{\gamma\, min}$

$$x_{a(b)\,\min} = \frac{2E_{\gamma\, min}}{\sqrt{s_{ee}}} \tag{3.3.21}$$

Again we have used (3.3.19) for the 4-vector of the momentum transfer in the $\gamma\gamma$ system.

The x limits from the production of the final state dissociative system

For photon dissociation we only require that the mass of the diffractive system be less than the value M_X. This constraint translates into a minimum x value for the momentum fraction of the struck quark in the photon, see (3.2.2).

The high energy approximation

The limits $x_{a(b)\,min}$ discussed above are satisfactory from the experimental viewpoint. However, we must be conscious of the fact that we must keep to the high energy limit, $s \gg |t|, Q^2 \gg \Lambda^2_{QCD}$, in order for the BFKL equation to remain valid. To control the high energy approximation we define a minimum value for the hard subprocess scatter, $\hat{s}$, where

$$\begin{aligned} \hat{s} &= x_a x_b s_{ee}, \\ \hat{s} &= x x_a x_b s_{ee}, \end{aligned} \tag{3.3.22}$$

for double photon production and single photon production respectively. We choose $\hat{s}_{min} = 10\,\mathrm{GeV}^2$ and $\hat{s}_{min} = 50\,\mathrm{GeV}^2$ for double photon production and $\hat{s}_{min} = 100\,\mathrm{GeV}^2$ and $\hat{s}_{min} = 50\,\mathrm{GeV}^2$ for single photon production. We choose the lower values of $\hat{s}_{min}$ for double photon production purely to boost the rate for this process. Choosing the more conservative higher values for $\hat{s}$ for the single photon production process guarantees that we exclude the contribution from the region where the BFKL equation breaks down ($\hat{s} \approx s_0$). We also take a lower maximum mass for the diffractive system, i.e. we choose $M_X^2 = 10\,\mathrm{GeV}^2$. We take the t lower limit as $1\,\mathrm{GeV}^2$ in order to keep perturbation theory valid and the upper limit as $5\,\mathrm{GeV}^2$ to keep control of the high energy approximation.

Specific Experimental Constraints

The two experiments we would like to make predictions for are LEP and a future LC. For LEP we calculate the cross section at $\sqrt{s_{ee}} = 91\,\mathrm{GeV}$ and $\sqrt{s_{ee}} = 189\,\mathrm{GeV}$ and calculate the number of events with projected integrated luminosities of $150\,\mathrm{pb}^{-1}$ and $50\,\mathrm{pb}^{-1}$ for the two data samples. The LEP tag angle 33 mrad and the thresholds for photon detection angle and energy, $|\cos\theta_\gamma| < 0.96$ and $E_\gamma > 300\,\mathrm{MeV}$ are used as input parameters. However, these parameters are an optimistic set of cuts, there is considerable experimental difficulty in distinguishing between photons and electrons at low angles. We therefore also take more conservative set of parameters, $|\cos\theta_\gamma| < 0.94$ and $E_\gamma > 1\,\mathrm{GeV}$ to alleviate the problem of particle identification.

Our choice of parameters for the calculations for the future LC take into account some of the essential design features [64]. As the future LC will be a single pass machine to achieve the required luminosity the beams must be pinched to a few nm in the vertical direction. This will greatly enhance unwanted electromagnetic effects: beamstrahlung, beam disruption, copious pair production, etc. as each beam interacts with the electromagnetic field of the entire opposing beam. To stop the background produced by such effects each design for a future LC incorporates a conical tungsten mask which covers an angle of $\approx 100\,\mathrm{mrad}$ from the beam direction. Whether or not such a region covered by the mask will be dead, or contain some sampling material is currently under discussion. With a view to taking these considerations into account we take the tag angle for the future LC to be both greater and smaller than that at LEP and discuss a range of both photon acceptance angles and energies. The results are presented for an approximate 6 month run at initial and established c.o.m energies of 500 GeV and 1000 GeV respectively.

We present our results for $ee \to ee\gamma X$ calculated using the GRS-G LO [56] pdf at the future LC in tables (3.1) and (3.2) and at LEP in table (3.3). We conclude that this process is measurable at the future LC (provided that the background can be identified and removed) and that it is not measurable at LEP. Tables (3.4) and (3.5) present our results for the lower rate inclusive process $ee \to ee\gamma\gamma$ at the energies of the future LC. We find that measurement is marginal at the future LC but possible provided that favourable criteria, i.e. very low angle photon and less critically low energy photon detection, are met in the construction of detectors close to the forward and backward regions. Analysis at LEP energies indicates that the rate for $ee \to ee\gamma\gamma$ is too small for the process to be seen there.

future LC $\sqrt{s_{ee}} = 500\,\mathrm{GeV}$, $\int dt\,\mathcal{L} = 5 \cdot 10^4 pb^{-1}$				
θ_{tag} mrad	θ_γ mrad	$E_{\gamma min}$ GeV	$\sigma\, pb$	Events
$\hat{s}_{min} = 100\mathrm{GeV}^2$				
20	100	0.3	0.31	15514
20	100	1	0.29	14399
20	250	0.3	0.14	6793
20	250	1	0.12	5770
20	500	0.3	0.06	2925
20	500	1	0.04	2100
100	100	0.3	0.41	20567
100	100	1	0.37	18499
100	250	0.3	0.18	8982
100	250	1	0.15	7635
100	500	0.3	0.08	3871
100	500	1	0.06	2773
$\hat{s}_{min} = 50\mathrm{GeV}^2$				
20	100	0.3	0.37	18681
20	100	1	0.33	16578
20	250	0.3	0.16	8155
20	250	1	0.15	7404
20	500	0.3	0.09	4334
20	500	1	0.05	2770
100	100	0.3	0.49	24705
100	100	1	0.44	22205
100	250	0.3	0.21	10615
100	250	1	0.19	9737
100	500	0.3	0.11	5695
100	500	1	0.07	3644

Table 3.1: The integrated cross section and number of events for $ee \to ee\gamma X$ at the future LC, $\sqrt{s} = 500$ GeV. Kinematic and experimental constraints as mentioned in the text

future LC $\sqrt{s_{ee}} = 1000\,GeV,\ \int dt\,\mathcal{L} = 5\cdot 10^4 pb^{-1}$				
θ_{tag} mrad	θ_γ mrad	$E_{\gamma min}$ GeV	$\sigma\,pb$	Events
$\hat{s}_{min} = 100\mathrm{GeV}^2$				
20	100	0.3	0.69	34491
20	100	1	0.62	30797
20	250	0.3	0.30	14898
20	250	1	0.27	13357
20	500	0.3	0.15	7624
20	500	1	0.10	4911
100	100	0.3	0.89	44589
100	100	1	0.80	39843
100	250	0.3	0.38	19033
100	250	1	0.34	17217
100	500	0.3	0.20	9823
100	500	1	0.13	6425
$\hat{s}_{min} = 50\mathrm{GeV}^2$				
20	100	0.3	0.78	39168
20	100	1	0.71	35446
20	250	0.3	0.38	18807
20	250	1	0.31	15383
20	500	0.3	0.20	9761
20	500	1	0.12	5904
100	100	0.3	1.01	50455
100	100	1	0.91	45711
100	250	0.3	0.49	24335
100	250	1	0.40	19759
100	500	0.3	0.25	12528
100	500	1	0.15	7574

Table 3.2: The integrated cross section and number of events for $ee \to ee\gamma X$ at the future LC, $\sqrt{s} = 1000$ GeV. Kinematic and experimental constraints as mentioned in the text

LEP $\theta_{tag} = 33$mrad					
$\sqrt{s_{ee}}$	θ_γ mrad	$E_{\gamma min}$ GeV	$\sigma\, pb$	$\int dt\, \mathcal{L}$ pb^{-1}	Events
$\hat{s}_{min} = 100\text{GeV}^2$					
91	280	0.3	$1.5 \cdot 10^{-2}$	180	2.60
91	350	1	$8.8 \cdot 10^{-3}$	180	1.65
189	280	0.3	$5.8 \cdot 10^{-2}$	50	2.85
189	350	1	$3.9 \cdot 10^{-2}$	50	1.91
$\hat{s}_{min} = 50\text{GeV}^2$					
91	280	0.3	$3.8 \cdot 10^{-2}$	180	6.77
91	350	1	$2.5 \cdot 10^{-3}$	180	4.59
189	280	0.3	0.12	50	5.86
189	350	1	$7.0 \cdot 10^{-2}$	50	3.50

Table 3.3: The integrated cross section and number of events for $ee \to ee\gamma X$ at LEP, $\sqrt{s} = 91, 189$ GeV. Kinematic and experimental constraints as mentioned in the text.

future LC $\sqrt{s_{ee}} = 500\,\mathrm{GeV}$, $\int dt\,\mathcal{L} = 5 \cdot 10^4 pb^{-1}$				
θ_{tag} mrad	θ_γ mrad	$E_{\gamma min}$ GeV	$\sigma\,pb$	Events
$\hat{s}_{min} = 10\mathrm{GeV}^2$				
20	100	0.3	$3.82 \cdot 10^{-4}$	19.11
20	100	1	$3.17 \cdot 10^{-4}$	15.87
20	250	0.3	$8.90 \cdot 10^{-5}$	4.45
20	250	1	$7.51 \cdot 10^{-5}$	3.75
20	500	0.3	$1.30 \cdot 10^{-5}$	0.65
20	500	1	$1.21 \cdot 10^{-5}$	0.60
100	100	0.3	$4.86 \cdot 10^{-4}$	24.29
100	100	1	$4.04 \cdot 10^{-4}$	20.22
100	250	0.3	$1.12 \cdot 10^{-4}$	5.60
100	250	1	$9.46 \cdot 10^{-5}$	4.73
100	500	0.3	$1.63 \cdot 10^{-5}$	0.81
100	500	1	$1.51 \cdot 10^{-5}$	0.76
$\hat{s}_{min} = 50\mathrm{GeV}^2$				
20	100	0.3	$2.39 \cdot 10^{-4}$	11.95
20	100	1	$2.37 \cdot 10^{-4}$	11.84
20	250	0.3	$2.13 \cdot 10^{-5}$	1.07
20	250	1	$2.13 \cdot 10^{-5}$	1.07
20	500	0.3	$4.90 \cdot 10^{-7}$	0.02
20	500	1	$4.90 \cdot 10^{-7}$	0.02
100	100	0.3	$3.06 \cdot 10^{-4}$	15.29
100	100	1	$3.03 \cdot 10^{-4}$	15.15
100	250	0.3	$2.71 \cdot 10^{-5}$	1.36
100	250	1	$2.71 \cdot 10^{-5}$	1.36
100	500	0.3	$6.20 \cdot 10^{-7}$	0.03
100	500	1	$6.20 \cdot 10^{-7}$	0.03

Table 3.4: The integrated cross section and number of events for $ee \to ee\gamma\gamma$ at the future LC, $\sqrt{s} = 500$ GeV. Kinematic and experimental constraints as mentioned in the text

future LC $\sqrt{s_{ee}} = 1000\,\text{GeV}$, $\int dt\,\mathcal{L} = 5 \cdot 10^4 pb^{-1}$				
θ_{tag} mrad	θ_γ mrad	$E_{\gamma min}$ GeV	$\sigma\, pb$	Events
$\hat{s}_{min} = 10\text{GeV}^2$				
20	100	0.3	$4.84 \cdot 10^{-4}$	24.20
20	100	1	$4.03 \cdot 10^{-4}$	20.17
20	250	0.3	$1.10 \cdot 10^{-4}$	5.51
20	250	1	$9.30 \cdot 10^{-5}$	4.65
20	500	0.3	$1.60 \cdot 10^{-4}$	0.80
20	500	1	$1.48 \cdot 10^{-5}$	0.74
100	100	0.3	$6.02 \cdot 10^{-4}$	30.08
100	100	1	$5.02 \cdot 10^{-4}$	25.11
100	250	0.3	$1.35 \cdot 10^{-4}$	6.80
100	250	1	$1.14 \cdot 10^{-4}$	5.74
100	500	0.3	$1.96 \cdot 10^{-5}$	0.98
100	500	1	$1.82 \cdot 10^{-5}$	0.91
$\hat{s}_{min} = 50\text{GeV}^2$				
20	100	0.3	$3.07 \cdot 10^{-4}$	15.33
20	100	1	$3.04 \cdot 10^{-4}$	15.18
20	250	0.3	$2.69 \cdot 10^{-5}$	1.34
20	250	1	$2.69 \cdot 10^{-5}$	1.34
20	500	0.3	$6.12 \cdot 10^{-7}$	0.03
20	500	1	$6.12 \cdot 10^{-7}$	0.03
100	100	0.3	$3.83 \cdot 10^{-4}$	19.15
100	100	1	$3.79 \cdot 10^{-4}$	18.97
100	250	0.3	$3.34 \cdot 10^{-5}$	1.67
100	250	1	$3.34 \cdot 10^{-5}$	1.67
100	500	0.3	$7.58 \cdot 10^{-7}$	0.04
100	500	1	$7.58 \cdot 10^{-7}$	0.04

Table 3.5: The integrated cross section and number of events for $ee \to ee\gamma\gamma$ at the future LC, $\sqrt{s} = 1000$ GeV. Kinematic and experimental constraints as mentioned in the text

3.4 The Normalisation of BFKL Cross Sections

The LO BFKL equation has two parameters which are not determined by the theory. This ambiguity has significant effects on its predictive power. The scale s_0 which appears in the logarithm of the centre of mass energy s, and μ^2 the scale at which α_s is evaluated are both free in LO, a full next to leading log analysis is required to gain insight into the physical origin of these two scales. In order to make predictions about cross sections from a purely LO perspective one must draw upon other sources of information both theoretical and experimental. Discussion about our own choices and those of others is presented here.

Our choice of the scale s_0 for the hard scatter which mediates the dissociative process $\gamma^* q \to \gamma q$ is simply the next largest scale apart from s i.e. $\max(|t|, Q^2)$. For the double photon production process $\gamma^*\gamma^* \to \gamma\gamma$ we chose a fixed value for the $z(= 3\alpha_s/\pi \log(s/s_0))$ energy variable, but in obtaining the $ee \to ee\gamma\gamma$ rate we are forced to make a choice and so again use the next largest scale form for s_0. The motivation for our choice comes from the accuracy of a previous study on vector meson production using BFKL dynamics [33]. The authors of that study perform the calculation of the function I^V_ν, corresponding to (2.2.34) of our work but with the replacement of a non-relativistic wavefunction as a model for the vector meson. Their choice for s_0 is

$$s_0 = |t| + Q^2 + m_V^2 \tag{3.4.23}$$

where $|t|, Q^2$ have their usual meanings and m_V is the mass of the vector meson. This choice was found to give a good agreement with the data [34]. We must be critical of our own choice of s_0 in light of (3.4.23) where the value is an analytic function of all the "other" invariant masses of the interaction. Our own choice does not have this analyticity. The consequence of our choice of largest "other" scale is displayed in the graphs where the central hard scatter is mediated by $\gamma q \to \gamma q$. There appears to be an unnatural change of the t slope at the point where $|t|$ becomes larger than Q^2 marking the region where we change s_0 from being Q^2 to $|t|$.

In inventing a functional form for s_0 based on the other scales that appear in the problem one is forced to consider all alternatives equally: experimental analysis is the obvious filtering mechanism.

For the authors of [38] s_0 is derived from considering the dynamics of the quarks on either end of the gluon ladder, arguing that typical rapidities of the gluons inside the ladder must lie between the rapidities of the quarks on the ends. The logarithms of energy at each order arise from the internal rapidity integration and thus s_0 is determined by the components of the 4-vectors of the quarks on the ends of the ladder. After identifying the transverse momenta as being of the order of Q they arrive at

$$s_0 = cQ_aQ_b \tag{3.4.24}$$

where c is the unknown scaling introduced and is subsequently identified with the longitudinal components of the quark 4-vectors and is given by

$$c = \frac{1}{\rho_{a\,\mathrm{max}}\rho_{b\,\mathrm{max}}} \tag{3.4.25}$$

where $\rho_{i\,\mathrm{max}}$ is typical maximum value of the Sudakov component given in (2.1.3). In the high energy limit this is estimated to be 0.1 giving

$$s_0 = 10^2 Q_aQ_b \tag{3.4.26}$$

This choice of $\rho_{i\,max}$ must be compared with the explicit value of 0.5 assumed in the non relativistic derivation of the vector meson wavefunction in [33], and it must also be pointed out that the variation of this maximum has a large effect on the normalisation of their cross section. The $\gamma^*\gamma^*$ total cross section has also been derived in the BFKL framework by Bartels et al. [39] where little discussion was made as to the origin of the unknown scales and s_0 is simply given by

$$s_0 = Q_aQ_b. \tag{3.4.27}$$

Throughout the work done in this thesis we have chosen a value for the strong coupling constant of $\alpha_s = 0.2$. This choice is motivated by the experimentally fitted value for vector meson production [34] data and gaps between jets data [27, 28]. In all other phenomenological studies of BFKL mechanics a similar value has been used;

0.25 for the calculation of vector meson production [33] and 0.22 was used by [39] for the calculation of the $\gamma^*\gamma^*$ total cross section. In keeping with their discussion on the origin of s_0 Brodsky et al. [38] give a detailed description of the dynamics of their choice of the scale at which the coupling is to be evaluated. They follow the arguments of [65] where the scale is determined by considering the one loop correction to the gluon propagator. The insistence on the disappearance of the quark loop contribution after integration over the loop momenta $\mathbf{k}^2$ gives us a value for the scale at which the coupling must be evaluated

$$\mu^2 = c_\mu Q_a Q_b \tag{3.4.28}$$

where $c_\mu = e^{-5/3}$ in the $\overline{MS}$ renormalisation scheme. They point out that this result strictly only applies to the BFKL Born, or two gluon, term in the full expansion and go on to approximate the value of the running coupling by this value when considering the entire BFKL series.

Brodsky et al. also identify an approach that can be used to determine the cut off scale defined to uphold the validity of the high energy approximation. This is expressed as

$$s > \frac{\kappa Q_a Q_b}{x_a x_b} \tag{3.4.29}$$

where κ is determined by demanding that the two gluon exchange graph gives a larger contribution than the electromagnetic contribution to $\gamma^*\gamma^* \to q\overline{q}$ in the high energy limit. With a value of 0.2 for the strong coupling constant the value of κ is approximately 100.

To illustrate the severity of the effects of altering the coupling and the unknown scale s_0 in figure (3.11) we show the effect on the normalisation of the $\gamma^* q \to \gamma q$ cross section of a $\pm 2.5\%$ alteration of the value of the coupling constant, and the effect of taking $s_0 \to 0.5 s_0$ and $s_0 \to 2 s_0$.

Which, if any, of the above schemes for choosing α_s and s_0 is the best can only be understood by going beyond the LLA where α_s starts to run and there is a non trivial dependence upon s_0 [20]. Data may also be used to suggest the correct procedure. At present we are not able to draw any firm conclusions.

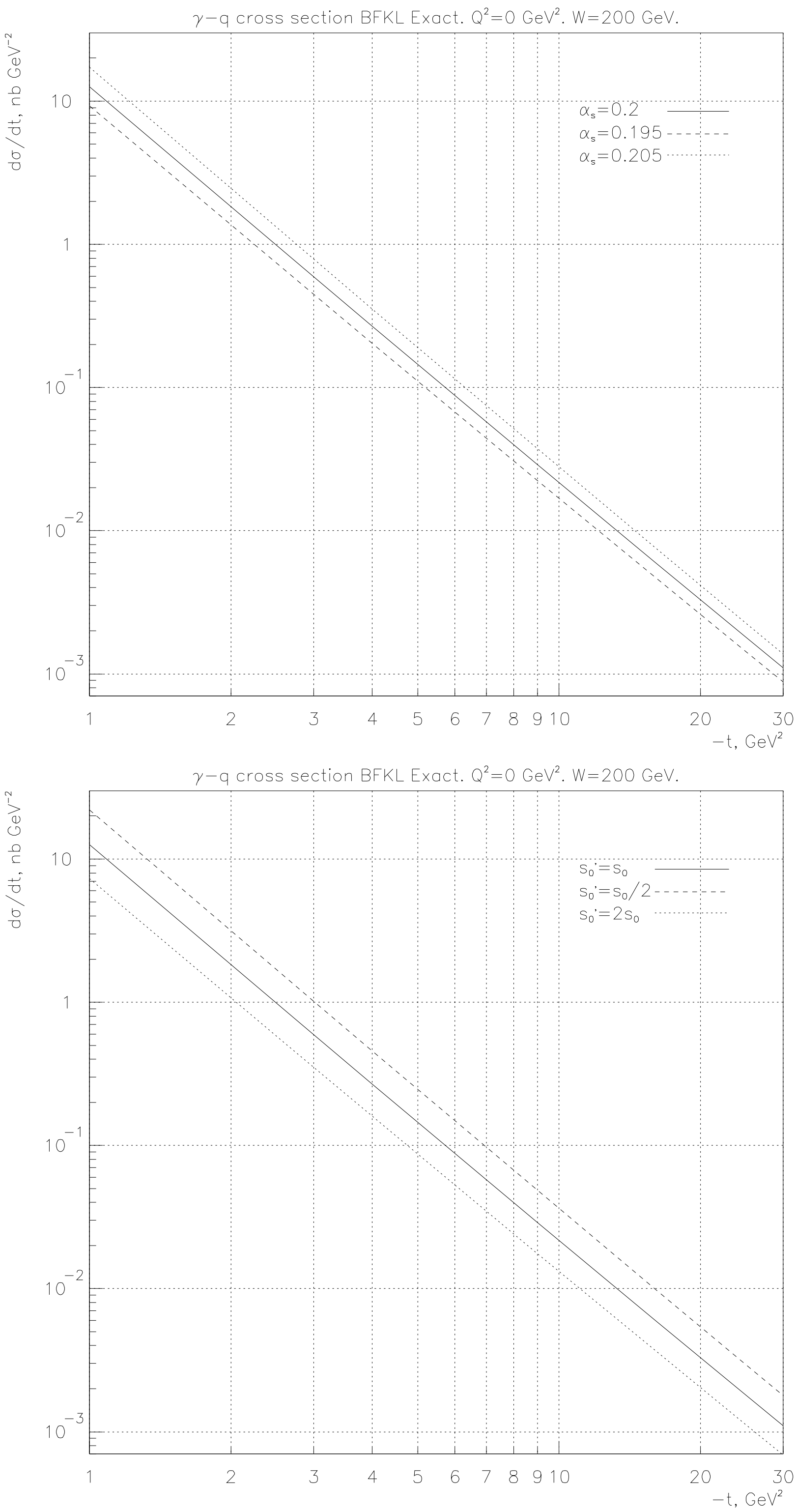

Figure 3.11: γq cross section. Exact BFKL result showing the effect of different values of the strong coupling α_s and different values for s_0. $\sqrt{s} = 200\text{GeV}$.

3.5 Example FORTRAN Program

Here we include an example of FORTRAN code used to produce the cross section for $ee \to ee\gamma X$.

```
!!!!!!!!!!!!!!!!!!!!!!!!!!!!!!!!!!!!!!!!!!!!!!!!!!!!!!!!!!!!!!!!!!!
! Calculation of the ee-> ee\gamX integrated cross section at
! a future linear collider.
!!!!!!!!!!!!!!!!!!!!!!!!!!!!!!!!!!!!!!!!!!!!!!!!!!!!!!!!!!!!!!!!!!!
! The diffractive high |t| mechanism is gam*q->gamq via BFKL
! Pomeron exchange. This version of the program is for the case
! when both electrons are anti-tagged which is far and away the
! highest rate case and takes a finite time to run !
!!!!!!!!!!!!!!!!!!!!!!!!!!!!!!!!!!!!!!!!!!!!!!!!!!!!!!!!!!!!!!!!!!!
! If the produced photon is out of range of the detector then it
! must die ! (x-section is defined as zero). The result for the
! threshold angle only holds for anti-tagged leptons.
!!!!!!!!!!!!!!!!!!!!!!!!!!!!!!!!!!!!!!!!!!!!!!!!!!!!!!!!!!!!!!!!!!!

IMPLICIT REAL*8 (a-h,o-z)

!!!!!!!!!!!!!!!!!!!!!!!!!!!!!!!!!!!!!!!!!!!!!!!!!!!!!!!!!!!!!!!!!!!
! Data blocks to perform integration.

REAL*8 rtseed(3),smind(2),tagd(2),gangd(3),egmind(2)

!!!!!!!!!!!!!!!!!!!!!!!!!!!!!!!!!!!!!!!!!!!!!!!!!!!!!!!!!!!!!!!!!!!
! \sqrt{s}= 500, 1000 and 2000 GeV through the running of the
! future LC. 50,100 GeV^2 to validate high energy approximation.
! Future LC smaller beam diam. (20 mrad) possible dead region
! (100 mrad). Photon detect angle 100,250,500 mrad. Photon
! threshold 300 MeV and 1 GeV.

data rtseed   /2.d3,1.d3,5.d2/
data smind    /1.d2,5.d1/
data tagd     /1.d-1,2.d-2/
data gangd    /5.d-1,2.5d-1,1.d-1/
data egmind   /1.d0,3.d-1/

! LEP sqrt{s}=91,189 GeV.\hat{s}_min=same.thetatag=33 mrad.
! egammamin=same, coupled with egamang=280,350 mrad

!!!!!!!!!!!!!!!!!!!!!!!!!!!!!!!!!!!!!!!!!!!!!!!!!!!!!!!!!!!!!!!!!!!
! Common blocks, pretty self explanatory.
```

```
COMMON /fixed/  pi,euler,alphas,alphaem,emass
COMMON /var/    egmin,tag,gang,rtsee,smin
COMMON /kount2/ kount2

!!!!!!!!!!!!!!!!!!!!!!!!!!!!!!!!!!!!!!!!!!!!!!!!!!!!!!!!!!!!!!!!!!
! External functions calls from the main routine. D0... is NAG
! and f is later in this file.

external D01BDF,f

!!!!!!!!!!!!!!!!!!!!!!!!!!!!!!!!!!!!!!!!!!!!!!!!!!!!!!!!!!!!!!!!!!
! Mathematical and physical constants (some quasi!).

pi      = 4*datan(1.0d0)
euler   = 0.5772156649d0
alphas  = 0.2d0
alphaem = 1.0d0/1.37d2
emass   = 5.d-4 ! GeV

!!!!!!!!!!!!!!!!!!!!!!!!!!!!!!!!!!!!!!!!!!!!!!!!!!!!!!!!!!!!!!!!!!
! Write the result somewhere.

open(11,file='FLC.dat')
write(11,*)'Future LC results for one produced photon and one'
write(11,*)'photon dissociating with anti-tagging of both leptons.'

!!!!!!!!!!!!!!!!!!!!!!!!!!!!!!!!!!!!!!!!!!!!!!!!!!!!!!!!!!!!!!!!!!
! Put the loops in for the data.

do i = 1,3
   rtsee = rtseed(i)
   do j = 1,2
      smin = smind(j)
      do k = 1,2
         tag = tagd(k)
         do l = 1,3
            gang = gangd(l)
            do m = 1,2
               egmin = egmind(m)

!!!!!!!!!!!!!!!!!!!!!!!!!!!!!!!!!!!!!!!!!!!!!!!!!!!!!!!!!!!!!!!!!!
! This part only does the |t| integration (1-D). The rest are
! nested in subroutines. t_max preserve hienlim (combined with
! shatmin)
```

```
               a=1.d0
               b=5.d0

               epsrel = 1.d-2

               call D01BDF(f,a,b,epsabs,epsrel,result,abserr)

!!!!!!!!!!!!!!!!!!!!!!!!!!!!!!!!!!!!!!!!!!!!!!!!!!!!!!!!!!!!!!!!!!
! Result in picobarns. Factor of 2 as we don't care which photon
! dissociates.

               cross  = 2.d0*3.89d8*result

!!!!!!!!!!!!!!!!!!!!!!!!!!!!!!!!!!!!!!!!!!!!!!!!!!!!!!!!!!!!!!!!!!
! 50000 pb^-1 for future LC, 180 pb^-1 for LEP low s
! and 50pb^-1 for high s.

               zlum   = 50000.d0

!!!!!!!!!!!!!!!!!!!!!!!!!!!!!!!!!!!!!!!!!!!!!!!!!!!!!!!!!!!!!!!!!!
! Total events over the ``lifetime'' of the experiment

               events = cross*zlum

!!!!!!!!!!!!!!!!!!!!!!!!!!!!!!!!!!!!!!!!!!!!!!!!!!!!!!!!!!!!!!!!!!
! Write the results in the same place as before

               write(11,*)'NEW DATA SET'
               write(11,*)'\sqrt{s} = ',rtsee,' GeV'
               write(11,*)'\hat{s}_min= ',smin,' GeV^2'
               write(11,*)'Electron anti tag= ',tag,' rad'
               write(11,*)'Photon detection minimum ',gang,' rad'
               write(11,*)'E_gamma threshold= ',egmin,' GeV'
               write(11,*)'Sigma = ',cross,' pb'
               write(11,*)'Which means ',events,' events at'
               write(11,*)'Luminosity = ',zlum,' pb^-1'

!!!!!!!!!!!!!!!!!!!!!!!!!!!!!!!!!!!!!!!!!!!!!!!!!!!!!!!!!!!!!!!!!!
! Wrap it up.

            enddo
         enddo
      enddo
   enddo
enddo
```

```
stop
end

!!!!!!!!!!!!!!!!!!!!!!!!!!!!!!!!!!!!!!!!!!!!!!!!!!!!!!!!!!!!!!!!!
! The integrand for the t integration.

real*8 function f(x)
  implicit real*8(a-h,o-z)

!!!!!!!!!!!!!!!!!!!!!!!!!!!!!!!!!!!!!!!!!!!!!!!!!!!!!!!!!!!!!!!!!
! Declare you NAG parameters and define your NAG arrays.

  PARAMETER (ndim=3,maxpts=10000000*ndim,lenwrk=(ndim*2)* &
       (1+maxpts/(2**ndim+2*ndim*ndim+2*ndim+1)))
  REAL*8 a(ndim),b(ndim),wrkstr(lenwrk)

!!!!!!!!!!!!!!!!!!!!!!!!!!!!!!!!!!!!!!!!!!!!!!!!!!!!!!!!!!!!!!!!!
! Common blocks again. Common error is getting these defined
! inconsistently in different locations.

  COMMON /var/    egmin,tag,gang,rtsee,smin
  COMMON /intvar/ xq,xa,xb,t
  COMMON /kount2/ kount2

!!!!!!!!!!!!!!!!!!!!!!!!!!!!!!!!!!!!!!!!!!!!!!!!!!!!!!!!!!!!!!!!!
! External integration routine and the integrand for the three x
! integrations. We integrate over t

  external D01FCF,bfkl

  t = x

!!!!!!!!!!!!!!!!!!!!!!!!!!!!!!!!!!!!!!!!!!!!!!!!!!!!!!!!!!!!!!!!!
! The maximum squared mass of the diffractive system

  Mx2 = 1.d1

!!!!!!!!!!!!!!!!!!!!!!!!!!!!!!!!!!!!!!!!!!!!!!!!!!!!!!!!!!!!!!!!!
! Define the lower limits for x_a, the longitudinal momentum of
! the electron taken by the photon. This is defined by how hard
! the final state photon must be in order to be detected. The
! upper limit is set by the angle that the final state photon can
! be detected at. We only insist that the second photon gets
! diffracted into a massive system of min mass M_X=\sqrt{10} GeV,
```

```
! we don't insist on finding it. This means that we are free to
! define the x_b limits as we wish \approx(0,1).

  a(1) = egmin/(0.5d0*rtsee)
  a(2) = 0.d0
  a(3) = 1.d0/(Mx2/t+1.d0)
  b(1) = dsqrt(t)/(0.5*rtsee*dtan(gang))
  b(2) = 1.d0
  b(3) = 1.d0

!!!!!!!!!!!!!!!!!!!!!!!!!!!!!!!!!!!!!!!!!!!!!!!!!!!!!!!!!!!!!!!!!
! Do the three x integrations.

  eps = 1.d-2
  ifail = -1
  minpts=0

  CALL D01FCF(ndim,a,b,minpts,maxpts,bfkl,eps,acc,lenwrk,wrkstr, &
      res,ifail)

  f = res
  kount2 = kount2 + 1

  return
end function f

!!!!!!!!!!!!!!!!!!!!!!!!!!!!!!!!!!!!!!!!!!!!!!!!!!!!!!!!!!!!!!!!!!
! The function called to by D01FCF to give a value of the gamgam
! x-section for a particular value of xa,xb,t,. i.e the value of
! this function is that in the paper modulo flux factors  and the
! replacement of s->xa*xb*xq*s.

real*8 function bfkl(ndim,x)
  IMPLICIT REAL*8 (a-h,o-z)

!!!!!!!!!!!!!!!!!!!!!!!!!!!!!!!!!!!!!!!!!!!!!!!!!!!!!!!!!!!!!!!!!!
! More NAG parameters and arrays.

  PARAMETER (lw=800,liw=lw/4)
  REAL*8 x(ndim),w(lw)
  INTEGER il(liw)

!!!!!!!!!!!!!!!!!!!!!!!!!!!!!!!!!!!!!!!!!!!!!!!!!!!!!!!!!!!!!!!!!!
! Pdflib number and character arrays.
```

```
  REAL*8 value(20)
  character*20 parm(20)

!!!!!!!!!!!!!!!!!!!!!!!!!!!!!!!!!!!!!!!!!!!!!!!!!!!!!!!!!!!!!!!!!!!
! Watch those common blocks.

  COMMON /fixed/  pi,euler,alphas,alphaem,emass
  COMMON /var/    egmin,tag,gang,rtsee,smin
  COMMON /intvar/ xq,xa,xb,t
  COMMON /kount/  kount

!!!!!!!!!!!!!!!!!!!!!!!!!!!!!!!!!!!!!!!!!!!!!!!!!!!!!!!!!!!!!!!!!!!
! Call the final integration over \nu.

  external D01AJF,ppamp

!!!!!!!!!!!!!!!!!!!!!!!!!!!!!!!!!!!!!!!!!!!!!!!!!!!!!!!!!!!!!!!!!!!
! Set the variables to be integrated over by D01FCF.

  xa = x(1)
  xb = x(2)
  xq = x(3)

!!!!!!!!!!!!!!!!!!!!!!!!!!!!!!!!!!!!!!!!!!!!!!!!!!!!!!!!!!!!!!!!!!!
! The nu integration is symmetric under \nu->-\nu, factor of two
! in result. Low values of \nu accurate.

  a = 0.d0   !numin
  b = 3.d0   !numax

!!!!!!!!!!!!!!!!!!!!!!!!!!!!!!!!!!!!!!!!!!!!!!!!!!!!!!!!!!!!!!!!!!!
! integration

  ifail=1
  epsrel = 1.d-2

  CALL D01AJF(ppamp,a,b,epsrabs,epsrel,result,abserr,w,lw, &
              iw,liw,ifail)

!!!!!!!!!!!!!!!!!!!!!!!!!!!!!!!!!!!!!!!!!!!!!!!!!!!!!!!!!!!!!!!!!!!
! Plus-plus result only. Contribution form plus-minus is
! negligible in the Q^2->0 limit. A=G/(2pi^10)*, dsig/dt=A^2/16/pi
! (s dep cancelled). G=2/3 for quark gam scatt. All numbers from
! the amplitude are condensed here
```

```
  ppres= (((alphas**2)*alphaem*2.0d0/9.0d0/t)**2)* &
 ((2*result)**2)/1.6d1/pi

!!!!!!!!!!!!!!!!!!!!!!!!!!!!!!!!!!!!!!!!!!!!!!!!!!!!!!!!!!!!!!!!!!!
! electron energy

  eenergy = 0.5d0*rtsee

!!!!!!!!!!!!!!!!!!!!!!!!!!!!!!!!!!!!!!!!!!!!!!!!!!!!!!!!!!!!!!!!!!!
! The result for the gamgam cross section multiplied by photon
! propagators and flux factors to get the differential x-section
! dsig(ee)/dt/dx_1/dx_2 that we want to integrate to get the
! x-section. To do this we use the approximation given by
! Frixione et al.


  fluxa = 2.d0*(1-xa)*((emass**2)*xa/((eenergy*(1-xa)*tag)**2 &
      +(emass*xa)**2)-1/xa)+(1.d0+(1-xa)**2)/xa*dlog &
       (((eenergy*(1-xa)*tag)**2+(emass*xa)**2)/(emass*xa)**2)

  fluxb = 2.d0*(1-xb)*((emass**2)*xb/((eenergy*(1-xb)*tag)**2 &
      +(emass*xb)**2)-1/xb)+(1.d0+(1-xb)**2)/xb*dlog &
       (((eenergy*(1-xb)*tag)**2+(emass*xb)**2)/(emass*xb)**2)

  qgcross = ((alphaem/2.d0/pi)**2)*ppres*fluxa*fluxb


!!!!!!!!!!!!!!!!!!!!!!!!!!!!!!!!!!!!!!!!!!!!!!!!!!!!!!!!!!!!!!!!!!!
! Photon pdfs: choose your favourite. 354 is GRS-LO.

  Q = dsqrt(t)

  Qhit=0

  parm(1)='NPTYPE'
  parm(2)='NGROUP'
  parm(3)='NSET'
  value(1)=3
  value(2)=5
  value(3)=4
  call pdfset(parm,value)

  call structp(xq,Q,Qhit,anom,upv,dnv,usea,dsea,str,chm,bot, &
    top,gl)
  fpro = (8.1d1/1.6d1*gl +(upv+dnv+2.*(usea+dsea+str+chm)))/xq
```

```
!!!!!!!!!!!!!!!!!!!!!!!!!!!!!!!!!!!!!!!!!!!!!!!!!!!!!!!!!!!!!!!!!!
! pdf*qg cross section = gg cross section

  bfkl = fpro*qgcross

  return
end function bfkl

!!!!!!!!!!!!!!!!!!!!!!!!!!!!!!!!!!!!!!!!!!!!!!!!!!!!!!!!!!!!!!!!!!
! The explicit form for the pp amplitude. We use the leading term
! in the small Q^2 limit, equivalent to MWDI's result.

real*8 FUNCTION ppamp(x)
  IMPLICIT REAL*8 (a-h,o-z)
  COMPLEX*16 wdigam,wgamma,z1

!!!!!!!!!!!!!!!!!!!!!!!!!!!!!!!!!!!!!!!!!!!!!!!!!!!!!!!!!!!!!!!!!!
! Watch it!

  COMMON /fixed/  pi,euler,alphas,alphaem,emass
  COMMON /var/    egmin,tag,gang,rtsee,smin
  COMMON /intvar/ xq,xa,xb,t
  COMMON /kount/  kount

!!!!!!!!!!!!!!!!!!!!!!!!!!!!!!!!!!!!!!!!!!!!!!!!!!!!!!!!!!!!!!!!!!
! \nu
  v = x

!!!!!!!!!!!!!!!!!!!!!!!!!!!!!!!!!!!!!!!!!!!!!!!!!!!!!!!!!!!!!!!!!!
! The BFKL z parameter. The scale in the logarithm is undetermined
! in LLA so we choose to set it as the highest other scale in the
! problem. We wish to impose a cut so that we only ever deal with
! a value of \hat{s} above a fixed value. This is to preserve the
! Regge energy limit.

  shat = xa*xb*xq*rtsee**2

  if (shat.le.smin) then

     ppamp = 0.d0

  else

!!!!!!!!!!!!!!!!!!!!!!!!!!!!!!!!!!!!!!!!!!!!!!!!!!!!!!!!!!!!!!!!!!
```

```
! All those months of algebra reduce nicely to this !!

     z=3*alphas/pi*dlog(shat/t)

     z1 = dcmplx(5.d-1,v)

     chi = -2*(euler+dreal(wdigam(z1)))
     fac2 = dexp(z*chi)
     fac3= v*(1.1d1+1.2d1*v**2)/((0.25d0+v**2)**2) &
            /(1.d0+v**2)*dtanh(pi*v)

     ppamp = fac2*fac3

  endif

  kount = kount + 1

  RETURN
END FUNCTION ppamp

!!!!!!!!!!!!!!!!!!!!!!!!!!!!!!!!!!!!!!!!!!!!!!!!!!!!!!!!!!!!!!!!!!!
! THAT'S ALL FOLKS (EOF)
```

Chapter 4

Conclusions

The aim of this thesis was to use the BFKL equation to predict event rates for high-$|t|$ diffractive photon production at HERA and single and double diffractive photon production at LEP and a future LC. These processes minimise the theoretical uncertainties involved in the calculation which have a non-perturbative nature in origin and provide as clean a test as possible of perturbative QCD in the Regge limit. Apart from the uncertainties in the BFKL equation itself, which will be reduced only when NLO corrections to the kernel and impact factors are known, this goal was achieved. The theoretical benefits are particularly attractive for the double photon production cross section. Unfortunately, our results indicate that this process is not realistically measurable in the foreseeable future. We have therefore also calculated the cross section for $\gamma^* q \to \gamma q$, and embedded it in the diffractive dissociative processes $\gamma^*\gamma^* \to \gamma X$ and $\gamma^* P \to \gamma X$. This introduces the phenomenological uncertainty associated with the parton distribution functions, which is more pronounced in the photon dissociation process. We presented results which can be tested at HERA and a future LC but not at LEP.

Turning to more theoretical points. The calculation of the $\gamma^*\gamma$-Pomeron vertex and its convolution with the BFKL eigenfunctions has been performed almost completely analytically. The techniques used here may well prove useful for future calculations.

Appendix A

Photon Polarisation Vectors

A.1 Photon Polarisation Vectors

Within Maxwell's Equations the definition of the (physically observable) $\underline{\mathrm{E}}$, $\underline{\mathrm{B}}$ fields are unchanged when the underlying (gauge) field undergoes the transformation

$$A^{\mu} \to A^{\mu} + \partial^{\mu}\chi. \tag{A.1.1}$$

This is the $U(1)$ local Abelian gauge invariance of electromagnetism. We can use this freedom to work with an A^{μ} that satisfies a Lorentz condition

$$\partial_{\mu}A^{\mu} = 0, \tag{A.1.2}$$

When expanding the field in terms of its normal modes this translates to

$$k_{\mu}\epsilon^{\mu} = 0 \tag{A.1.3}$$

where ϵ^{μ} is the polarisation vector of a photon travelling with 4-momenta k^{μ}. This condition reduces the field degrees of freedom to three, rather than the four that is dictated by Lorentz invariance, and completely defines the polarisation vectors for virtual particles. However, for real photons this condition doesn't define A^{μ} completely as we are free to make a further transformation

$$A^{\mu} \to A^{\mu} + \partial^{\mu}\tilde{\chi} \tag{A.1.4}$$

provided that $\tilde{\chi}$ satisfies the massless Klein-Gordon equation:

$$\Box\tilde{\chi} = 0 \tag{A.1.5}$$

This gauge freedom means that we can add any multiple of k^μ to ϵ^μ

$$\epsilon^{'\mu} = \epsilon^\mu + \xi k^\mu \tag{A.1.6}$$

For a real photon this new polarisation vector also satisfies the gauge condition $\epsilon^{'\mu}k_\mu = 0$. This allows us to choose ξ such that the time component of $\epsilon^{'\mu}$ is zero, turning the Lorentz condition into a 3-vector condition:

$$\mathbf{k}.\boldsymbol{\epsilon} = 0 \tag{A.1.7}$$

This reduces the number of independent polarisation vectors for a real photon to two, $\epsilon_\mu^{(1)}, \epsilon_\mu^{(2)}$, both transverse to $\mathbf{k}$ the propagation direction.

We require three Lorentz invariant expressions for the polarisation vectors of the incident, virtual photon and two for the final state real photon. These vectors are then placed explicitly in the trace of the Feynman amplitude and used to compute a polarisation sum over the unmeasured final state polarisation and an average over the initial state polarisation.

A.1.1 The Initial Polarisation State

Transversely Polarised Photons

As we have defined the third spatial direction as the axis of travel of the incident photon we are free to define one of the transverse polarisation vectors as a *general*, normalised vector in the transverse plane.

$$\epsilon_{i\mu}^{(1)} = \epsilon_{i\mu\perp}^{(1)} \ , \ \ (\epsilon_{i\mu\perp}^{(1)})^2 = -1. \tag{A.1.8}$$

Choosing Lorentz gauge $\epsilon_{i\mu}q_1^\mu = 0$ and another vector that is orthogonal to $\epsilon_{i\mu\perp}^{(1)}$,$(p_{2\mu})$ we can construct the second transverse polarisation vector:

$$\epsilon_i^{\mu(2)} = N\epsilon^{\mu\nu\rho\sigma}q_{1\nu}p_{2\rho}\epsilon_{i\mu\perp}^{(1)}, \tag{A.1.9}$$

where $\epsilon^{\mu\nu\rho\sigma}$ is the four dimensional completely antisymmetric tensor. Under the properties of this tensor and normalising this reduces to

$$\epsilon_i^{\mu(2)} = \frac{2}{s}\epsilon^{\mu\nu\rho\sigma}p_{1\nu}p_{2\rho}\epsilon^{(1)}_{i\mu\perp} \tag{A.1.10}$$

Longitudinally Polarised Photons

The longitudinal polarisation vector is orthogonal to $\epsilon^{(2)}_{i\mu}$, $\epsilon^{(1)}_{i\mu}$ and $q_{1\mu}$. The general form for such a vector is

$$\epsilon_i^{\mu(0)} = \tilde{N}\epsilon^{\mu\nu\rho\sigma}q_{1\nu}\epsilon^{(1)}_{i\rho}\epsilon^{(2)}_{i\sigma} \tag{A.1.11}$$

which becomes

$$\epsilon_i^{\mu(0)} = \frac{1}{\sqrt{Q^2}}\epsilon^{\mu\nu\rho\sigma}(p_{1\nu} - \frac{Q^2}{s}p_{2\nu})\epsilon^{(1)}_{i\rho\perp}(\frac{2}{s}\epsilon_{\sigma\alpha\beta\gamma}p_1^\alpha p_2^\beta)\epsilon^{(1)}_{i\gamma\perp}. \tag{A.1.12}$$

When this is computed it gives the following expression for the longitudinal polarisation vector:

$$\epsilon_i^{\mu(0)} = \frac{1}{\sqrt{Q^2}}p_1^\mu + \frac{\sqrt{Q^2}}{s}p_2^\mu \tag{A.1.13}$$

which is independent of the choice of $\epsilon^{(1)}_{i\mu\perp}$.

A.1.2 The Final Polarisation State

The final state photon is on-shell so we only have to be concerned about the two transverse polarisation states. We require a covariant expression for the two polarisation vectors in terms of other 4-momenta of the problem $(p_1^\mu, p_2^\mu, \epsilon^{(1)}_{i\mu\perp})$.

With the final state photon on-shell

$$\epsilon_f^{(i)}.q_2 = 0 \tag{A.1.14}$$

and with the freedom of Lorentz gauge we are free to add any multiple of q_2^μ to $\epsilon_f^{\mu(i)}$ without affecting physical observables. As

$$q_2^\mu = p_1^\mu + \frac{\mathbf{q}_2^2}{s}p_2^\mu + q_2^{\mu\perp} \tag{A.1.15}$$

this means that we can fix

$$\epsilon_f^{\mu(i)} = A^{(i)} p_2^\mu + n_\perp^{\mu(i)} \tag{A.1.16}$$

The on-shell condition fixes the normalisation $A^{(i)}$ giving

$$\epsilon_f^{\mu(i)} = -\frac{2n_\perp^{(i)}.q_\perp}{s} p_2^\mu + n_\perp^{\mu(i)}. \tag{A.1.17}$$

The rotational symmetry of the problem allows us the freedom to choose a particular $n_\perp^{\mu(i)}$ without biasing physical observables. With this freedom we choose the initial state polarisation vectors

$$n_\perp^{\mu(i)} = \epsilon_i^{\mu(i)}. \tag{A.1.18}$$

References

[1] P. Ciok et al., Nuovo Cimento **8** (1958) 166; K. Nui, Nuovo Cimento **10** (1958) 994; G. Cocconi, Phys. Rev. **111** (1958) 1699.

[2] M. Good and R. G. Walker, Phys. Rev. **120** (1960) 1857.

[3] P. D. B. Collins, "An Introduction to Regge Theory & High Energy Physics". Cambridge University Press (1977); R. J. Eden, P. V. Landshoff, D. I. Olive, J. C. Polkinghorne, "The Analytic S-Matrix". Cambridge University Press (1966).

[4] A. Donnachie and P. V. Landshoff, Phys. Lett. **B 296** (1992) 227.

[5] For a complete listing of the D0 papers on diffractive phenomena visit `http://www-d0.fnal.gov`.

[6] For a complete listing of the CDF papers on diffractive phenomena visit `http://www-cdf.fnal.gov/cdf.html`.

[7] For a complete listing of the H1 papers on diffractive phenomena visit `http://www-h1.desy.de:80/`.

[8] For a complete listing of the ZEUS papers on diffractive phenomena visit `http://www-zeus.desy.de/`.

[9] G. Ingelman and P. Schlein, Phys. Lett. **B152** (1985) 256.

[10] A. Donnachie and P. V. Landshoff, Phys.Lett. **B437** (1998) 408; P.V. Landshoff, Lecture at Workshop on New Trends in HERA Physics, Ringberg, Germany, June 1999. hep-ph/9907392.

[11] For a review of QCD and diffraction see: M. Wüsthoff and A. D. Martin, hep-ph/9909362 and references therein.

[12] V. N. Gribov and L. N. Lipatov, Sov. J. Nucl. Phys. **15** (1972) 438; L. N. Lipatov, Sov. J. Nucl. Phys. **20** (1975) 438; G. Altarelli, G. Parisi, Nucl. Phys. **B26** (1977) 298; Yu. L. Dokshitzer, Sov. Phys. JETP. **46** (1977) 641.

[13] Ya. Ya. Balitsky and L. N. Lipatov, Sov. J. Nucl. Phys. **28** (1978) 822; E. A. Kuraev, L. N. Lipatov, V. S. Fadin, Phys. Lett. **B60** (1975) 50; Sov. Phys. JETP. **44** (1976) 443; Sov. Phys. JETP. **45** (1977) 199.

[14] J. R. Forshaw and D. A. Ross, "QCD and the Pomeron", Cambridge University Press (1997).

[15] V. V. Sudakov, Sov. Phys. JETP. **3** (1956) 65.

[16] L. N. Lipatov, Sov. Phys. JETP. **63** (1986) 904.

[17] A. H. Mueller and G. P. Salam, Nucl.Phys. **B475** (1996) 293.

[18] A. H. Mueller and B. Patel, Nucl. Phys. **B425** (1994) 471.

[19] J. Bartels and H. Lotter, Phys. Lett. **B309** (1993) 400.

[20] L. N. Lipatov and V. S. Fadin, Sov. J. Nucl. Phys. **50** (1989) 712; JETP. Lett. **89** (1989) 352; V. S. Fadin and R. Fiore, Phys. Lett. **B 294** (1992) 286; V. S. Fadin and L. N. Lipatov, Nucl. Phys. **B406** (1993) 259; **B477** (1996) 767; Phys. Lett. **B429** (1998) 127; V. S. Fadin, R. Fiore and A. Quartarolo, Phys. Rev. **D50** 2265; **D50** (1994) 5893; **D53** (1996) 2729; V. S. Fadin, R. Fiore and M.I. Kotsky, Phys. Lett. **B387** (1996) 593; Phys. Lett. **B359** (1995) 181; V. S. Fadin, M. I. Kotsky and L. N. Lipatov, hep-ph/9704267; V. S. Fadin et al., Phys. Lett. **B422** (1998) 287; G. Camici and M. Ciafaloni, Phys. Lett. **B386** (1996) 341; Nucl. Phys. **B 496** (1997) 305; M. Ciafaloni and G. Camici, Phys. Lett. **B412** (1997) 396 and erratum Phys. Lett. **B430** (1998) 349; J. R. Forshaw, G. P. Salam, R. S. Thorne, J. Phys. **G25** (1999) 1495; R. S. Thorne, Phys. Rev.

D60 (1999) 054031; S. J. Brodsky, V. S. Fadin, V. T. Kim, L. N. Lipatov, G. B. Pivovarov, hep-ph/9901229; C. R. Schmidt, hep-ph/9904368.

[21] J. R. Forshaw and P. J. Sutton, Euro. Phys. J. **C14** (1998) 285.

[22] D. A. Ross, Phys.Lett. **B431** (1998) 161; Yu. V. Kovchegov and A. H. Mueller, Phys. Lett. **B439** (1998) 423; N. Armesto, J. Bartels, M. A. Braun, Phys. Lett. **B442** (1998) 459; E. Levin, hep-ph/9806228.

[23] G. P. Salam, JHEP. **9807** (1998) 019; J. R. Forshaw, D. A. Ross, A. Sabio Vera, Phys. Lett. **B455** (1999) 273; M. Ciafaloni, D. Colferai, G. P. Salam, hep-ph/9907409.

[24] J. R. Forshaw: "High-t Diffraction" contribution to the DIS99 Workshop, Zeuthen, Germany, April 1999.

[25] J. D. Bjorken, Phys. Rev. **D47** (1992) 101.

[26] A. H. Mueller and W- K. Tang, Phys. Lett. **B284** (1992) 123.

[27] ZEUS Collaboration: M. Derrick et al., Phys. Lett. **B369** (1996) 55; H1 Collaboration: "Rapidity Gaps Between Jets in Photoproduction at HERA" contribution to The International Europhysics Conference on High Energy Physics, Jerusalem, Israel, August 1997.

[28] CDF Collaboration: F. Abe et al., Phys. Rev. Lett. **74** (1995) 855; Phys. Rev. Lett. **80** (1998) 1156; Phys. Rev. Lett. **81** (1998) 5278; D0 Collaboration: S. Abachi et al., Phys. Rev. Lett. **74** (1994) 2332; Phys. Rev. Lett. **76** (1996) 734; Phys. Rev. Lett. **81** (1998) 5278.

[29] B. E. Cox and J. R. Forshaw, Phys. Lett. **B434** (1998) 133; B. E. Cox: "Double Diffraction Dissociation at large $|t|$ in Photoproduction at HERA" contribution to The International Europhysics Conference on High Energy Physics, Jerusalem, Israel, August 1997.

[30] I. F. Ginzburg, S. L. Panfil, V. G. Serbo, Nucl. Phys. **B284** (1987) 685.

[31] I. F. Ginzburg and D. Yu. Ivanov, Phys. Rev. **D54** (1996) 5523.

[32] J. R. Forshaw and M. G. Ryskin, Zeit. Phys. **C68** (1995) 137; D.Yu. Ivanov, Phys. Rev. **D53** (1996) 3564; D. Yu. Ivanov and R. Kirschner, Phys. Rev. **D58** (1998) 4026.

[33] J. Bartels, J. R. Forshaw, H. Lotter, M. Wüsthoff, Phys. Lett. **B375** (1996) 301.

[34] H1 Collaboration: "Production of J/Ψ Mesons with large $|t|$ at HERA" contribution to The International Europhysics Conference, Jerusalem, Israel, August 1997; ZEUS Collaboration: "Study of Vector Meson Production at Large $|t|$ at HERA" contribution to The International Europhysics Conference, Jerusalem, Israel, August 1997; H1 Collaboration: "Diffractive J/Ψ production" contribution ZEUS Collaboration: "Study of Vector Meson Production at Large $|t|$ at HERA and Determination of the Pomeron Trajectory" contribution to ICHEP98, Vancouver, Canada, July 1998; to the International Europhysics Conference on High Energy Physics, Tampere, Finland, July 1999; ZEUS Collaboration: "Recent Results from Decay Angle Analyses of ρ^0 Photoproduction at High Momentum Transfer from ZEUS" contribution to the DIS99 workshop, Zeuthen, Germany, April 1999; ZEUS Collaboration: "Study of Diffractive Production of Vector Mesons at Large Q^2 or at Large $|t|$ at HERA" contribution to the International Europhysics Conference on High Energy Physics, Tampere, Finland, July 1999.

[35] B. E. Cox, J. R. Forshaw, L. Lönnblad, hep-ph/9908464.

[36] J, Kwiecinski and L. Motoya, Phys. Lett. **B438** (1998) 203; J, Kwiecinski and L. Motoya, Acta Phys. Polon. **B30** (1999) 1817.

[37] D. Yu. Ivanov and M. Wüsthoff, Eur. Phys. J. **C8** (1999) 107.

[38] S. J. Brodsky, F. Hautmann, D. E. Soper, Phys. Rev. **D56** (1997) 6957; S. J. Brodsky, F. Hautmann, D. E. Soper, Phys. Rev. Lett. **78** (1997) 803; **79** (1997) 3544E.

[39] J. Bartels, A. De Roeck, H. Lotter, Phys. Lett. **B389** (1996) 742.

[40] A. Bialas, W. Czyz, W. Florkowski, Eur. Phys. J. **C2** (1998) 683.

[41] J. Kwiecinski and L. Motkya, hep-ph/9905567.

[42] N. G. Evanson and J. R. Forshaw, Phys. Rev. **D60** (1999) 034016.

[43] L. N. Lipatov and G. V. Frolov, Sov. J. Nucl. Phys. **13.3** (1971) 333.

[44] H. Cheng and T. T. Wu, Phys. Rev. **D1.123** (1970) 3414.

[45] J. A. M. Vermaseren, 'Symbolic Manipulation with FORM, Tutorial and Reference Manual', CAN * (1991).

[46] I. S. Gradshteyn and I. M. Ryzhik, "Tables of Integrals, Series and Products" 5^{th} edition. Academic Press (1994).

[47] S. Munier and H. Navelet, hep-ph/9909263.

[48] A. de Rujula et al, Phys. Rev. **A10** (1974) 1649.

[49] J. Bartels, J. R. Forshaw, H. Lotter, L. N. Lipatov, M. G. Ryskin, M. Wüsthoff, Phys. Lett. **B348** (1995) 589.

[50] A. Wagner: "TESLA: Status, Tasks, Perspectives". Talk given at the 4^{th} workshop of the 2^{nd} ECFA/DESY joint study on physics and detectors for a linear electron-positron collider, Oxford, March 1999. `http://hepnts1.rl.ac.uk/ECFA_DESY_OXFORD/`.

[51] P. N. Burrows, private communication.

[52] H. Plothow-Besch, Comp. Phys. Comm. **75** (1993) 396; H. Plothow-Besch, Int. J. Mod. Phys. **A10** (1995) 2901.

[53] A. D. Martin, R. G. Roberts, W. J. Stirling, Phys. Rev. **D51** (1995) 4756.

[54] H. L. Lai et al., Phys. Rev. **D55** (1997) 1280.

*e-mail:form@can.nl

[55] M. Glück, E. Reya, A. Vogt, Z. Phys. **C67** (1995) 433.

[56] M. Glück, E. Reya, M. Stratmann, Phys. Rev. **D51** (1995) 3220.

[57] G. A. Schuler and T. Sjöstrand, Phys. Lett. **376B** (1996) 193.

[58] M. Drees and K. Grassie, Z. Phys. **C28** (1985) 451.

[59] L. E. Gordon and J. K. Storrow, Nucl. Phys. **B489** (1997) 405.

[60] C. F. v. Weizsäker, Z. Phys. **88** (1934) 612; E. J. Williams, Phys. Rev. **45** (1934) 729.

[61] A. I. Lebedev. "Corrections to Weiszäcker-Williams Approximation for Low-Q^2 Inelastic *ep*-scattering", "Physics at HERA", Proceedings of the Workshop, DESY, Hamburg, eds. W. Buchmüller and G. Ingelman (1991) 613.

[62] L. V. Bezrokuv, E. B. Bugaev, Sov. J. Nucl. Phys. **32** (1980) 847.

[63] S. Frixione, M. L. Mangano, P. Nason, G. Ridolfi, Phys. Lett. **B319** (1993) 339.

[64] D. J. Miller, contribution to RADCOR, Barcelona, Spain, Sept 1998, hep-ex/9901039.

[65] G.P. Lepage and P. B. Mackenzie, Phys. Rev. **D48** (1993) 2250; S. J. Brodsky, G. P. Lepage and P. B. Mackenzie, Phys. Rev. **D23** (1983) 228.